A Yap-dependent mechano-regulatory loop directs cell migration for embryo axis assembly

Ana Sousa Ortega

Thesis supervisors:
Juan Ramón Martínez Morales
María Almuedo Castillo

UNIVERSIDAD PABLO DE OLAVIDE SEVILLA

A Yap-dependent mechano-regulatory loop directs cell migration for embryo axis assembly

Ana Sousa Ortega

Thesis supervisors:
Juan Ramón Martínez Morales, PhD
María Almuedo Castillo, PhD

Sevilla, May 2023

Thesis dissertation submitted for the PhD degree in Biotechnology, Engineering and Chemical Technology.

Acknowledgments

The research presented in this thesis was carried out in the Department of Developmental Biology in El Centro Andaluz de Biología del Desarrollo (CSIC-UPO-JA).
A 4-month stay was carried out in St Anne's University Hospital International Research Center (Brno, Czech Republic), under the supervision of Giancarlo Forte and Jorge Oliver De La Cruz.

I especially have to thank Javier Vázquez, Rocío Polvillo and Jorge Corbacho from Juan Ramón Martínez-Morales' laboratory, Estefanía Sanabria from María Almuedo's laboratory, and Alejandro Campoy from the CABD Advanced Microscopy and Imaging facility for their contributions and help to this work. I also have to thank the CABD Proteomics, Advanced Microscopy and Imaging, Aquatic Vertebrates and Functional Genomics facilities for their excellent technical assistance.

This thesis work was supported by grants awarded to Juan Ramón Martínez Morales from the Spanish Ministry of Science, Innovation and Universities (AEI): (References BFU2017-86339P) and by the Marie Sklodowska-Curie H2020-MSCA-IF- 2018-ST MechaPattern 834610 and La Caixa Junior Leader Incoming from Fundación "la Caixa" awarded to María Almuedo Castillo.

“Reserve your right to think, for even to think wrongly is better than not to think at all”

Hypatia (philosopher, astronomer, and mathematician of the 4th century BC)

To my lab
and to my family

Abbreviations

A-P: anterior posterior

AJ: Adherens junction

C&E: convergence and extension

D-V: dorsoventral

DEGs: Differentially expressed genes

ECM: extracelular matrix

EMT: epithelial to mesenchymal transition

EVL: enveloping layer

F-actin: Filamentous actin

FA: Focal adhesion

FAK: focal adhesion kinase

FGF: fibroblast growth factor

GO: gene ontology

IF: intermediate filaments

L-R: left-right

LINC: linker of nucleoskeleton and cytoskeleton

LynTm: Lyn-tdTomato

PCA: principal component analysis

PCP: planar cell polarity

pH3: Phospho histone 3

qPCR: quantitative PCR

TAZ: Transcriptional co-activator with PDZ-binding domain

TJ: tight junctions

WT: *wild-type*

YAP: Yes-associated protein

YSL: yolk syncytial layer

Abstract/Resumen

Gastrulation is a decisive process that occurs during embryonic development, in which a relatively homogenous group of cells is transformed into an embryo with established body axes and presenting the three germ layers. This is achieved through complex cell rearrangements that are tightly controlled by the interplay of the different types of morphogenetic inputs. In the animal kingdom, striking divergences exist in embryonic development, as they evolve and adapt to different environments, egg architecture and speed of development. However, even though large differences can be found among the different species, the underlying logic and principles governing the gastrulation movements are conserved. The set of cell movements observed during gastrulation is not exclusive to this process, as they are also generally involved in organogenesis, tissue regeneration, and cancer progression. Therefore, understanding how the gastrulation movements are coordinated and controlled is essential not only to understand axes formation, but also how tissues and organs are built, and even which are the mechanisms underlying oncogenic growth and metastasis. The key role of mechanical inputs during tissue morphogenesis is becoming increasingly evident, however little is known about how these inputs shape and regulate gastrulation. Among the most well-known transcriptional activators that cells use to interpret mechanical signals are YAP proteins, yet their role in gastrulation remains elusive. Our detailed analysis of *yap1* and *yap1b* double mutants in medaka fish shows that these mechanosensors are required for the assembly of the primary embryo axis: a key event for the establishment of the vertebrate body plan. Using quantitative imaging and live-sensors, we show that Yap activity is required for the proper migration of dorsally converging cells towards the embryo midline. Thus, mutant cells display reduced velocity and migratory persistence resulting in shorter cell displacements in many cases insufficient to reach the midline. Combining RNA-seq with previous DamID-seq data, we characterize the transcriptional program directly activated by Yap proteins, which mostly entails the recruitment of actin cytoskeleton regulators, ECM molecules and focal adhesion components. Moreover, we show that Yap activation depends itself on intracellular tension, closing a positive feedback loop that maintains directed cell migration.

Keywords: Morphogenesis, gastrulation, mechanobiology, Yap proteins

La gastrulación es un proceso decisivo que se ocurre durante el desarrollo embrionario, en el que un grupo de células relativamente homogéneo se transforma en un embrión con ejes corporales y que posee las tres capas germinales. Esto se logra a través de reordenamientos celulares complejos que están controlados estrictamente por la interacción de los diferentes tipos de información morfogenética. En el reino animal, existe una gran divergencia en el desarrollo embrionario, ya que este evoluciona adaptándose a los diferentes ambientes, a la morfología del huevo y a la velocidad de desarrollo. Sin embargo, aunque pueden encontrarse grandes diferencias entre las distintas especies, se conservan la lógica y los principios subyacentes que rigen los movimientos de gastrulación. El conjunto de movimientos celulares observados durante la gastrulación no es exclusivo de este proceso, ya que también pueden estar involucrados en la organogénesis, la regeneración de tejidos y la progresión del cáncer. Por lo tanto, comprender cómo se coordinan y controlan los movimientos de la gastrulación es esencial no solo para comprender la formación del eje, sino también cómo se construyen los tejidos y órganos, e incluso cuáles son los mecanismos subyacentes al crecimiento oncogénico y la metástasis. El papel clave de las señales mecánicas durante la morfogénesis de los tejidos se está volviendo cada vez más evidente, sin embargo, se poco sabe sobre cómo estas señales dan forma y regulan la gastrulación. Entre los activadores transcripcionales más conocidos que utilizan las células para interpretar señales mecánicas se encuentran las proteínas YAP, aunque su papel en la gastrulación sigue siendo difícil de saber. Nuestro análisis de los mutantes dobles *yap1* y *yap1b* en medaka muestra que estos mecanosensores son necesarios para el ensamblaje del eje central del embrión. Usando análisis de imagen cuantitativo y sensores *in vivo*, demostramos que la actividad de Yap es necesaria para la migración de las células que convergen dorsalmente hacia la línea media del embrión. Además, caracterizamos el programa transcripcional activado directamente por las proteínas Yap, observando que están principalmente involucradas en el reclutamiento de reguladores del citoesqueleto de actina, moléculas de la matriz extracelular y componentes de adhesión focal. Por último, mostramos que la activación de Yap depende de la tensión intracelular, cerrando un ciclo de retroalimentación positiva que mantiene la migración celular dirigida.

Palabras claves: Morfogénesis, gastrulación, mecanobiología, proteínas YAP

Introduction

Morphogenesis

How tissues and organs emerge during development to shape embryos is a fundamental question that has intrigued scientists for centuries and is far from being fully understood. The formation of an embryo entails the production of billions of cells from one single cell, and their organization into tissues that acquire a 3D shape in a specific spatio-temporal sequence. After the emergence of developmental genetics in the 80's and 90's, the classical approach to understand this process, known as morphogenesis, was mainly if not exclusively gene-centric. However nowadays, we acknowledge that morphogenesis is determined by the interplay of different information modules, which can be classified into genetics, biochemistry, geometry and mechanics (Collinet & Lecuit, 2021; Gilmour et al., 2017; Leptin, 2005).

Genetic information

With the emergence of molecular genetics at the end of the twentieth century, the prevailing idea was that developmental processes were a sequence of cell decisions determined by genes, that culminate in cell differentiation. In this hypothesis, individual genes have a quantitative effect and the cooperation of their individual actions was responsible for the developmental trajectories of each cell (Fig 1A) (Slack, 2002). This idea has its basis in key findings, such as the one obtained by Roux in 1888. Roux killed an individual blastomere of a two-cell stage frog embryo, observing that the remaining live portion only gives rise to part of an organism. These observations inspired Roux's mosaic theory of embryonic differentiation, in which the fate of each cell in an embryo is pre-specified very early and follows fixed trajectories (Collinet & Lecuit, 2021; De Robertis & M, 2006). The identification of morphogens and "master genes" also strengthen the idea of a genetic program controlling development (Pradel & White, 2002). Wolpert indicated that morphogens could provide positional information to cells, and therefore explain the wide variety of differentiation patterns. He proposes diverse models as a possible solution to the French flag problem, which refers to the ability of a system to form a pattern with unvaried sizes, even when parts are removed or added. The best-known is the gradient model, in which cells activate a set of downstream genes

in a morphogen concentration-specific manner (Sharpe, 2019; Wolpert, 1969). Besides, master genes are defined as genes whose expression is sufficient to direct the complete genetic program that specifies a particular cell lineage. Two classic examples of master regulators able to reprogram cell identity are the transcription factors MyoD and PAX6. The single addition of MyoD enables cells derived from the three germ layers to differentiate into muscle cells (Chan & Kyba, 2013; Weintraub et al., 1989). Besides, PAX6 is capable of promoting ectopic eye development (Gehring & Ikeo, 1999; Halder et al., 1995).

However, several observations contrasted with this deterministic model, and brought up the necessity of other mechanisms to explain development. Driesch and Morgan showed that when blastomeres of two-cell stage frog or sea urchin embryos were separated, they could regenerate the missing part (Collinet & Lecuit, 2021; Morgan, 1895). These findings indicated that during development cells could interact with each other and their surrounding environment, and adopt different possible fates in a manner that is not predetermined.

As previously indicated, nowadays, morphogenesis started to be understood as a mechanism controlled not only by genetic programmes but also by biochemical, mechanical and geometrical information. The constant updated instructions and coordination between these types of morphogenetic signals define the time, the region and the scale that drives tissue shape changes.

Biochemical information

Biochemical properties define the production and degradation rate, the activation and inhibition kinetics, as well as the diffusion and transport constants of a specific molecule (Fig 1B-C). Thus, the rate of chemical reactions influences its local concentration and activation time (Wartlick et al., 2011). Striking spatial-temporal molecular patterns can emerge from the coupling of these parameters. The generated biochemical gradient is read and interpreted by cells, which induce specific changes in gene expression depending on the concentration and the activity of the morphogen. Thus, a homogeneous field of cells is transformed into discrete regions with its own

differentiation programmes (Rogers & Schier, 2011; Sagner & Briscoe, 2017). A paradigmatic example is the vertebrate somite formation that depends on a system of traveling signaling gradients. The level of WNT and fibroblast growth factor (FGF) establish the region of cells that are competent to respond to the segmentation clock, which defines the formation of a somite. The signaling range of these gradients is controlled by mechanisms such as transcription of these genes, regulation of receptors maturation, or modulation of ligand activity by secreted antagonist (Hubaud & Pourquié, 2014). Finally, biochemical information can also be found on a cellular scale, determined by the polarized accumulation of specific molecules in the cell. This directs and defines the orientation of cell polarity, cell shape and cell dynamics. (Collinet & Lecuit, 2021). The important role of this information during morphogenesis is illustrated in a study showing that the basal localization of focal adhesion components in neuroepithelial precursors is required for optic cup folding in medaka fish. Ojoplano protein sustains the polarized formation of focal contacts essential to transmit the mechanical cues that drive the folding of the optic cup (Fig 1D) (Martinez-Morales et al., 2009).

Mechanical information

Time and length scales of morphogenetic processes can also be controlled by mechanical parameters such as elasticity, viscosity and friction. The stress propagation within a tissue or a cell is determined by these factors, and therefore the deformation rate upon a given mechanical input (Fig 1E). The rheological properties of a tissue are defined by those of its individual cells, the extracellular matrix, and the strength of cell-cell adhesions. Mechanical forces can generate gradients of stress similar to the already explained biochemical gradients of morphogens, for example when a localized stress is dissipated by friction (Collinet & Lecuit, 2021; Kindberg et al., 2020). Studies in *C. elegans* propose that to guarantee the robustness of the anterior-posterior polarization in the embryo, viscosity must dominate over friction, as there is a biological need for contractile flow to affect not only the adjacent regions but also the distant ones. This is achieved through a particular turnover of cortical components and regulation of

filamentous actin (F-actin) polymerization and/or myosin activation (Mayer et al., 2010). The role of tissue mechanics has also been studied in vertebrate body axis elongation. In this study they uncover a N-cadherin-dependent gradient along the A-P axis which sustains an increase in mechanical integrity, enabling a tissue transition from a fluid-like to a jamming behavior that drives axis elongation. These tissue properties and persistent stresses at supracellular scales allow effective cell rearrangements, and thus guide morphogenetic flows at the growing end (Mongera et al., 2018).

Additionally, mechanical cues can activate mechanotransduction pathways, which in turn induce biochemical and genetic responses, such as cytoskeleton remodeling, cell proliferation or differentiation. The mechanosensation and mechanotransduction in cells are executed by specialized structures including tight and adherens junctions (AJ) as well as focal adhesions (FA), which sense mechanical stimuli arising from the neighboring cells or the extracellular matrix (ECM), respectively (Fig 1F). These structures are fundamental for cells to timely adapt to the continuous modification of their surrounding environment. For instance, under exposure to shear stress due to the blood flow, endothelial cells activate the transcription of genes involved in proliferation and cytoskeleton remodeling (Fig 1G) (Dasbiswas et al., 2018; Farge, 2011). Also, it has been observed that epithelial monolayers cultured on high-stiffness substrate lead to an increase in proliferation, and that the inhibition of myosin generates a decrease in tension and proliferation rate (Martino et al., 2018; C. M. Nelson et al., 2005). Another example highlighting the key role of ECM in morphogenesis is the requirement of Matrigel, a mixture of ECM components, for all organoids formation. In the case of human somite organoids, known as somitoids, matrigel is required for the epithelization and the establishment of apical-basal polarity (Sanaki-Matsumiya et al., 2022).

Geometrical information

Morphogenetic processes occur in an environment defined by the geometrical configuration of the tissue, which is determined by its dimensionality, size and curvature. These geometrical factors enable the interaction between different parts of a cell, tissue or embryo, and define boundary conditions in space and time. Simulations

using an *in silico* model of a *Drosophila* developing embryo suggest that precise geometrical features, like the cephalic furrow or endoderm invagination, are required to reproduce the experimentally observed flows (Fig 1H) (Collinet & Lecuit, 2021; Dicko et al., 2017). Durdu and collaborators determine that during the migration of lateral line primordium in zebrafish, the presence of microluminal structures is necessary to spatially constrain FGF signaling (Fig 1I). This local accumulation of FGF defines in turn the frequency and position of rosette-like mechanosensory organs formation (Durdu et al., 2014). Another example in which tissue conformation modulates the local concentration of morphogens is the restriction of intestinal stem cells at the base of the villi during chick and mouse embryonic development. Buckling force shapes the morphogenetic field, forming a local maximum of epithelial signals, in particular Shh, at the tip of each villus. This induces feedback signaling between the underlying mesenchyme and the epithelium to ultimately restrict stem cells to the base of each intestinal projection (Fig 1J) (Shyer et al., 2015). Thus, geometrically imposed restrictions modulate and complement mechanical, biochemical and genetic information during morphogenesis.

Interplay between the different modules of information

Even though here the morphogenetic information is classified into four sections, they are all tightly connected. Thus, it is a challenging task to study them independently as during morphogenesis they are constantly influencing each other. The great interplay between the four types of morphogenetic information was notable in the examples discussed above. Genetic programs determine which molecules are synthesized in each cell, but these programs can be modified under specific mechanical stress or a specific concentration of morphogens, which are at the same time regulated by biochemical parameters such as the production and degradation rate or its diffusion constants. Moreover, the space of action of a morphogen can be constrained by geometrical barriers, or the mechanical properties of the tissue, which are defined by the cytoskeleton architecture and cell adhesions of cells. Therefore, the sophisticated morphology of tissues, organs and organisms emerged from the tight coordination of a

complex system of signaling that controls the behavior of cells. As the ultimate target of every morphogenetic program is a change in multicellular organization, a still open question is how tissue shape changes are read and interpreted by individual cells to control their gene expression, fate and morphology. The different levels of shape control and their recently discovered mechanisms of feedback and cross-talk are beginning to explain the impressive robustness of morphogenetic processes (Gilmour et al., 2017; Hannezo & Heisenberg, 2019). One example of this robustness is the fast adaptation and normal development of zebrafish embryos, in which 30% of their cells were removed at blastula stages. As tissue patterning and organ proportions must adapt to their body size, signaling gradients need to be scaled in an integrated and coordinated manner during embryo development (Almuedo-Castillo et al., 2018).

Thus, morphogenetic information defines tissue dynamics. These dynamics comprise; bending or invagination, which gives rise to tissue out-of-plane deformation, tissue extension and flow, comprehending planar expansion and rotational flows, tissue branching, which generates 3D arborization, and hollowing, consisting of internal fluid-filled lumen formation. Then, morphogenesis is responsible for bringing cell populations together to create new interactions and build complex three-dimensional structures (Collinet & Lecuit, 2021). One fundamental process during animal embryogenesis that involves impressive morphogenetics events is gastrulation. During this process, the main embryonic axes are established and the germ layers are specified and shaped, thus generating the internal organization as well as the external form of developing bilaterians (Chea et al., 2005; Leptin, 1999, 2005; Solnica-Krezel & Sepich, 2012; Tam & Loebel, 2007).

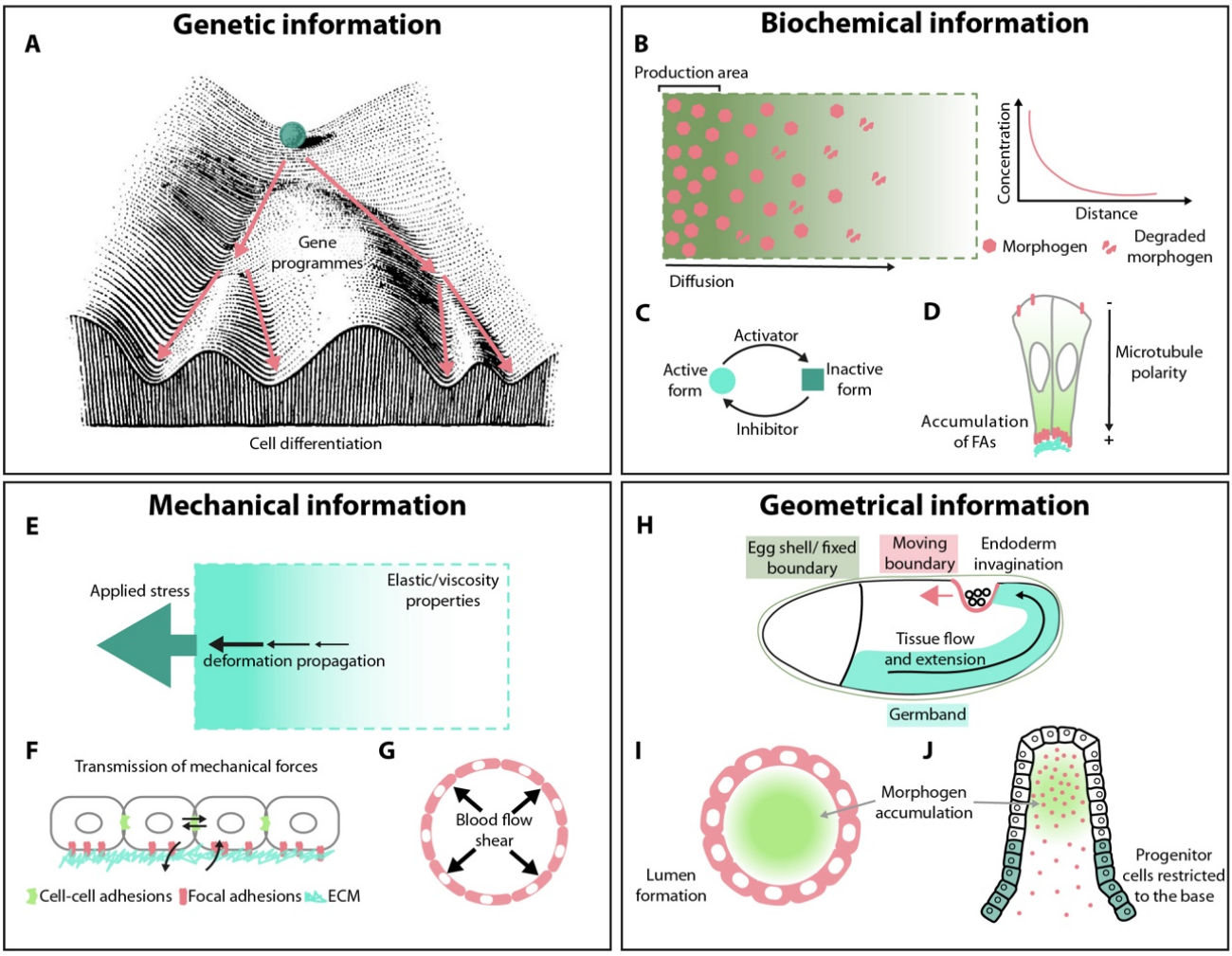

Figure 1. Modules of morphogenetic information. (A) Genetic information. Cell-fate trajectories landscape determine by genetic programmes. Blue ball represents an undifferentiated cell. Pink arrows indicate different cell fate decisions driven by specific genes. **(B-D) Biochemical information.** (B) The diffusion rate of a molecular specie (pink hexagon), synthesized in a restricted zone and exposed to degradation. The graph illustrates the exponential decay of a molecule concentration as a function of distance. (adapted from Collinet & Lecuit, 2021). (C) Activation and inhibition of a specific molecule. (D) Polarized formation of focal adhesions (FAs) in neuroepithelial precursors as an example of cell polarization. Microtubule orientation is indicated. Blue lines represent the basal lamina (adapted from Martinez-Morales et al., 2009). **(E-G) Mechanical information.** (E) The propagation of deformation due to an applied stress in a tissue, which depends on the elastic, viscosity and friction coefficients (adapted from Collinet & Lecuit, 2021). (F) Endothelial cells under the exposure of shear stress due to the blood flow. (G) Epithelial cells sensing mechanical stimuli (black arrows) arisen from neighboring cells and extracellular matrix (ECM), through cell-cell adhesions and focal adhesions, respectively. **(H-J) Geometrical information.** (H) The invagination and movement of the posterior endoderm acts as a moving boundary that restricts the extension of germbands, during fly gastrulation. Eggshell acts as fixed boundary (adapted from Collinet & Lecuit, 2021). (I) Microluminal structures as a spatial constrain to a morphogen (green gradient). (J) The local maximum formation of epithelial signals at the tip of each villus, as a result of the geometrical configuration. This localized signaling lead to the restriction of intestinal stem cells to the base of each intestinal projection (adapted from Gilmour et al., 2017).

Gastrulation

The diverse and sophisticated body architecture of animals is achieved during embryonic development through the coordination of a limited set of cell behaviors; including cell division and death, shape changes, cell contact remodeling and cell migration; all controlled by the diverse morphogenetic cues. The earliest and one of the most crucial processes of embryogenesis is gastrulation. At the beginning of this process, embryos consist of a relatively small number of cells with similar morphologies and are arranged in simple structures. During gastrulation complex and large rearrangements of cells occurs, which results in the embryo acquiring an organized and multilayered structure with distinguishable germ layers and established embryonic axis, including anteroposterior (A-P), dorsoventral (D-V) and left-right (L-R) (Leptin, 2005; Solnica-Krezel, 2005; Solnica-Krezel & Sepich, 2012). In triploblastic animals, including all bilaterians such as arthropods or chordates, the gastrula consists of three germ layers; ectoderm, which generates the epidermis and nervous system, mesoderm, which give rise to bone, muscle, connective tissue, circulatory and urogenital systems, and endoderm, which produces the gastrointestinal tract and associated structures. Thus, gastrulation requires key signaling pathways to induce cell differentiation as well as large-scale cell movements to segregate germ layers progenitors into different positions along the body axes (Pinheiro & Heisenberg, 2020).

Even though gastrulation in different animal species is conserved in its most fundamental aspects, it has also many species-specific divergent features. This process is very flexible and appears to have changed rapidly during evolution to respond to differences in the environment and egg architecture. The diversity in yolk distribution across species illustrates this; *Xenopus* displays a yolk-rich egg, and during its development, the yolk is portioned into a subset of cells, whereas birds and fish, although they also have a yolk-rich egg, the yolk does not fraction into the dividing cells. Otherwise, mammal eggs don't present yolk at all (Fig 2). Therefore, discovering unifying principles of development or postulating a common gastrulation ancestor is extremely

challenging. Even though we can find many cell behaviors and morphogenetic mechanisms shared between different species (Leptin, 2005).

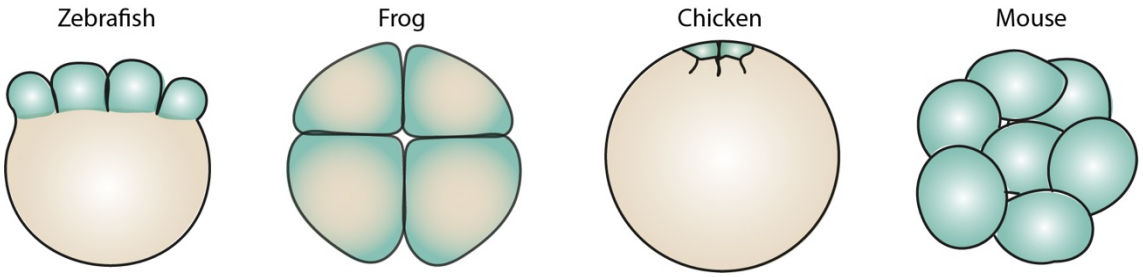

Figure 2. 8-cell stages embryos of four vertebrate model organisms. Cells' cytoplasm is represented in blue, the plasmatic membrane in black and the yolk in light brown (adapted from Solnica-Krezel, 2005).

The essence of gastrulation is that a homogeneous mass of cells is transformed into a structured and highly asymmetric body plan. For this to happen, different populations of cells receive specific instructions to undergo differentiation and move toward their final position. The complete set of determinants driving gastrulation movements is still not well understood. Since disruption of cell fates usually lead to defects in gastrulation, it is crucial to understand how cell fates are determined.

Axes specification and cell fate determination

Surprisingly, in the development of evolutionary widely distant species, we can find homologous genetic pathways controlling cell fate determination. One example of this is the Hox genes complexes, present in all animals, which control cell fate determination between A-P axis (Forlani et al., 2003; Pradel & White, 2002). Besides, the patterning of D-V axis is determined by a gradient of TGF-β family members, which is thought to be a molecular mechanism conserved from a common ancestor of vertebrates and invertebrates. Nonetheless, there are significant differences between these models. High activity levels of BMP2/4 determine the ventral side in vertebrates, whereas the peak activity of its homolog in *Drosophila*, Dpp, is on the dorsal side, due to a D-V inversion at the base of chordates (Su et al., 2019). Another observed divergence is that this signaling pathway only patterns ectoderm in *Drosophila* and sea urchins, while in chordates is responsible for ectodermal well as endomesodermal subdivisions (Balemans & Van Hul, 2002; Leptin, 2005; Ross et al., 2001). Finally, a crucial molecule

for mesoderm induction and the establishment of L-R axis is Nodal. This member of TGF-β family is conserved across the majority of vertebrate and invertebrate deuterostomes species, even though, temporal and spatial changes have occurred in Nodal expression during evolution. In all studies in vertebrates, *nodal* is expressed in the organizer and in the left lateral plate of mesoderm during embryogenesis (Chea et al., 2005; Coutelis et al., 2014), while in echinoid echinoderms is expressed on the presumptive oral side of the embryo. In addition, the germ layers where nodal is expressed varies in different phyla; in most of the invertebrate deuterostomes is present in the ectoderm, while in vertebrates is present in the mesoderm (Chea et al., 2005).

The determination of regions within the embryo that will give rise to the germ layers occurs simultaneously with the establishment of body axes. Specific transcription factors can be recognized in each population of germ layers' precursors, which will further direct their differentiation. In vertebrates Brachyury expression, under the control of Nodal, determines the mesendodermal primordium differentiation (B. L. Martin & Kimelman, 2010; Smith et al., 1991; Technau, 2001). The evolutionarily conserved gene Goosecoid is expressed in the group of mesodermal cells forming the gastrula organizer in vertebrates, which gives rise to the head process (Blum et al., 1992; Rivera-Pérez et al., 1995). Snail and Twist determine mesoderm in *Drosophila* but also have key morphogenetic functions in the mesoderm of vertebrates at late gastrula stages (Kang & Massagué, 2004; Leptin, 2005).

All of these factors participate in directing cell behaviors and morphogenetic movements during gastrulation. A remarkably small number of choreographed cell behaviors are used repeatedly to determine the animal body plan, including cell shape changes, apical and constriction, and cell migration.

Cell behaviors shaping gastrulation

Cell shape changes

The shape of the cell is defined by its intrinsic material properties and active stresses as well as by external regulation through mechanical and chemical signaling (Dasbiswas et al., 2018). Cell shape transitions are mediated by the remodeling of cell adhesions, the

actomyosin network and the microtubule system. As these structures are involved in nearly all aspects of cellular morphogenetic behavior, it is difficult to analyze them independently. Disruption of the actin cytoskeleton results in global effects and phenotypes difficult to interpret. For this reason, the role of this network has mostly been studied by the analysis of its regulators and modifiers, including members of the RHO GTPases family and Myosin II. These modulators have been proven to have crucial roles in determining cell shape during division, growth, and morphogenetic events such as gastrulation, discussed later in detail (Leptin, 2005; W. J. Nelson, 2009).

Apical constriction

An epithelium is typically formed by cells that are polarized along their apical-basal axes and are connected through apical cell-cell adhesion complexes. Apical constriction consists on the shrinking of the apical surface of epithelial cells, generally the exterior or lumen-face cell surface. This often leads to cell morphology changes from columnar or cuboidal to trapezoidal, wedge-shaped or bottle-shaped. These cell geometry modifications have different consequences depending on the physiological context. Apical constrictions in cells maintaining cell-cell adhesions can lead to the bending of the epithelial tissue, enabling the formation of three-dimensional structures. Apical constrictions of individual cells can result in cell extrusion or cell ingression from epithelial tissues. (R. E. Keller, 1981; A. C. Martin & Goldstein, 2014). A common machinery, including actin, myosin and adherens junctions (AJs) is required in this process. F-actin and myosin form the contractile network, either arranged into bundles or into a more loosely organized mesh underlying the plasma membrane, known as apical actomyosin cortex. The shrinkage of the apical cortex is driven by actin-myosin contractions. Apical AJs are involved in establishing cell polarization and linking the cells, enabling actin-myosin contractions to drive tissue shape changes (Fig 3A) (A. C. Martin & Goldstein, 2014; Solnica-Krezel & Sepich, 2012).

Cell intercalation

Cell-cell intercalation is a process in which neighboring cells exchange places. Intercalation can occur within a single plane (mediolateral) or between adjacent planes in a multilayered tissue (radial). The common factors orchestrating this process are

cadherins, non-muscle myosin and RHO GTPases, however, the execution can differ depending on the type of intercalation and the cell identity (Walck-Shannon & Hardin, 2014).

Epithelial mediolateral intercalations require that cells maintain their adhesions as well as their motility. To do this, cells shrink their junctions oriented perpendicular to the extension axis, followed by a restoration of the isodiametric shapes (Fig 3B). By contrast, mesodermal mediolateral intercalation arises from protrusive activity that is polarized to the mediolateral edges of intercalating cells. These protrusions are thought to be attached to the neighboring cells and provide traction for the movement. In both cases, cells are highly oriented and often require Wnt/planar cell polarity (PCP) pathway signaling (Fig 3C). The core molecules of this signaling are asymmetrically distributed on cell membranes, and mediate the polarization of cells through the control of E-cadherin distribution, formation of protrusions and myosin contractility (Yang & Mlodzik, 2015).

Radial cell intercalations, mostly independent of Wnt/PCP signaling, seems to be context-dependent. In early development, long-range morphogen signals, such as FGF or EGF, control the directed protrusive activity. Ultimately, the final position of cells also requires the presence of cell adhesions (Fig 3D) (Gong et al., 2004; Gray et al., 2011; Walck-Shannon & Hardin, 2014).

Cell migration

Cells show a large repertoire of migration modes with impressive plasticity, allowing them to switch between different migration strategies in response to their environmental cues and the activity of different molecular pathways. Cells can move as individuals or as a group.

Single-cell migration is classically divided into mesenchymal and amoeboid modes. Mesenchymal migration, typical of fibroblast and some cancer and stem cells, is characterized by a strong dependence on ECM adhesion, the presence of elongated morphology and actin-based protrusion at their leading edge, and the ability to create strong traction forces on the substrate through contractile actin network (Fig 3E). By contrast, in ameboid migration, cells display rounder morphology, undergo constant fast extensions and retraction of membrane protrusions, and present weak adhesions to the substrate. This mode of migration usually leads to higher migration velocity and it is used

by a wide range of cells, including primordial germ cells or immune cells (Fig 3F) (Abercrombie, 1997; Ruprecht et al., 2015; SenGupta et al., 2021).

Additionally, cells can also migrate collectively as groups. This kind of movement has an essential role during tissue remodeling, wound closure and cancer cell invasion. During collective migrations, external cues must be transmitted to the entire group of cells. This generates a front-rear polarity at a supracellular level. In the front, leader cells display stable protrusions towards the substrate, whereas at the rear end, the follower cells present small transient lamellipodia. In the protrusions, focal adhesions are formed to exert traction forces. Finally, leader cells can also remodel the substrate by secreting metalloproteinases and other ECM components, thus influencing the overall migration (Fig 3G) (Friedl & Gilmour, 2009; Leptin, 1999; SenGupta et al., 2021).

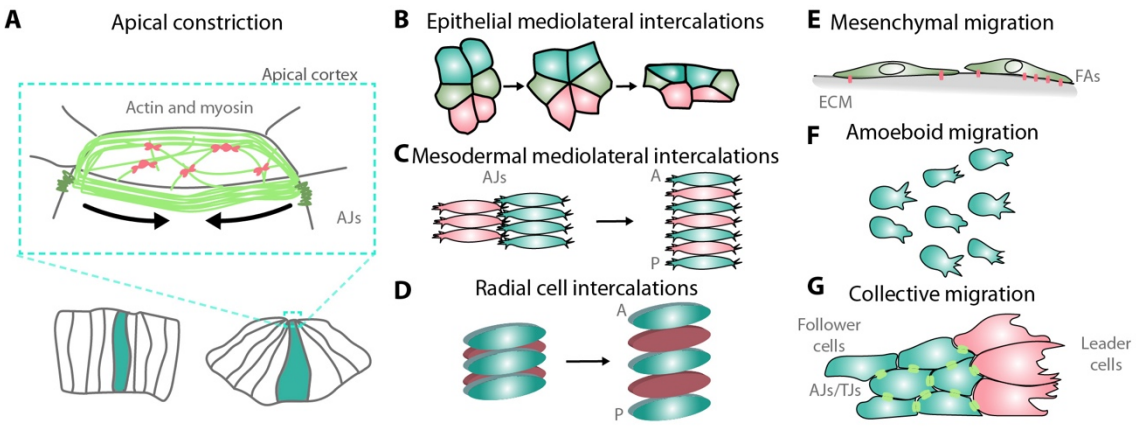

Figure 3. Cell behaviors involved in gastrulation. **(A) Apical constriction** driving epithelial tissue bending. Shrinking of the apical cortex (magnification shown in the blue rectangle) is mediated by contractions of the actomyosin network. F-actin is represented in light green and myosin in pink. Apical adherens junctions (dark green) link cells, allowing actomyosin contractions to drive tissue shape changes (adapted from Martin & Goldstein, 2014). **(B-C) Cell-cell intercalations** in which neighboring cells exchange places within the same plane, maintaining their adhesions (epithelial mediolateral intercalation in B) or creating protrusions (mesodermal mediolateral intercalation in C), or between adjacent planes (radial intercalation in D) (adapted from Solnica-Krezel & Sepich, 2012; Walck-Shannon & Hardin, 2014). **(E-G) Cell migration** can be as a single cell, presenting elongated morphology and strong dependence to ECM adhesions (mesenchymal migration in E) or displaying a rounder shape and weak ECM adhesions (ameboid migration in F), or as a group (collective migration in G) (adapted from SenGupta et al., 2021).

These cell behaviors are combined to perform complex and large-scale cell rearrangements. During gastrulation, these cell rearrangements are classified into four evolutionarily conserved movements; epiboly, internalization, convergence, and extension.

Morphogenetic movements during gastrulation

Emboly

Emboly, or internalization, is the gastrulation movement in which the future mesodermal and endodermal cells are internalized beneath the prospective ectoderm. These rearrangements result in the endoderm taking the most internal position, the ectoderm as the most external layer, and the mesoderm between them (Fig 4). This ingression occurs through an opening in the embryo, known as ventral furrow in *Drosophila*, blastoderm margin in fish, blastopore in amphibians and primitive steak in amniotes (Solnica-Krezel, 2020; Standring, 2021; Stern, 2004). The underlying cellular behaviors of the internalization differ between species but must involve some form of epithelial-to-mesenchymal transition (EMT), in which cell-cell adhesions are disassembled, cell polarity is lost and cells acquire migratory and invasive properties. This is usually followed by a migration of endodermal and mesodermal progenitors away from the area of internalization (Thiery et al., 2009; Wu et al., 2007). In *Drosophila*, the epithelium invaginates through apical constriction, giving rise to the ventral furrow. The future mesoderm is localized in the most internal region of this folding, which experiences an EMT to break away from the invaginated epithelium and start migrating (Fig 4A) (Ko & Martin, 2020; Solnica-Krezel & Sepich, 2012). Above the prospective blastopore in frogs, processes of apical constriction mediate the involution of a cohesive tissue, consisting of future mesoderm and part of the endoderm. Only when this tissue is internalized, mesodermal cells break away from it (R. E. Keller, 1981). In the emboly of sea urchins or amniotes, EMT precedes internalization. Thus, mesodermal and endodermal progenitors at the primitive streak undergo EMT to migrate individually into the embryo (Fink & McClay, 1985; Tam & Loebel, 2007). Finally, during zebrafish emboly, both processes, ingression and involution, are observed. Mesodermal and endodermal progenitors migrate through the blastoderm margin as synchronized individuals in dorsal regions, or as a cohesive tissue in lateroventral regions (Pinheiro & Heisenberg, 2020; Solnica-Krezel & Sepich, 2012).

Epiboly

Epibolic movements are responsible for germ layers spreading and thinning. The nature of epiboly is defined by the size and geometry of the embryo. In single-layer epithelium blastulae, like those of mammalian embryos, it occurs an expansion of the surface while keeping the thickness constant. In contrast, epiboly in multilayered blastula usually implies a thinning of the tissue (Fig 4).

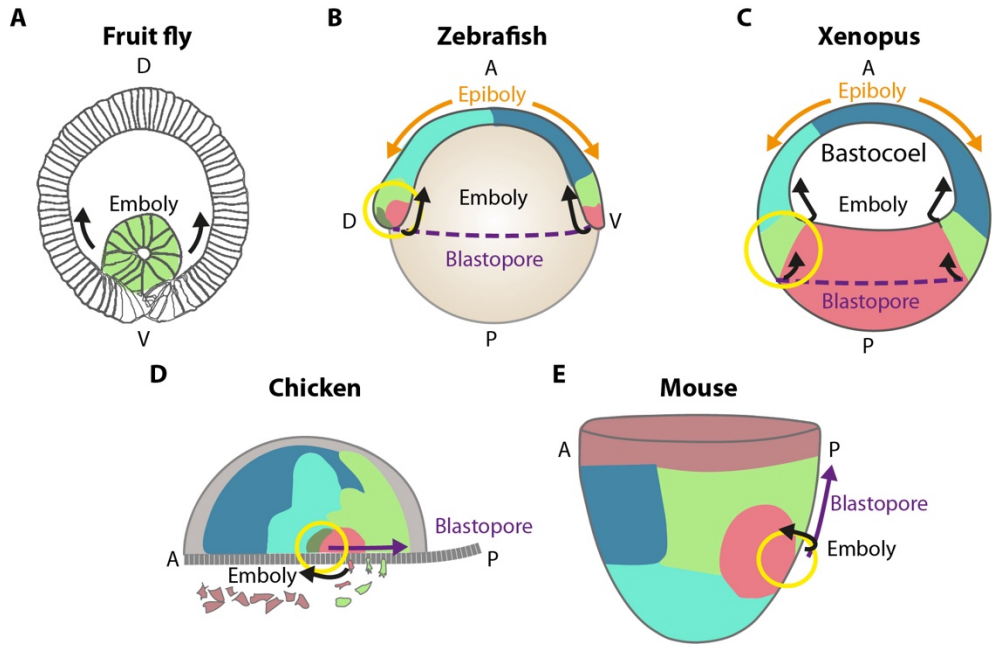

Figure 4. Gastrulating movements in diverse animal models. Cross-sections of early gastrula fate maps of fly fruit (A), zebrafish (B), frog (C), chicken (D), and mouse (E). Emboly (black arrows) and epiboly (orange arrows) movements are indicated. Blastopore are represented as a purple arrow or line. Spermann-Mangold organizer is indicated as a yellow circle. Germ layer are identified as follow: mesoderm and its precursors (light green), prechordal mesoderm (dark green), endoderm and its precursors (pink), epidermis (dark blue), neuroectoderm (light blue), various extraembryonic tissues (brown, gray). Abbreviations: A: anterior, P: posterior, D: dorsal, V: ventral (adapted from Solnica-Krezel & Sepich, 2012).

A great variety of cellular mechanisms can be involved in epibolic movements. In amniotes, the main mechanism is cell division within the plane of the epithelium, followed by a growth in cell volume (Solnica-Krezel, 2005). In frogs and fish, a key cell behavior during epiboly is the radial intercalation of deeper cells to more superficial layers. As these intercalations are not polarized with respect to the embryonic axis, they lead to an isotropic expansion of tissue (R. E. Keller, 1981; Solnica-Krezel & Sepich, 2012; Warga & Kimmel, 1990). Cell shape changes can also contribute to the expansion of cell layers. The cells of the superficial epithelium of zebrafish, known as enveloping layer (EVL), undergo a flattening and expansion of their surface without a significant volume

change. This process is thought to be mainly driven by cortical contractions of the actomyosin belt, formed at the blastoderm margin, and the membrane removal in an adjacent layer, the yolk syncytial layer (YSL), to which EVL is attached (Marsal et al., 2017; Solnica-Krezel, 2020). Lin and collaborators show that direct cell migration also mediates epibolic movements in zebrafish, leading to the expansion of the tightly packed cell mass at the embryo equator towards the vegetal pole (F. Lin et al., 2009).

Convergence and extension

Convergence movements narrow the germ layers along the mediolateral axis, and simultaneously extension movements elongate them anteroposteriorly, thus defining the animal body plan. The initiation of convergence and extension (C&E) movements differs between species. In frogs and fish, they start once the germ layers are specified and epiboly has been in progress for a while. By contrast, in amniote gastrulation, the anterior extension of the primitive streak is concurrent with C&E movements (Solnica-Krezel, 2020; Solnica-Krezel & Sepich, 2012). These morphogenetic events are driven by a combination of cell behaviors that have different importance depending on the species. However, to ensure proper C&E, cells have to achieve mediolaterally-elongated cell morphology and polarized motile protrusions, which enables the intercalation of mesenchymal cells. These cell shape changes and movements simultaneously lead to a narrowing and elongation of the body axis, as well as a preferential segregation of the anterior and posterior cells (Solnica-Krezel, 2005; Yin et al., 2009). Studies in zebrafish and chick point out to polarized cell divisions, in which daughter cells are aligned within the A-P axis, as an additional mechanism underlying vertebrate embryo elongation. In medaka gastrulating embryos, this mechanism drives, at least in part, the elongation of the central nervous system primordium (Gong et al., 2004; Hirose et al., 2004; Sausedo et al., 1997). Finally, cell migration can also mediate C&E processes. For example, during zebrafish development, lateral mesoderm converges towards the midline in a directed manner. Moreover, cells closer to the animal pole move preferentially anteriorly and those closer to the vegetal pole are biased posteriorly (Sepich et al., 2005). Interestingly, undirected cell migration can also contribute to tissue spreading. This is observed in zebrafish endodermal precursors and is controlled by Nodal signaling. Once these cells have been internalized during emboly, they start migrating in an undirected manner,

thus expanding randomly over the yolk. After the first half of gastrulation, endodermal cells switch from a random walk behavior to directed convergence movements towards the A-P axis (Pézeron et al., 2008). Striking similarities are found during chick gastrula, in which internalized cells first move away from the blastopore without any bias towards the midline, and at midgastrula stage, they start to migrate towards the midline, initiating dorsal convergence (Solnica-Krezel, 2005).

Consequently, even though these morphogenetic movements do not always have the same underlying cellular mechanism in all species (i.e. these must be experimentally determined for each individual case) they do share many features. Often, the differences observed are the result of the adaptation to changes in environmental conditions, egg architecture and the speed of development. However, all the morphogenetic movements during gastrulation can be achieved by a small number of cell behaviors. Thus, the study of mechanisms that regulate them is crucial to better understand gastrulation and other morphogenetic processes (Leptin, 2005; Solnica-Krezel & Sepich, 2012).

In this thesis, I will focus on how mechanical cues are able to shape these morphogenetic events during gastrulation. This module of morphogenetic information is one of the less understood and recent studies have proven its crucial role during morphogenesis.

Mechanical cues and mechanotransducers

Mechanical forces play a crucial role in morphogenetic events transmitting detailed information across space, which leads to changes in cellular properties and behaviors. Cells sense and transform these mechanical cues into a biological response through intracellular molecules known as mechanosensors. These are mainly proteins that display molecular changes in response to mechanical stimulation. The nature of these molecular changes can differ widely, including post-translational modifications, intracellular protein shuttling, protein unfolding, and new interactions generation (Martino et al., 2018).

Tissues and cells are able to sense, generate and transmit forces by different mechanisms, but the cytoskeleton is involved in most of them. The broad functions of the cytoskeleton are to spatially organize the contents of the cells, to physically and biochemically connect the cells to the external environment, and to generate coordinated forces that enable cell movements and shape changes (Fletcher & Mullins, 2010). The cytoskeleton's mechanical properties are determined by the dynamics, geometry, and polarity of their components, which include actin fibers, microtubules, and intermediate filaments (IFs). The contractility of the cytoskeleton is mediated by the stress fibers, consisting of F-actin and myosin II coupling through crosslinking proteins. When myosin II hydrolyzes ATP, these structures generate forces that are transmitted across tissues through cell adhesions. In this manner, individual cellular forces can lead to tissue-scale changes (Heisenberg & Bellaïche, 2013; Kindberg et al., 2020)

Microtubules and IFs also contribute to the mechanical properties of the cells. For example, microtubules mediate the intracellular transport of molecules within a cell, required for the establishment of cell polarity. Besides, IFs are assembled in many cells in response to mechanical stresses and contribute to the mechanical integrity of eukaryotes' nuclei. However, most of the morphogenetic forces are thought to be driven by the actomyosin cytoskeleton in coordination with cell adhesions (Fletcher & Mullins, 2010; Kindberg et al., 2020).

Cell-cell adhesions

Cells within epithelial and endothelial tissues are held together by cell-cell junctions, which are essential for tissue homeostasis. Tissues are constantly facing mechanical forces that provide key context information for their function, but at the same time generate a stress, which needs to be adjusted in order to ensure their integrity. There are different types of cell-cell bindings with distinct functions and molecular compositions; adherens junctions (AJs), tight junctions (TJs), and desmosomes. All of them act in parallel as mechanotransducers at cell-cell contacts (Angulo-Urarte et al., 2020).

Adherens junctions present different sizes and compositions, but classic cadherins are a common component. They are generally connected to the actin cytoskeleton through a β-catenin and α-catenin binding. The coupling of the cadherin clusters to F-actin is essential to stabilize AJs and avoid their degradation (Hong et al., 2013). In addition, AJs remodeling depends on mechanical forces, as tension-dependent α-catenin unfolding allows the recruitment of vinculin and other adaptor proteins, which connect with F-actin. This results in the maturation and growth of the AJs and the additional recruitment of F-actin, promoting a self-reinforcing process that strengthens the binding of AJs and the actin cytoskeleton (Angulo-Urarte et al., 2020). This mechanosensory function enables AJs to react dynamically to forces, regulating intracellular tension, and activating cellular responses.

Tight junctions seal layers of cells enabling the separation of compartments with different compositions. They are formed by transmembrane proteins, including claudins, occluding and junctional adhesion molecules, and cytoplasmic proteins, such as ZO proteins. TJs are anchored to F-actin and microtubules via ZO and cingulin family proteins. These proteins have a crucial role in maintaining intracellular tension, and thus in the regulation and transmission of forces within the monolayer. ZO proteins also have a mechanosensitive role, as cytoskeletal-derived tensional forces lead to ZO conformational changes that allow the recruitment of cytoskeleton-regulating proteins, such as ROCK, or the sequestration of transcription factors (Angulo-Urarte et al., 2020; Spadaro et al., 2017).

Desmosomes are strong cell-cell adhesions that have a crucial role in maintaining the integrity of tissues, especially of those frequently exposed to mechanical stress, such as epithelial cells in the skin or cardiomyocytes. Desmosomes are formed by desmosomal cadherins, plakoglobins, and plakophilins. These junctions are coupled to IFs through desmoplakins. Interestingly, pulling forces promote the linkage of classical cadherins to α-catenin and/or recruitment of desmosomal proteins and IFs to AJs in a plakoglobin-dependent manner (Angulo-Urarte et al., 2020; Choi et al., 2009; Weber et al., 2012).

In conclusion, there is a clear link between the different types of cell junctions, and they work together to interpret the mechanical cues and transduce them into the proper signaling response.

ECM-cell adhesions

Cell adhesions to the ECM through FAs have also a central role in mechanical signaling, as they are able to interpret, transmit and buffer the forces across tissues during a morphogenetic event. ECMs are conformationally and compositionally diverse networks of glycosaminoglycans, proteoglycans, and fibrous proteins, including collagen, elastin, fibronectin, and laminin, which have structural and adhesive functions (Alberts et al., 2002; Dzamba & DeSimone, 2018). The composition and structure of the ECM are tightly controlled in a tissue-specific manner during development and in adulthood, in order to favor cell and organ function.

FAs are large multiprotein signaling hubs, which basic composition consists of heterodimeric integrin receptors, adaptors such as talin or vinculin coupled to F-actin, and FA kinase (FAK) and SRC kinase, which control numerous downstream pathways. However, FA structure is highly variable in response to ECM composition and mechanics. In fact, forces exerted on FAs or even the space and adhesion sites available in the ECM promote conformation changes in FA mechanosensitive proteins, which expose cryptic-bindings sites, resulting in the recruitment of further proteins, the rearrangement of the cytoskeleton and the activation of myosin II. This causes the reinforcement of the binding site, and ultimately the activation of downstream signals (Schiller & Fässler, 2013). For example, integrin binding to the ECM activate paxillin, a scaffold protein at FA, which promotes the recruitment of structural and signaling molecules that drive cell migration (López-Colomé et al., 2017).

Interestingly, the formation of new adhesions needs Arp2/Arp3-mediated actin polymerization, while their maturation requires myosin II-mediated cell contractility, the activity of formins, and stiff ECM. Actomyosin contractility promotes the recruitment of vinculin to the FAs and the inhibition of F-actin depolymerization, reinforcing the adhesion site and increasing cell tension. Moreover, downstream signals

like cell spreading or resistance to rigid substrate increase FAK activation in a positive loop (Martino et al., 2018). On the other hand, soft ECM or myosin II inhibitors result in a decrease in FA stability (Huttenlocher & Horwitz, 2011; Schiller & Fässler, 2013). Thus, the maturation of FAs is regulated by the mechanical properties of the ECM, wherein stiffer substrates promote larger, stronger, and enduring cell adhesions (Kindberg et al., 2020; Martino et al., 2018; Nardone et al., 2017).

Besides, FAs have also an impact on the shape of the nucleus. The F-actin connects FAs to the perinuclear actin cap, consisting of actomyosin bundles wrapped around the nucleus (Khatau et al., 2009). Additionally, the linker of nucleoskeleton and cytoskeleton (LINC) complex provides a direct mechanical coupling between the cytoskeleton and nuclear components across the nuclear envelope (Méjat & Misteli, 2010). These connections provide the direct propagation of mechanical forces from the cell periphery to the nucleus.

Conclusively, cells not only respond to changes in ECM composition and mechanics, but they also adjust their own mechanical state by remodeling their cytoskeleton and adhesions, modulating their elasticity, or generating contractile responses upon applied forces.

Mechano-dependent shuttling proteins

The mechanical information sensed by FAs and cell-cell adhesions, and its propagation across the cytoskeleton, can activate downstream proteins promoting their subsequent shuttling to the nucleus, which eventually may lead to changes in gene expression. Among the first proteins described to shuttle to the nucleus to control gene expression in response to mechanical cues are: the TJ protein, ZO-1, whose nuclear localization is inversely related to cell density and the maturation of cell-cell contacts (Balda & Matter, 2000; Gottardi et al., 1996), tyrosin kinase c-Abl, which moves from FAs to the nucleus to integrate adhesion and cell cycle signals or to regulate cell morphology in response to growth factors (Lewis et al., 1996; Plattner et al., 1999), and β-catenin, a protein mostly present at AJs that display a nuclear localization in response to cytoskeleton

remodeling (Gumbiner, 1995; Martino et al., 2018; Orsulic & Peifer, 1996). A number of other proteins have been shown to translocate to the nucleus in a mechanical-dependent manner, being Yes-associated protein (YAP) and WW Domain Containing Transcription Regulator 1 (TAZ) one of the most studied.

YAP and TAZ proteins

The vertebrate paralogs YAP and TAZ, as well as their homolog in *Drosophila* Yorkie, are transcriptional effectors of the Hippo pathway. These paralogs share many common structural features; a TEAD-binding domain, 14-3-3-binding domain, one or two WW domains, a transcriptional activation domain that in vertebrates can be phosphorylated by Src/Yes tyrosine kinase family, and ends in a short PDZ-domain recognition sequence. In vertebrates, the core of the Hippo pathway consists of MST1/2 kinases, which together with SAV1 adapter protein, phosphorylate and activate a complex of LATS1/2 kinases and their cofactor MOBKL1A/B. In turn, this complex binds and phosphorylates the transcriptional coactivators YAP/TAZ, resulting in their inactivation by nuclear exclusion, followed by proteasomal degradation (Dong et al., 2007; Huang et al., 2005). On the other hand, inactivation of the Hippo core kinases leads to the accumulation of YAP/TAZ in the nucleus, where they bind mainly to members of the TEAD family of transcriptional factors, promoting the expression of target genes (Fig 5). The most studied target genes of YAP/TAZ are involved in stem cell activity, cell proliferation, and survival. The function of these paralogs has been proven to be essential during early development. In drosophila, Yorkie is required for the proliferation of several embryonic tissues, and its aberrant activation induces tissue overgrowth (Fernández et al., 2011; Hamaratoglu et al., 2006; Piccolo et al., 2014). Mutants of Hippo pathway components in mice, such as NF2, MST1/2 and LATS2, lead to death at relatively early embryonic stages due to a defective development of extraembryonic tissues (McClatchey et al., 1997; Piccolo et al., 2014). In divergence with the overexpression phenotype, YAP/TAZ double mutants die before implantation. Whereas, *YAP*$^{-/-}$ mutants with functional TAZ die shortly after gastrulation, displaying shortened and disorganized body axis, defective neural morphogenesis and abnormal yolk sac vasculature (Morin-Kensicki et al., 2006; S. Piccolo et al., 2014). Besides, the Hippo pathway is also a central regulator of organ size and its dysregulation leads to tumorigenesis, as shown in many overgrowth tissue

phenotypes when the Hippo pathway activity was reduced (Galli et al., 2015; Karaman & Halder, 2018; Neto-Silva et al., 2010; Zhao et al., 2010). In mice liver, overexpression of YAP induces cell proliferation in a TEAD-dependent manner resulting in a fourfold increase in liver mass. Consistently, severe heart enlargement is caused by Salvador/WW45, Mst1/2, and Lats2 inactivation or YAP overexpression. On the other hand, YAP depletion produces a decrease in cell proliferation, an increase in apoptosis, and a defective morphogenesis of liver and heart formation. In line with this, YAP also promotes progenitor cell proliferation after an induced damage, showing its positive role in liver and heart regeneration (Camargo et al., 2007; S. Piccolo et al., 2014; Varelas, 2014). The existence of a strong link between cancer and Yap is illustrated in breast cancer cells or skin tumors in mice, where YAP/TAZ-TEAD together with the activator protein-1 (AP-1) form a complex that synergistically activates target genes directly involved in the regulation of S-phase entry and mitosis, resulting in an oncogenic growth (Zanconato et al., 2016). Even though the activity of Hippo effectors has been historically associated with cell growth and tumorigenesis, recent studies have shown that the activation of YAP can directly induce the transcription of genes involved in cell-matrix interaction, ECM composition, and cytoskeleton integrity (Calvo et al., 2013; Morikawa et al., 2015; Nardone et al., 2017).

Given the importance of these Hippo pathway effectors, a critical question is how they are controlled. Since their identification, several upstream regulators have been discovered, including classical signaling molecules such as G-protein coupled receptors (GPCRs) and RAS-MAPK signaling (Calvo et al., 2013; Morikawa et al., 2015; Nardone et al., 2017). However, the strongest effects on Hippo pathway activity are exerted by mechanical signals. Although YAP and TAZ can have different roles in the cell, they are both sensitive to substrate stiffness, cell-cell interaction, and cell spreading (Dupont et al., 2011; Martino et al., 2018; Nardone et al., 2017; Oliver-De La Cruz et al., 2019). AJs serve as a binding site for Hippo pathway members, and the loss of these cell-cell adhesion components can promote the nuclear localization of YAP in different contexts (Fig 5A) (Karaman & Halder, 2018; Zhao et al., 2011). Besides, adhesions to fibronectin, via FAK-Src-PI3K signaling pathway, induce the inhibition of LATS1/2 and thus YAP nuclear accumulation. These regulations of the Hippo pathway by AJs and FAs are

thought to be involved in the proliferation inhibition by cell contacts and in the presence of active YAP in spread cells (N.-G. Kim et al., 2011; N.-G. Kim & Gumbiner, 2015). Also, cells in stiff environments experience forces via FAs that are in turn transmitted to the nucleus, leading to its flattening. This shape change stretches nuclear pores, which reduces their mechanical resistance to molecular transport and increases YAP nuclear import (Elosegui-Artola et al., 2017). YAP/TAZ activity can also be controlled in a Hippo/LATS-independent manner. This was shown using single-cell micropatterned fibronectin islands of different sizes and with a defined available area for cell-ECM adhesions. Cells individually plated on big islands displayed a spread morphology and nuclear YAP/TAZ, which was independent of the actual area available for cell-ECM interactions. This indicates that this activation is not determined by cell-cell or ECM-cell contacts. Neither, Rac1-GEFs inhibition, disrupting microtubules, nor depletion of LATS1/2 affect YAP/TAZ localization under tested conditions. Instead, Rho or actin cytoskeleton inhibition prevents YAP/TAZ transcriptional activity, indicating that this regulation mainly depends on Rho GTPase activity and the tension of the actomyosin cytoskeleton (Dupont et al., 2011). Recent studies indicate the mechanically sensitive ion channel, Piezo 1, as another mechanism that can impact in YAP/TAZ function (Fig 5B) (Duchemin et al., 2019; Pathak et al., 2014).

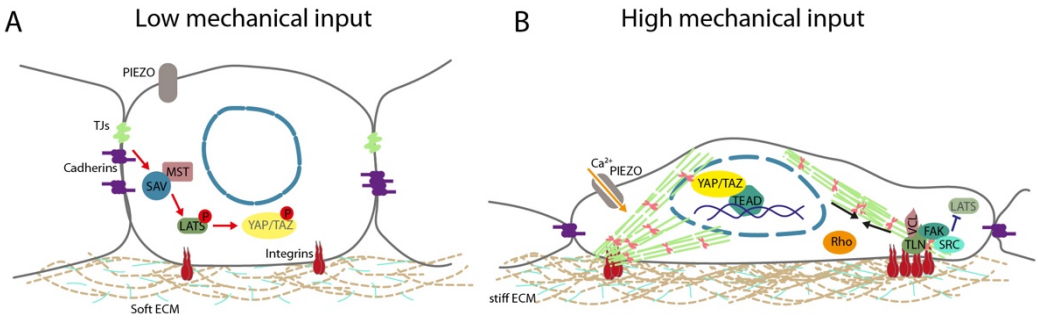

Figure 5. Yap/TAZ mechano-regulation. (A) Cells on a soft substrate with low mechanical input, activate Hippo core kinases, MST1/2 and LATS1/2, leading to the inactivation of YAP/TAZ by nuclear exclusion and subsequent degradation. Cell-cell adhesions can promote the activation of the Hippo pathway. **(B)** Cells in stiff environments or under high mechanical inputs display nuclear YAP/TAZ, where they bind to TEAD and promote the expression of their target genes. FAs can drive the shuttle of YAP/TAZ to the nucleus through different mechanisms: the inhibition of LATS1/2 via FAK-Src-PI3K, promoting the stretching of nuclear pores, or inducing actomyosin contraction. Cell spreading promotes YAP/TAZ activation, in a Hippo/LATS-independent manner. Piezo activation can also lead to the nuclear localization of YAP. Red arrows indicate activation. Abbreviations: TJs: tight junctions, ECM: extracellular matrix, VCL: Vinculin, TLN: Talin. (Figure adapted from Karaman & Halder, 2018).

Despite the role of YAP/TAZ paralogs in integrating the mechanical signals to control cell growth, cell specification, and cell morphology changes, the mechanistic link between these mechanosensors and gastrulation morphogenetic movements has remained elusive. This is precisely the main goal of this thesis.

Objectives

The main goal of this thesis work was to expand the knowledge about how mechanical inputs influence morphogenetic movements during gastrulation. Being Yap a well-known transcriptional mechanotransducers, our specific objectives were:

1. Understand the role of Yap proteins during the gastrulation stages in medaka, one of the teleost fish model species.

2. Study the genetic program controlled by Yap activation.

3. Analyze the interplay between Yap activity and intracellular tension driven by cell cytoskeleton changes.

4. Examine the possible molecular and mechanical mechanisms that regulate Yap activity during gastrulation.

Materials and Methods

Strains and fish maintenance

The medaka (*Oryzias latipes*) iCab wild-type strains, whose developmental stages are illustrated in Figure 6, the transgenic lines *tg*(*4xGTIIc*:eGFP) and the mutant strains *yap1Δ7pb* and *yap1bΔ136pb* were maintained under previously described experimental conditions (Vázquez-Marín et al., 2019). To generate the medaka line *tg(4xGTIIc:eGFP),* the plasmid *4xGTIIc:eGFP* with flanking Tol2 sites (Miesfeld et al., 2015) was injected at 10ng/µl together with in vitro transcribed Tol2 RNA (50 ng/µl) into one-cell-stage iCab embryos (this line was generated by Felix Loosli). GFP positive embryos were raised to adulthood and outcrossed to iCab WT fish to establish the transgenic line *tg(4xGTIIc:eGFP)*.

Animal experiments were carried out according to ethical regulations. Experimental protocols have been approved by the Animal Experimentation Ethics Committees at the Pablo de Olavide University and CSIC (license number 02/04/2018/041).

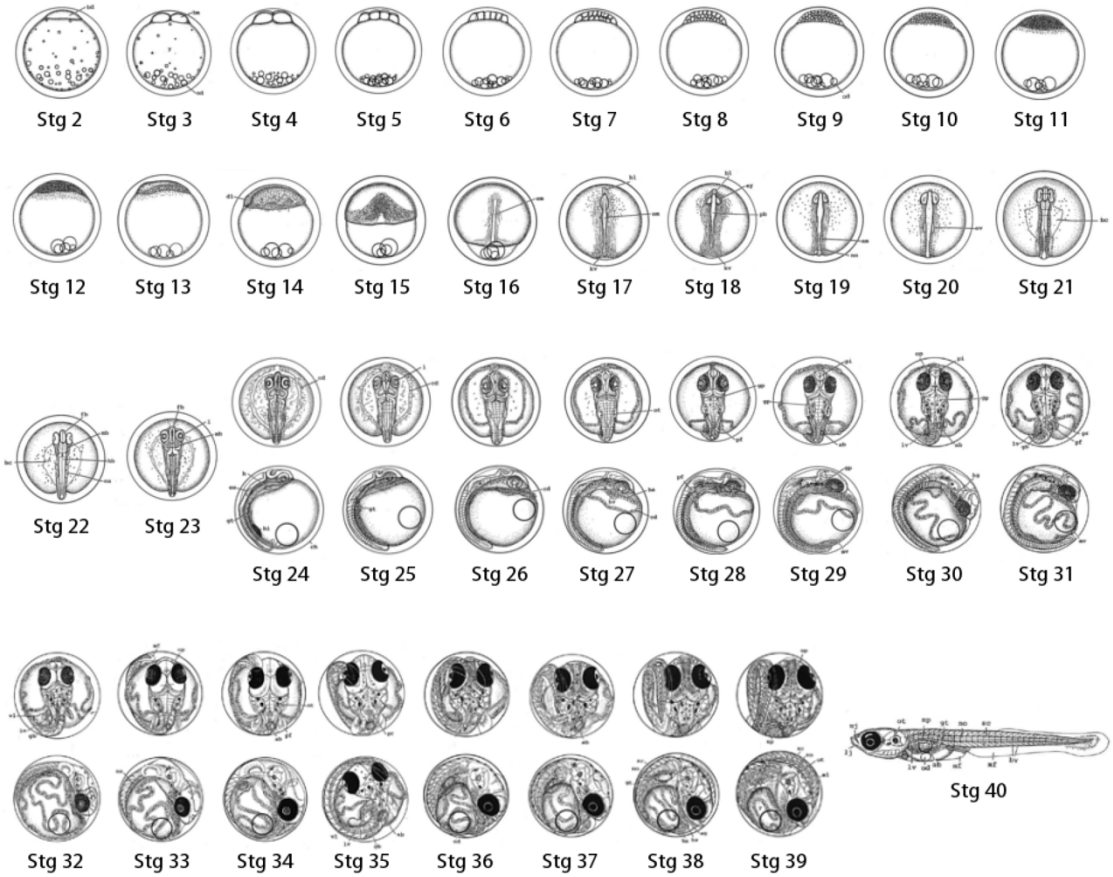

Figure 6. Medaka developmental stages. Graphic representation of the principal morphological characteristics of each developmental stage during the development of medaka (*Oryzias latipies*) (Adapted from Iwamatsu, 2004).

3D reconstruction of *yap1/yap1b* mutant embryos

Wild type, *yap1* single mutant and *yap1/yap1b* double mutant siblings at stage 17 were fixed with PFA 4% at 4°C for 2-3 days. Samples were washed extensively in PBS-0.2% Tween and stained with phalloidin Alexa-488 (Invitrogen) in PBS-0.2% Tween solution supplemented with 5% DMSO (1:50) overnight (o/n) at 4°C. After extensive washing steps with PBS-0.1% Tween, samples were stained with DAPI (1:1000), mounted in FluoroDish 35 mm plates (WPI) and imaged in a Leica SP5 microscope using a 20x multi-immersion objective. Embryos were imaged dorsoventrally taking images of 50 stacks of 3 µm-length each with a pixel size of 0.379 x 0.379 µm. Tridimensional models were acquired using Imaris 8. After imaging the embryos, each one of them was individually genotyped.

Whole-mount embryo immunostaining

Embryos collected from *yap1*$^{+/-}$;*yap1b*$^{+/-}$ adult fishes were fixed at stage 16 using 4% PFA. Fixed embryos were dechorionated with forceps. Embryos were washed with PBS-0.2% Tween, treated with cold acetone at −20 °C for 20 min, then incubated with freshly prepared blocking solution (10% fetal bovine serum in PBS-0.2% Tween) at room temperature (RT) for 2 h. The primary antibodies anti-active caspase-3 antibody (BD Biosciences, 559565) and anti-phospho-Histone H3 (Ser10) antibody (Millipore 06-570) were diluted 1:500 in blocking solution and embryos were incubated o/n at 4 °C. Embryos were then subsequently washed with PBS-0.2% Tween and incubated o/n at 4 °C in the dark with the Alexa Fluor TM 555 Goat anti-rabbit antibody (Invitrogen #A32727), diluted as well 1:500 in blocking solution. Finally, embryos were washed with PBS-0.2% Tween and incubated o/n at 4 °C with DAPI (Sigma) diluted 1:1000 in PBS-0.2% Tween. For imaging, embryos were embedded in 1% low-melting-point agarose and mounted in FluoroDish 35 mm plates. Confocal laser scanning microscopy was performed using a Zeiss LSM 880 microscope. Images were processed using ImageJ (Schindelin et al., 2012). For quantification of apoptotic and proliferative cells, masks were applied for both channels. The mask generated for the red channel was segmented using the Watershed algorithm. Only the regions marked with the primary antibody that also corresponded to nuclei with a 6-200 µm^2 area were considered to avoid debris.

Apoptotic and proliferative cells were counted on the embryo surface and extrapolated to the total number of nuclei (quantified as described above using the corresponding DAPI images). After imaging, embryos were genotyped by PCR to identify *yap1*/*yap1b*-related genotypes. To analyze whether experimental groups were significantly different, two-sided Student's t-tests were performed.

Analysis of cell movements during gastrulation

WT, *yap1* single mutant and *yap1/yap1b* double mutant siblings were injected at one-cell stage with H2B-GFP mRNA (Addgene, #53744) at a final concentration of 25 ng/µL. The embryos were incubated for 3 h at 28°C and o/n at 25°C. The most promising candidates were then selected the day after in a fluorescent binocular and dechorionated following a three-step protocol with minor modifications (S. R. Porazinski et al., 2010). First, embryos were rolled in sandpaper (2000 grit size, waterproof) to weaken their outer structure. Then, the embryos were incubated for 30 min at 28°C in pronase at 20 mg/ml. Finally, after several washing steps, embryos were incubated for 60 min in hatching enzyme at 28°C and transferred into a Petri dish with BSS 1x medium supplemented with penicillin-streptomycin and 1-heptanol 3.5 mM (Sigma) to block contractile rhythmical movements. Overnight movies (8-9 h) were acquired using a Leica SP5 microscope with a 20x objective. Frames with a pixel size of 0.189 x 0.189 μm^2 were taken every four minutes. Each frame, 2 confocal section separated 10 µm were acquired, maximum projected, and processed with an unsharp mask (radius sigma = 15 and mask weight = 0.60) and median filter (radius = 2.0). Manual cell tracking analysis was carried out using ImageJ (Schindelin et al., 2012). Alternatively, a more precise, semi-automatic cell tracking was also performed using TrackMate (Tinevez et al., 2017) (blob diameter = 7.9 and threshold = 0.23). The resulting data were analyzed using R. Cells tracked in less than 15 frames and/or localized initially near the midline were excluded. Lateral or midline cell trajectories were determined according to their central position with respect to the midline. Variance test and two-sided Student's t-tests were performed to estimate the statistical significance among the different experimental conditions.

RNA-seq

Library preparation

Individual wild type, *yap1* single mutant and *yap1/yap1b* double mutant embryos at stage 16 were homogenized in TRIzol (Ambion). Samples were centrifuged at full speed and the supernatant was transferred to a fresh tube. Chloroform was then added to split the RNA (upper aqueous phase) from the DNA fraction (lower phase). The DNA fraction was precipitated by adding glycogen and 100% ethanol and incubating it at RT for 20 min. This fraction was then centrifuged at maximum speed for 30 min at 4°C. After three washing steps using 75% ethanol, the DNA pellet was then resuspended in 30 µL of TE buffer. The RNA fraction was precipitated by adding RNA-grade glycogen (ThermoFisher Scientific) and isopropanol and following the same steps applied to the DNA fraction. The RNA pellet was resuspended in 12 µL of nuclease-free water. Each embryo was genotyped using its corresponding purified DNA fraction. The RNA samples were merged according to their genotype to generate from three to four biological replicates. Prior to library preparation, contaminating DNA remnants were degraded using the *TURBO DNA-free kit* (Ambion). Each RNA library was finally sequenced using an Illumina HiSeq 2500 system.

Downstream bioinformatic analysis

Reads were pre-processed trimming the Illumina universal adapters and the first 12 bases of each read to avoid k-mers using *Trimmomatic* (Bolger et al., 2014). Reads shorter than 50 bp and those with an average quality lower than 20 were filtered out (HEADCROP:12 MINLEN:50 AVGQUAL:20). Potential rRNA sequences were removed using *sortmerna* (Kopylova et al., 2012). Processed reads were then mapped against the last version of the medaka genome (ASM223467) using Hisat2 (D. Kim et al., 2019). Only reads with a high mapping quality (*samtools view -q 60*) were considered for further steps of the bioinformatics analysis. The software *htseq-count* was used to count the number of reads per gene (GTF from Ensembl version 99 was used as a reference). The subsequent analysis was performed using DEBrowser v1.14.2 (Kucukural et al., 2019). Genes with less than 10 reads on average were discarded (RowMeans < 10) and data were normalized following the relative log-expression (RLE) method. Potential batch

effects were removed using ComBat. Differential gene expression analysis was carried out using the R package DESeq2 (padj < 0.05; -log FC = 1; https://www.r-project.org/). GO Terms were analyzed using GProfiler (Raudvere et al., 2019). The lists of *yap1* and *yap1b* DamID peaks obtained previously (Vázquez-Marín et al., 2019) were concatenated and, after assigning the closest gene using *Bedtools*, they were compared to the list of downregulated genes in our bulk RNA-seq to identify which genes are potential direct binding targets for Yap1 and Yap1b. As the Ensembl version used for the RNA-seq analysis is more recent that the one used for the DamID-seq analysis (Ensembl version 89), those genes which may have changed their identifier were not considered for this analysis. The statistical significance for the comparison between control and identified overlapping DamID peaks was calculated applying a two-proportion Z-test.

Whole-mount in situ hybridization

cDNA from medaka embryos at stage 24 was used to amplify part of the coding sequence of medaka *no-tail* (ntl), *goosecoid* (gsc), *sox3*, *yap1* and *marcksl1b* genes. PCR products were cloned into pSC-A-amp/kan Strataclone plasmids (Agilent) to generate probes for whole-mount *in situ* hybridization (ISH) experiments (Table S1). Probes were synthesized using digoxigenin-11-UTP nucleotides (Roche) and the T3 or the T7 polymerase (Roche) depending on the insert orientation. ISH was performed following a previous protocol (Thisse & Thisse, 2008). Medaka embryos at stage 15, 16, 17 and 18 were fixed in 4% PFA for two days, dehydrated in methanol, and stored at −20 °C.

Fluorescent *in situ* hybridization (FISH) was performed on medaka embryos at stage 16 using specific probes for *marcksl1b*. We followed the same protocol as for ISH, with the following modifications from incubation with the anti-DIG antibody on: samples were first Incubated with blocking Buffer (2% Blocking Reagent from ROCHE in MABTween 1x) for 1 h, and then with anti-digoxigenin-POD antibody (11207733910 Roche, 1:150 in Blocking Buffer) for at least 2 h at RT. The embryos were then washed six times with PBS 0.1% Tween at RT and then o/n at 4 °C. Later, the embryos were washed again with PBS-0.1% Tween and three times with Borate buffer (100 mM Borate Buffer, 0.1%Tween), and stained with TSA amplification solution (50 µg/ml TSA Fluorescein 5 mg/ml in 100 mM Borate Buffer, 0.1%Tw, 2% DS, 0.003% H2O2) for 1h at RT in the dark. Finally,

embryos were incubated overnight at 4 °C with DAPI (Sigma) diluted 1:1000 in PBS-0.2% Tween. Stained embryos were mounted in FluoroDish plates as described previously. Confocal laser scanning microscopy was performed using a Zeiss LSM 880 microscope with a 40x objective. Only embryos that were mounted with their dorsal-anterior axis oriented in parallel to the cover glass bottom were used for the analysis. Maximum projection images were processed using ImageJ (Schindelin et al., 2012). A list of primers used to generate the RNA probes is provided in Table S1.

To quantified marcksl1b expression, mean gray values of the GFP channel were obtained from 56 µm2 regions of maximum projection images using ImageJ. To establish a correlation between m*arcksl1b* and cell density, we determined the centroid position of each nucleus using TrackMate, excluding the centroids that were closer than eight pixels and those nuclei at the border of the image. Then, we calculated the mean of the distance between the five closest neighbors for each nucleus. Based on the *marcksl1b* expression pattern, we distinguished two different areas; an active area which shows a specific expression pattern for *marcksl1b* and an inactive area in which cells are not expressing *marcksl1b*. We represented the XY position of the nuclei's centroids, with a circle or a triangle if they were localized in the active or the inactive area, respectively. The color gradient of each nucleus was dependent on the mean distance to its five closest neighbors. To analyze whether experimental groups were significantly different, two-sided Student's t-tests were performed.

mRNA Generation and injection

DNA plasmids containing *yap1::mcherry, utrophin::GFP* (Nicolás-Pérez et al., 2016), *paxillin::mKate* (Sidhaye & Norden, 2017) (Addgene 105974) *and lynTdTomato* were linearized with NotI and then transcribed using the mMESSAGE mMACHINE SP6 Kit (Ambion) to synthesize capped mRNA. RNA was injected into one-cell-stage embryos; *yap1::mcherry* (80 pg/embryo), *utrophin::GFP* (150 pg/embryo), *paxillin::mKate* (125 pg/embryo) and l*ynTdTomato* (100 pg/embryo). For the phenotypic rescue experiments of *yap1*-/-;*yap1b*-/- embryos with Paxillin, we injected 300 pg per embryo of *paxillin::mKate* mRNA.

Embryos injected with *utrophin*::GFP and paxillin::*mKate* or *lynTdTomato* mRNA were fixed in PFA 4% at stage 16 for two days. Fixed embryos were washed with PBS-0.1% Tween, dechorionated with forceps, and incubated overnight at 4 °C with DAPI (Sigma) diluted 1:1000 in PBS-0.1% Tween. Embryos were imaged with a Zeiss LSM 880 microscope (63x objective), taking images of a pixel size of 0.132 x 0.132 μm^2 and a voxel depth of 0.24 µm. Only embryos that were mounted with the dorsal-anterior axis oriented in parallel to the cover glass bottom were used for analysis. Imaged embryos were genotyped later to identify *yap1/yap1b*-related genotypes. Images were processed using ImageJ (Schindelin et al., 2012). For each image and channel, a maximum projection was generated. For XZ projections we used the Volume viewer plugin from ImageJ. To analyze the 3D morphology of the nuclei we applied first a Gaussian Blur 3D filter (X, Y and Z sigma value was set to 2.0) to the blue channel. Then, we segmented and created a 3D mask of these nuclei using plugin interactive watershed segmentation (SFC FIJI plugin 1.2.0). 3D nuclei reconstructions were performed by applying Reslice, without avoiding interpolation and 3D Viewer (v4.0.3) to DAPI signal channel. To obtain the geometrical and morphological parameters we used the plugins 3D Geometrical measure and 3D shape measure from ImageJ (v3.96.3). Downstream analyses were carried out using R. Nuclei smaller than 100 and bigger than 350 (volume unit) were excluded.

Focal adhesions and cell morphology quantifications were performed using ImageJ. To analyze focal adhesions, we first carried out a manual segmentation and then created a mask of paxillin::mKate signal. Then, we applied Skeletonize and measured the length of the segmented signal. To perform cell morphology analysis, we manually segmented utrophin::GFP signal, or LynTdTomato and utrophin::GFP merged signals, and measured cell area, compactness (ratio of cell area to the area of the circle having the same perimeter), and number of filopodia. Number of filopodia was defined as the number of elements which area is larger than 0.077 μm^2, as obtained from the subtraction between the total cell area and the area obtained when applying an opening morphological filter (element: disk, radius: 1.1 µm) (plugin MorphoLibJ 1.4.2.1) (Fig S1). To analyze whether experimental groups were significantly different, two-sided Student's t-tests were performed.

To generate *marcksl1b* Knockdown embryos we synthesized *marcksl1b* gRNA using the primers indicated in Table S1, and the mMachine T7 kit (Ambion). The obtained gRNAs were quantified using Qubit RNA BR Assay Kit (ThermoFisher). Then, 2 nL containing 3 ng of purified Cas13d protein and 250 pg of gRNA were injected in one-cell stage embryos. The depletion of marcksl1b were confirmed by qPCR (detailed in qPCR section).

Yolk extraction

Removal of yolk material was performed on medaka embryos at stage 15, using microcapillaries, to obtain a 30-40% reduction of embryo perimeter. Following a 2 h incubation, embryos were fixed with PFA 4% for two days to perform ISH of marcksl1b, as described in the previous section. Yap-active area was quantified using ImageJ (Schindelin et al., 2012). To analyze cell morphology and quantify cell density, yolk removal and fixation were also performed on embryos injected with *utrophin::GFP* mRNA. Fixed embryos were stained with DAPI and then imaged with a Zeiss LSM 880 microscope (objective 40x). Only embryos mounted in such a way that their dorsal-anterior axis was oriented in parallel to the cover glass bottom were used for the analysis. Maximum projection images were processed using ImageJ 65. For cell quantification, mask and Analyze Particle were applied for the DAPI channel. Only nuclei displaying an area bigger than 7.1 µm2 were considered, to avoid including cellular debris in the measurements. To follow Yap/Tead activation, yolk extraction and fixation were performed on embryos of the transgenic line tg(4xGTIIc:eGFP). GFP signal was quantified as described in the previous section for marcksl1b expression. To analyze whether experimental groups were significantly different, two-sided Student's t-tests were performed.

Drug treatments

Medaka embryos were dechorionated *in vivo* following a previous protocol (S. R. Porazinski et al., 2010) with minor modifications. First, embryos were rolled in sandpaper (2000 grit size, waterproof) to weaken their outer structure. Then, the embryos were incubated for 30 min at 28°C in pronase at 20 mg/ml. Finally, after several

washing steps, embryos were incubated for 60 min in hatching enzyme at 28°C and transferred into a Petri dish with BSS 1x medium. Embryos at stage 15 were incubated with DMSO, Rho Kinase Inhibitor III (555553, Merck) at 250 µM, Myosin II ATPase inhibitor (Blebbistatin, 203391, Merck) at 300 µM, tyrosin kinase inhibitor (Dasatinib, SML2589, Merck) at 150 µM, or Phosphatases types 1 and 2A inhibitor (Calyculin, C5552, Merck) at 0.7 µM dissolved in water for 2 h. Then embryos were fixed with PFA 4% for two days to perform ISH and FISH as described in the previous section. Embryos of the transgenic line tg(4xGTIIc:eGFP) were also treated with the above-mentioned drugs, and their GFP signal quantified as previously described. Embryos injected with utrophin::GFP and lynTdTomato mRNA were also treated with DMSO or Rho Kinase Inhibitor and fixed. Fixed embryos were then imaged with a Zeiss LSM 880 microscope and their nuclear morphology analyzed as indicated in the previous section. To analyze whether experimental groups were significantly different, two-sided Student's t-tests were performed.

Embryos compression

For each condition, batches of 25 medaka dechorionated embryos were subjected to confined compression using a Univert device, equipped with a customized compression chamber (CellScale, Waterloo, ON; Figure S9A). Embryos, placed in the compression chamber, already filled E3 medium (9 ml), were mechanically stimulated by a motorized vertical indentor up to the configured axial distance (Fig S9A). A rubber ring placed between the indentor piece and the samples' chamber controlled the compression fit and precision (± 1 µm) (Figure S9A). Embryo batches were compressed to 80% of their diameter, which corresponds to a uniaxial displacement of 250 µm, for a period of 20 min. Non-compressed control embryos were confined in parallel in E3 medium.

qPCR

To measure gene expression levels after compression, mRNA from medaka embryos was isolated using easy-BLUE Total RNA Extraction Kit (iNtRON Biotechnology, Inc. Korea). Then, cDNA retrotranscription was performed using the iScript cDNA Synthesis kit (Bio-Rad). Afterwards, the concentration was measured in a Qubit fluorometer. The

expression levels of *ctgfa*, *lats2*, *lamc1* and *marcksl1b* were quantified by RT-qPCR (CFX96 Touch Real-Time PCR Detection System), normalizing the results with the housekeeping gene *ef1a*. All qPCR reactions were performed in triplicate with SsoAdvanced Universal SYBR Green Supermix in a total volume of 10µL (Primers sequences listed in table S1). To analyze significant differences, two-sided Student's t-tests were performed.

Results

In the results shown Javier Vázquez Marín greatly contributed to the initial description of *yap* mutants' phenotype (Fig 7D-G and Fig 8), the acquisition of *in vivo* movies (movie S2, S3 and Fig S2), and the RNA-seq analysis (Fig 12, 13, 14 and Fig S3, S4, Table S2, SuppDatasets 1, 2 and 3). Jorge Corbacho contributed to the compression protocol and qPCR analysis (Fig 26C and 27C).

Yap paralogs are required for proper axis development in medaka

Gastrulation relies on extensive cellular rearrangements responsible to place the three germ layers in their correct topological position, while directing the formation of the embryo body axis (R. Keller, 2005). Previous work in different vertebrate species, including our work in medaka (Vázquez-Marín et al., 2019), hinted to a potential role for the mechanosensor Yap during axis development. To gain insight into the role of Yap family proteins in this process, we focused on the phenotypic consequences of mutating both *yap* paralogs, *yap1* and *yap1b* in gastrulating medaka embryos.

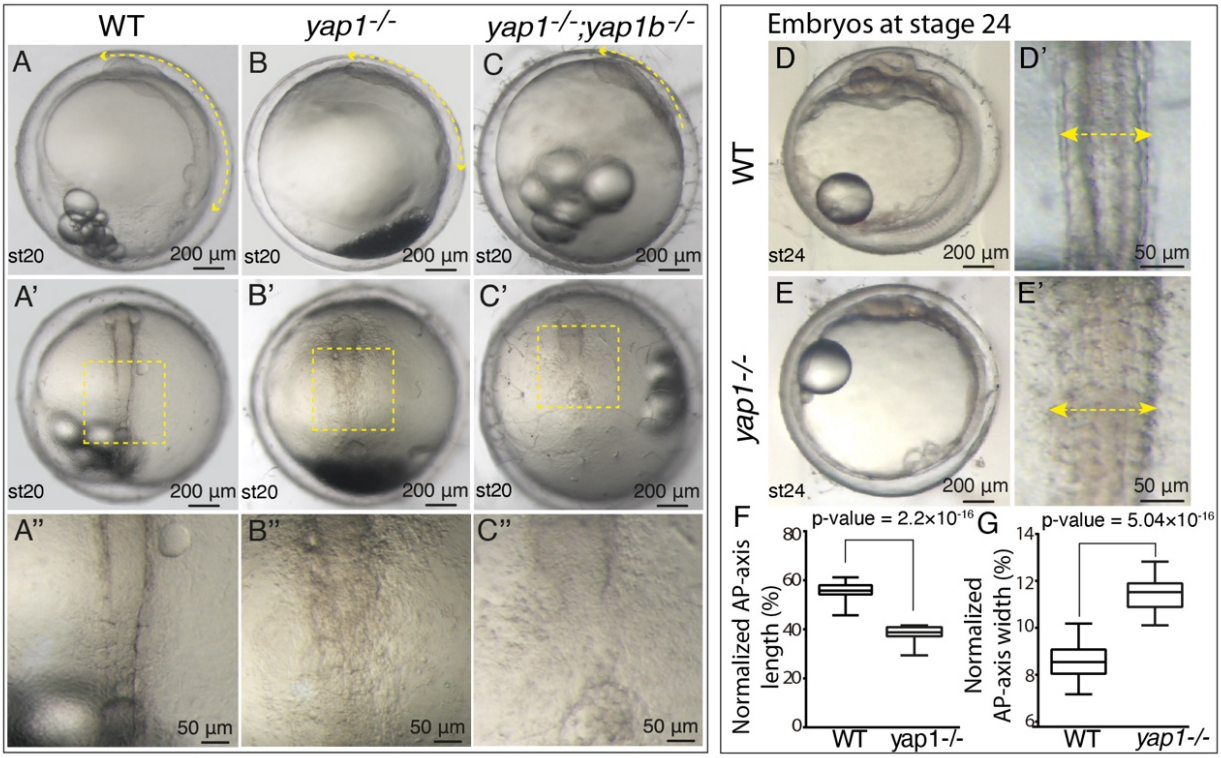

Figure 7. Analysis of yap mutants' phenotype. (A-C) Brightfield images of WT, *yap1*$^{-/-}$ and *yap1*$^{-/-}$;*yap1b*$^{-/-}$ embryos at stage 20 (post gastrulation stage) (A-C). Yellow double-headed arrows highlight the shortening and the widening of the A-P axis (A-C). A''- C'' correspond to the magnifications indicated with a yellow square in their corresponding A'- C' images. **(D, E)** Brightfield images of WT and *yap1*$^{-/-}$ embryos at stage 24. Yellow double-headed arrows highlight the shortening and the widening of the A-P axis (D-E). D', E' correspond to magnifications of the axis**. (F, G)** Quantification of the normalized length (F) and width (G) of WT and *yap1*$^{-/-}$ embryo A-P axis at stage 24. P-value < 0.0001 (F and G adapted from Javier Vázquez Marin's thesis)**.** Boxes represent the quartiles; the whiskers indicate the maximum and minimum values; points indicate independent embryos ($N^{embryos} \geq 4$). Two-sided Student's t-tests were performed to evaluate statistical significance. Scales bars are 200 µm (A-E and A'-C'), 50 µm (A''-C''and D'-E').

When we examined *yap1-/-* medaka embryos at stage 20 (hereinafter referred as 'single mutants'), we observed that somite formation was affected, and the anterior-posterior (A-P) axis was wider and shorter (Fig 7A, B). Despite these defects, the somitogenesis recovered, and the primary embryo axis (although still shorter and wider) was eventually formed in single mutant embryos at later stages (stage 24), as previously reported (S. Porazinski et al., 2015; Vázquez-Marín et al., 2019) (Fig 7D-E). Remarkably, *yap1-/-;yap1b-/-* double mutants (hereinafter *yap* double mutants) displayed much stronger developmental defects, as posterior axis assembly and somites were not apparent at stage 20 (Fig 7A, C). Moreover, *yap* double mutants did not survive after stage 23.

To further characterize the mutants' phenotype, we performed a DAPI and Phalloidin staining to visualize nuclei and filamentous actin during late gastrulation (stages 16-17) (Fig 8A-C).

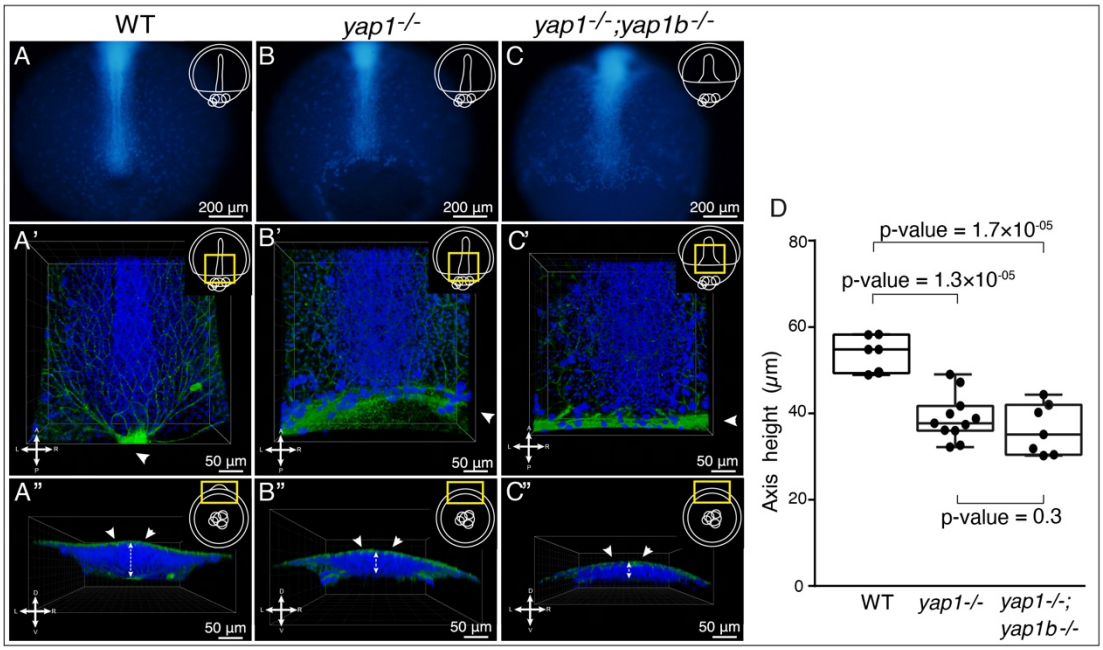

Figure 8. Defective axis assembly in yap mutants. (A-C) DAPI staining, in which nuclei are labeled in blue, were performed in WT, *yap1*$^{-/-}$ and *yap1*$^{-/-}$;*yap1b*$^{-/-}$ embryos fixed at stage 16-17 (late gastrula) (A, B and C). Whole embryos are shown under the fluorescent stereo microscope. DAPI and Phalloidin immunostained confocal images show the posterior axis of WT, *yap1*$^{-/-}$ and *yap1*$^{-/-}$;*yap1b*$^{-/-}$ embryos at stage 16-17 (nuclei in blue and filamentous actin in green) (A', B' and C'). XZ projections of the DAPI and Phalloidin immunostaining, showing the D-V height of the axis of WT, *yap1*$^{-/-}$ and *yap1*$^{-/-}$;*yap1b*$^{-/-}$ embryos (A'', B'' and C'') Embryos' orientations are indicated with a cross (A: anterior, L: left, R: right, P: posterior). Yellow rectangles in schematic embryo representations indicate the area depicted in each image. **(D)** Quantification of the D-V height of the axis (white arrows in A''-C'') in WT, *yap1*$^{-/-}$ and *yap1*$^{-/-}$;*yap1b*$^{-/-}$ embryos at stage 16-17. P-value < 0.0001**.** Boxes represent the quartiles; the whiskers indicate the maximum and minimum values; points indicate independent embryos ($N^{embryos} \geq 4$). Two-sided Student's t-tests were performed to evaluate statistical significance. Scales bars are 200 µm (A-C) and 50 µm (A''-C'' and A''-C'').

Confocal analysis followed by 3D reconstructions showed how, in WT embryos, A-P axis assembly becomes apparent and actin network concentrates at the epiboly front, particularly at the closing blastopore (Fig 8A-A'', 8D and Movie S1). In contrast, in *yap* single mutants, actin staining appeared more diluted at the delayed blastopore margin and a decreased density of cells at the midline was observed, confirmed by the measurements of D-V height of the axis (Fig 8B- B'', 8D and Movie S1). In agreement with our previous findings, *yap* double mutants completely fail to assemble their posterior part, displaying a significantly reduced dorso-ventral (D-V) accumulation of cells at the midline, and without an apparent definition of the presumptive neural plate and paraxial mesoderm masses (Fig 8C-C'', Fig 8D and Movie S1).

Yap has a crucial role in proliferation and cell survival (Huang et al., 2005; Yosefzon et al., 2018; Zanconato et al., 2016), and an increase in cell death in yap mutants has been reported after neurulation at stage 20-22 (S. Porazinski et al., 2015; Vázquez-Marín et al., 2019). Therefore, we evaluated if a possible explanation for the observed phenotype was a change in cell death and proliferation rates in *yap* double mutants during gastrulation. To this end, we quantified the number of apoptotic and proliferative cells labeled by caspase 3 and pH3, respectively, in WT and *yap* double mutants in late gastrulation embryos at stage 16 (Fig 9A-D).

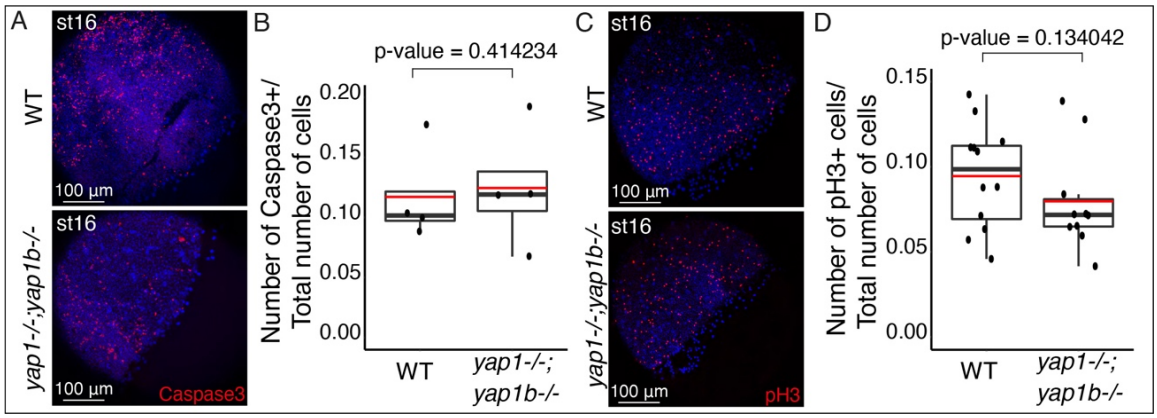

Figure 9. Analysis of cell death and proliferation rates in yap double mutant embryos. (A) Confocal images show Caspase 3+ cells in red and DAPI in blue in WT and *yap1*$^{-/-}$;*yap1b*$^{-/-}$. **(B)** Quantification of caspase 3-positive cells per total number of cells in WT and *yap1*$^{-/-}$;*yap1b*$^{-/-}$ embryos. P-value = 0.414234. **(C)** Confocal images show pH3+ cells in red and DAPI in blue in WT and *yap1*$^{-/-}$;*yap1b*$^{-/-}$. **(D)** Quantification of pH3+ cells per total number of cells in WT and *yap1*$^{-/-}$;*yap1b*$^{-/-}$ embryos. P-value = 0.134042. Boxes represent the quartiles; the whiskers indicate the maximum and minimum values; points indicate independent embryos ($N^{embryos} \geq 4$). Two-sided Student's t-tests were performed to evaluate statistical significance. Scales bars are 100 µm (A, C).

We did not observe significant differences in cell death nor proliferation density between WT and *yap* double mutant embryos at these earlier stages of development (Fig 9A-D). Given that variations in cell death and proliferation could be ruled out as responsible for the gastrulation defects, we decided to explore alternative mechanisms behind the axis assembly failure.

Yap is needed for a correct cell migration during gastrulation

In teleost embryos, axis assembly is achieved by dorsal migration and lateral intercalation of the precursors at the midline (Solnica-Krezel & Sepich, 2012). Since we observed a clear failure in midline cell stacking in our *yap* mutants, we asked ourselves if directed cell migration was altered. To assess that, we analyzed cell trajectories during gastrulation using live imaging in medaka embryos. In WT embryos, cells move dorsally from the lateral regions towards the central axis in a straight manner (Fig S2A and Movie S2). *Yap* single mutants seem to display lower accuracy in their directionality and cells are slightly delayed when reaching the embryo axis (Fig S2B and Movie S2). Displacement defects are markedly accentuated in *yap* double mutant embryos, where many cells display abnormal trajectories and deficient migration towards the midline (Fig S2C and Movie S2).

To further confirm these observations, we performed a high throughput cell-tracking analysis to measure the main parameters involved in directed migration (Fig 10A-D). First, we measured cell displacement, which quantifies how much a cell moves from its start point (Fig 10A), and represented this parameter with a color gradient (Fig 10E, F). We could observe that unlike in WT embryos, long-displacing cells (i.e. red and yellow trajectories) were rarely detected in *yap* double mutants, whereas short-displacing cells (i.e. blue and green trajectories) predominate (Fig 10E, F). The statistical analysis of these measurements confirmed our observations, as displacement mean values were significantly lower in *yap* double mutants compared to WT embryos (Fig 10G). The second parameter we evaluated was the migratory persistence of cells, which quantifies how long a cell keeps the same direction (Fig 10B). This analysis revealed that the migratory persistence of *yap* mutant cells is significantly reduced compared to WT cells (Fig 10H). Finally, we also measured the cell trajectory length (Fig 10C) and the mean velocity (Fig 10D). Similarly to the previous parameters, we could clearly observe that WT cells move faster and through longer tracks than *yap* mutant cells (Fig 10I, J).

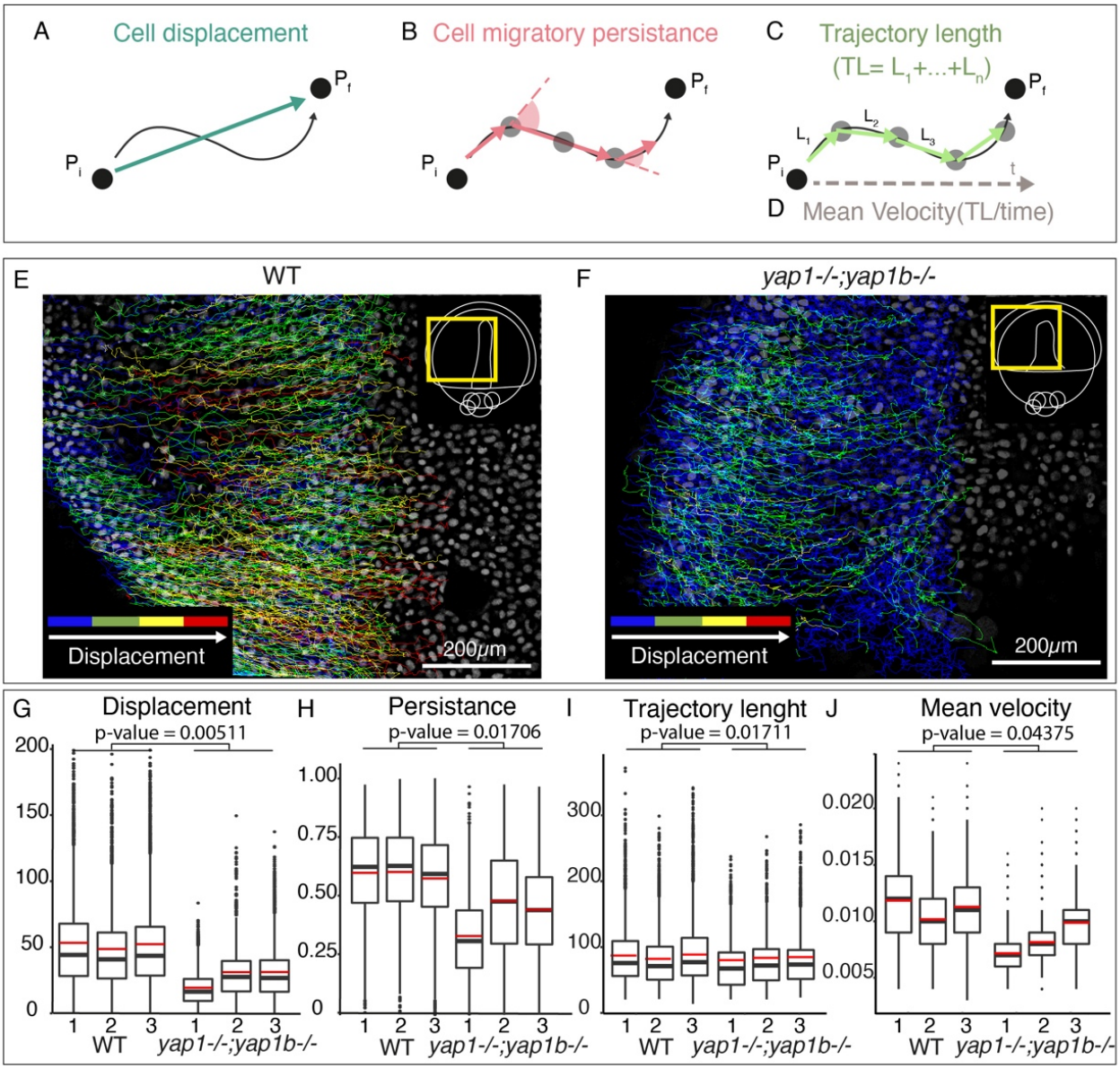

Figure 10. Defective directed cell migration in gastrulating yap mutant embryos. (A-D) Schematic representation of the parameters quantified in the cell-tracking analysis**.** Cell displacement (in blue) is the distance between the start and end position of a cell (A). Cell migratory persistence (in pink) measures for how long a cell keeps the same direction of movement (B). Cell trajectory length (in green) represents the sum of every cell displacement that occurs between two consecutive time points (C). Cell mean velocity (in brown) measures the distance between two cells' positions divided by the time difference (D). Black points represent a cell. Gray points represent the positions that a cell takes through the different time points during its migration. P_i: initial position. P_f: final position. TL: trajectory length. L: length. **(E-F)** Total individual cell migratory tracks over 8 h in WT and *yap1*$^{-/-}$*;yap1b*$^{-/-}$ embryos. The color code of the trajectory lines indicates the cells' displacement. Displacement values were represented as: Blue = 20-50; Green = 50-80; Yellow = 80-130; Red > 130. Yellow rectangles in schematic embryo representations indicate the area depicted in each image. **(G)** Quantification of cell displacement in WT and *yap1*$^{-/-}$*;yap1b*$^{-/-}$ embryos. P-value = 0.005111. **(H)** Quantification of cell migratory persistence in WT and *yap1*$^{-/-}$*;yap1b*$^{-/-}$ embryos. P-value = 0.01706. **(I)** Quantification of cell trajectory length. P-value = 0.01711. **(J)** Quantification of the cell mean velocity in WT and *yap1*$^{-/-}$*;yap1b*$^{-/-}$ embryos. P-value = 0.04375. Boxes represent the quartiles; the whiskers indicate the maximum and minimum values. Red and black lines indicate the median and the mean, respectively. To analyze whether experimental groups were significantly different, a variance test followed by a two-sided Student's t tests were performed on the means of WT and *yap1*$^{-/-}$*;yap1b*$^{-/-}$ embryos ($N^{embryos}$ = 3, n^{cells} ≥1391). Scale bars are 200 µm (E-F).

However, when we analyzed convergent and extension movements of cells at the midline, these migratory parameters were not significantly altered. Only the displacement of *yap* mutant cells is slightly reduced, which might be explained by the fact that the mutants have a shorter embryo axis (Fig 11).

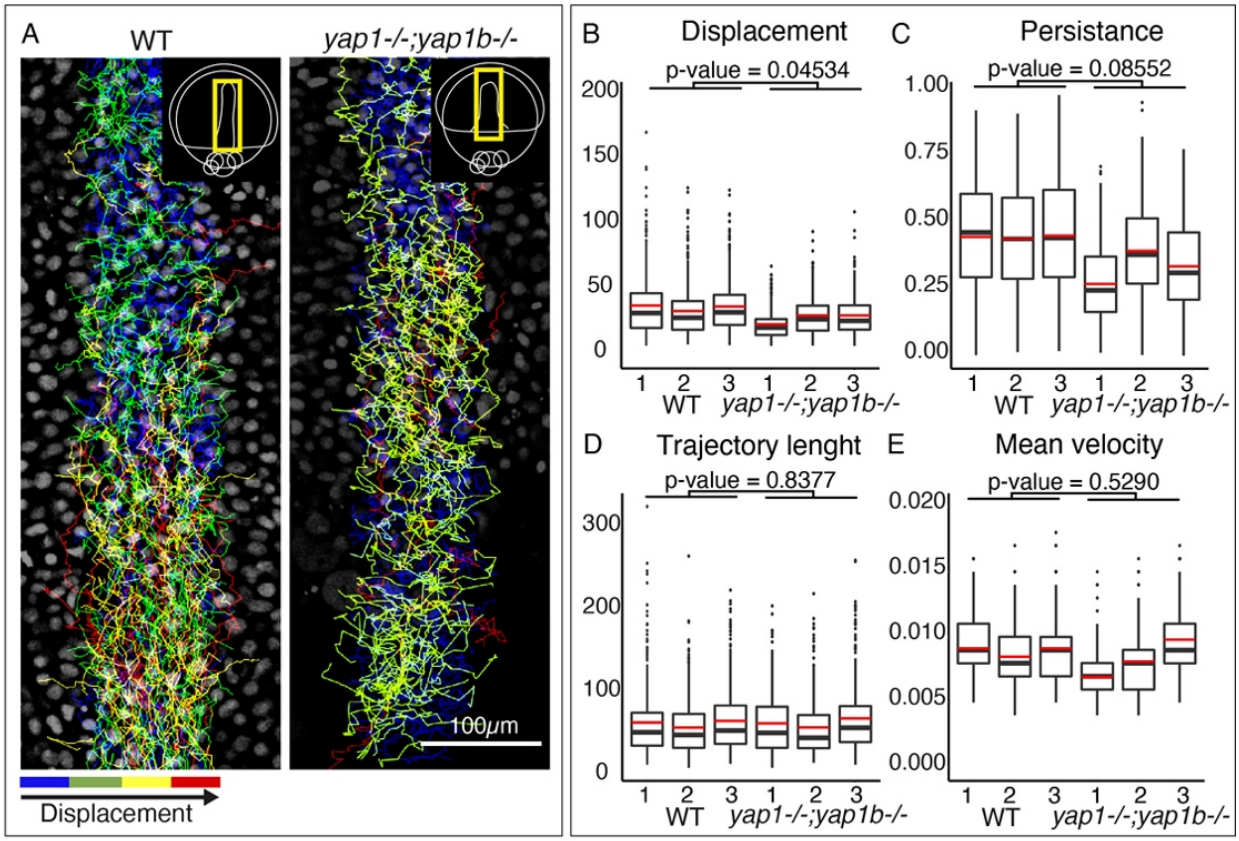

Figure 11. Midline cell migration in gastrulating WT and *yap* mutant embryos. (A) Total individual cell migratory tracks over 8 h in the midline of WT and *yap1*$^{-/-}$;*yap1b*$^{-/-}$ embryos. The color code of the trajectory lines indicates the cells' displacement (distance between the start and end position of a cell). Displacement values were represented as: Blue = 10-20; Green = 20-40; Yellow = 40-60; Red > 60. Yellow rectangles in schematic embryo representations indicate the area depicted in each image. **(B)** Quantification of cell displacement in WT and *yap1*$^{-/-}$;*yap1b*$^{-/-}$ embryos. P-value = 0.04534. **(C)** Quantification of cell migratory persistence, measuring for how long a cell keeps the same direction of movement, in WT and *yap1*$^{-/-}$;*yap1b*$^{-/-}$ embryos. P-value 0.08552. **(D)** Quantification of cell trajectory length, measuring the total length of a cell trajectory P-value = 0.8377. **(E)** Quantification of the cell mean velocity, measuring distance between two cells' positions divided by the time difference, in WT and *yap1*$^{-/-}$;*yap1b*$^{-/-}$ embryos. P-value = 0.5290. Boxes represent the quartiles; the whiskers indicate the maximum and minimum values. Red and black lines indicate the median and the mean, respectively. To analyze whether experimental groups were significantly different, a variance test followed by a two-sided Student's t tests were performed on the means of WT and *yap1*$^{-/-}$;*yap1b*$^{-/-}$ embryos ($N^{embryos}$ = 3, n^{cells} ≥ 271). Scale bars are 100 µm(A).

Taken together, these results indicate that Yap proteins play an essential role in direct cell migration in gastrulating embryos, specifically of dorsal cells converging to the midline.

Yap transcriptional programs primarily regulate cytoskeleton organization and cell adhesion components

Diverse molecular cues have been shown to direct polarized cell movements during gastrulation, such as cell-to-cell adhesion, interaction with the ECM, or chemotaxis (Solnica-Krezel & Sepich, 2012). On the other hand, Yap proteins have been shown to activate context-dependent transcriptional programs (Zanconato et al., 2015; Zhao et al., 2008). Therefore, in order to get a complete picture on how Yap might be directing cell trajectories, we performed a comparative RNA-seq analysis of WT, *yap* single and double mutant embryos at mid-late gastrulae stage (stage 16) (Fig 12A, B). Using this approach, we identified 717 and 1178 differentially expressed genes (DEGs) in *yap* single and double mutants compared to WT embryos, respectively (Fig 12A, B, Supplementary dataset 1). Principal components analysis (PCA) of the obtained results showed differential clustering of WT samples vs *yap* single and double mutants (Fig 12C), supporting our previous finding that both *yap1* and *yap1b* control very similar transcriptional programs (Vázquez-Marín et al., 2019). For that reason, we focused further analyses on *yap* double mutants most severe phenotype.

To understand the mechanisms underlying Yap activity, we next studied Gene Ontology (GO) terms enrichment in the DEGs in *yap* double mutants *vs* WT (Fig 12D-H). We explored four different GO categories: molecular function, cellular component, biological process and KEGG pathway. In the molecular function category, we identified integrin binding as the most significantly enriched GO term, followed by others such as acting binding or cell adhesion (Fig 12D). Very consistent results were also obtained for the remaining GO categories (Fig 12F-H). Thus, significantly enriched GOs terms identified in *yap* double mutants were related to cell-ECM adhesion (i.e. focal adhesion (FA) or collagen-containing ECM), Hippo signaling, and actin cytoskeleton regulation/organization (Fig 12D-H; Supplementary data set 2).

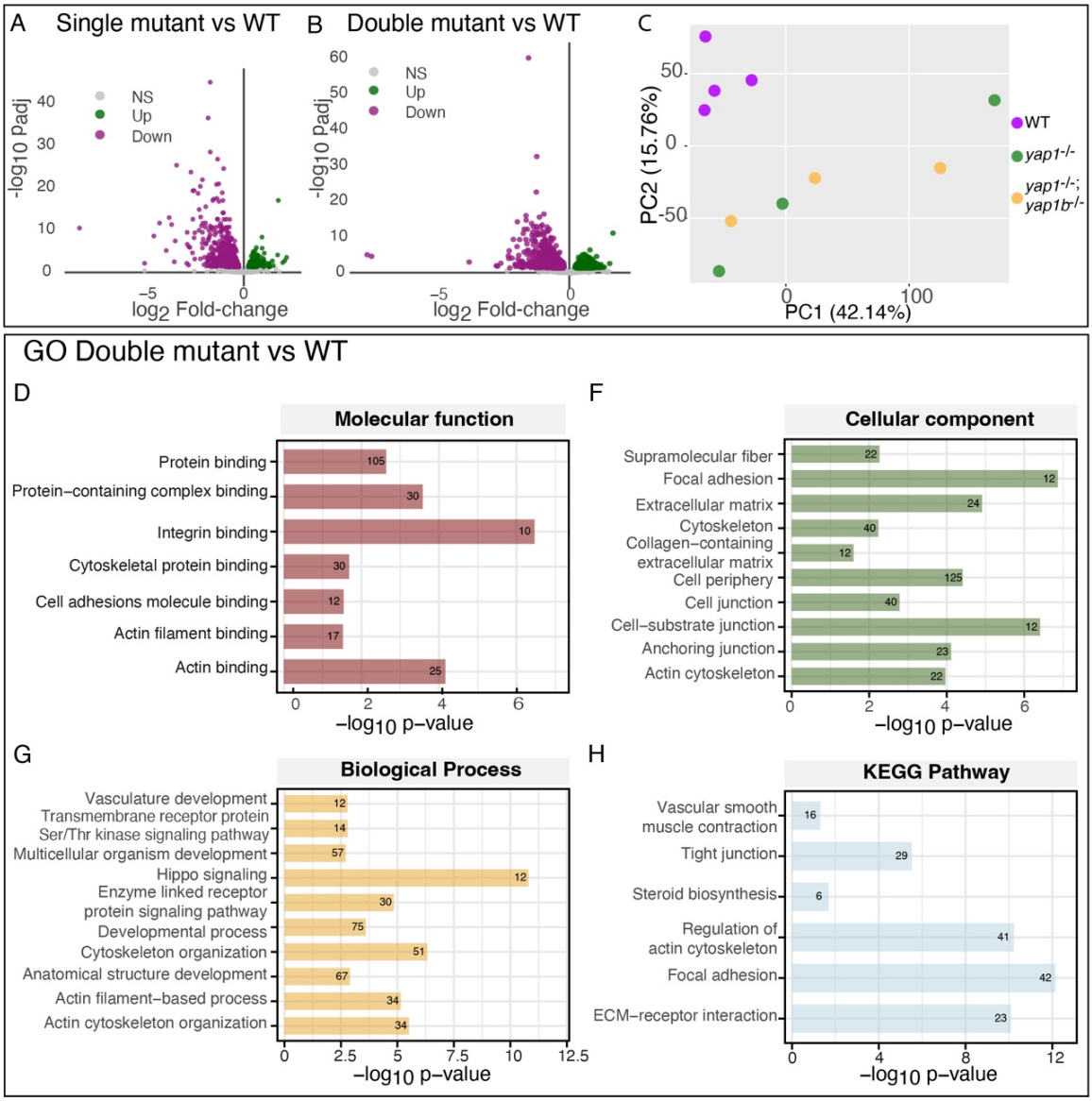

Figure 12. Characterization of Yap-dependent transcriptional programs. (A-B) Volcano plot graphs showing differentially expressed genes (DEGs) between WT to *yap1*$^{-/-}$ embryos (A) and WT to *yap1*$^{-/-}$;*yap1b*$^{-/-}$ embryos (B). Gray dots: no differentially expressed genes; Green dots: up-regulated genes in *yap1*$^{-/-}$;*yap1b*$^{-/-}$; Magenta dots: down-regulated genes in *yap1*$^{-/-}$;*yap1b*$^{-/-}$. Differential gene expression analysis was carried out using the R package DESeq2 (padj < 0.05; -log FC = 1). **(C)** PCA graph showing the RNA-seq data variability between WT, *yap1*$^{-/-}$, and *yap1*$^{-/-}$;*yap1b*$^{-/-}$ embryos. **(D-H)** Gene Ontology (GO) enrichment of the DEGs in *yap1*$^{-/-}$;*yap1b*$^{-/-}$ embryos compared with WT, classified in molecular function (D), cellular component (F), biological processes (G) and KEGG Pathway (H).

Similar GO enrichments were obtained when DEGs between yap single mutants *vs* WT were considered (Fig S3A-C). These data indicate that Yap paralogs primarily regulate the expression of actomyosin cytoskeleton and ECM-cell adhesion components (Table S2; Supplementary dataset 2).

Cellular rearrangements during gastrulation are often coordinated with lineage restriction and germ layers specification. To verify whether cell fate is compromised in *yap* mutants, we examined in more detail our RNA-seq datasets, which in principle did not yield significantly enriched GO terms consistent with that hypothesis (Fig 12D-H and S3A-C). For further confirmation, we checked the expression of a battery of 10 conserved specifiers of each germ layer. No significant differences were observed for key mesoderm, endoderm, and neuroectoderm markers when their expression was compared between *yap* mutant and WT embryos (Fig 13A). The only genes that appeared significantly downregulated correspond to early non-neural ectoderm (i.e., epidermal) specifiers (Fig 13A). To confirm these observations, we compared the expression patterns of a mesoendodermal marker, *no-tail* (*ntl*), an endodermal marker, *goosecoid* (*gsc*), and an ectodermal marker, *sox3* (Fig 13B) by in situ hybridization. In agreement with our RNA-seq data, these three germ-layer markers did not appear down-regulated in *yap* mutants. However, their expression patterns appeared wider in *yap* mutants, which suggests a failure in cell convergence, in line with the defective migration of cells that we observed (Fig 13B).

A

Neuroectoderm markers

Gene name	P_{adj}
sox2	0.1307
tfap2a	0.2181
prdm1a	0.8668
chrd	0.2500
otx2b	0.8185

Non-neuroectoderm markers

Gene name	P_{adj}
dlx3b	$1.59 \cdot 10^{-5}$
gata2a	$7.27 \cdot 10^{-13}$
tp63	$4.28 \cdot 10^{-10}$
foxi1	0.0081
bmp2b	0.0520

Mesoderm markers

Gene name	P_{adj}
tbxta	0.6032
wnt8a	0.0223
aldh1a2	0.0663
cdx4	0.1340
gsc	0.6336
gata5	0.7235
pcdh8	0.4956
shha	0.7747
tbx16	0.2520
pax2a	0.5571

Endoderm markers

Gene name	P_{adj}
sox17	0.9305
sox32	0.3822
foxa2	0.5293
foxd3	0.7692
etv5a	0.5432
cyp26a1	0.8562
eml2	0.0524
lmo4a	0.5431
ackr3a	0.3958
prex1	0.5863

B

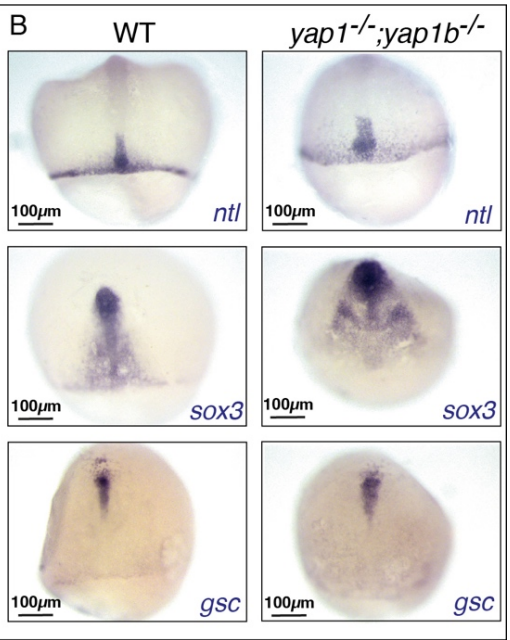

Figure 13. Cell fate acquisition is not affected in *yap* mutant embryos. (A) Differential expression of the 10 most conserved markers of each germ layer in *yap*$^{-/-}$;*yap1b*$^{-/-}$ compared to WT embryos. Adjusted p-values are shown. Red indicates significantly down-expressed genes in *yap1*$^{-/-}$;*yap1b*$^{-/-}$ embryos compared with WT; Green indicates significantly up-expressed genes in *yap1*$^{-/-}$;*yap1b*$^{-/-}$ embryos compared with WT. **(B)** *ISH* analysis of the expression of *ntl* (mesodermal marker), *sox3* (ectodermal marker) and *gsc* (endodermal marker) in WT and *yap1*$^{-/-}$ and *yap1*$^{-/-}$embryos at stg 16. Scale bars = 100 µm.

Taken together, these analyses indicate that what is behind the cell migration defects is a failure in the activation of the genetic program controlling cytoskeleton reorganization and cell adhesion, rather than a general problem in cell fate acquisition.

To gain further insight into the genetic program controlled by Yap proteins, we compared our RNA-seq data with DamID-seq results we previously obtained in stage 16 medaka embryos (Vázquez-Marín et al., 2019). Using the DamID-seq technique, we generated maps of chromatin occupancy for Yap1 and Yap1b in gastrulating embryos. Then, by cross-comparing genes neighboring Yap paralogs binding sites with our list of DEGs, we could determine which of these genes are potential direct targets (i.e. genes downregulated in *yap* double mutants in which Yap binds to nearby regulatory regions according to our DamID-seq results). We observed that a significantly high percentage of these DEGs are direct targets of Yap1/Yap1b (Fig 14A), and that these genes have a very similar list of associated enriched GOs terms as the entire set of DEGs (Supplementary dataset 2).

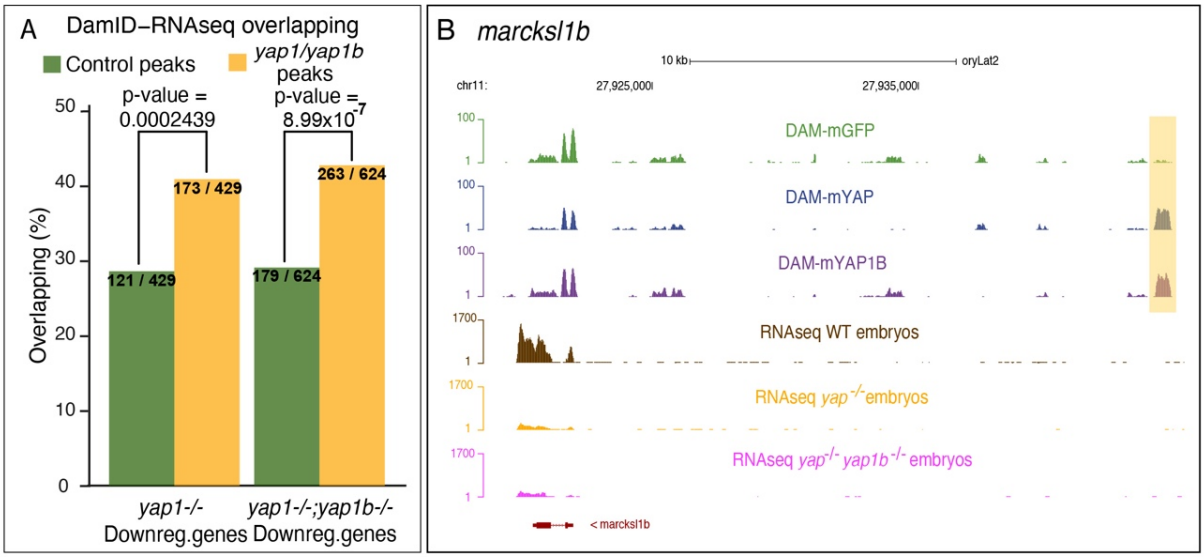

Figure 14. Direct downstream genes of Yap1/Yap1b. (A) Quantification of the overlap between genes associated to regions targeted by Yap1/Yap1b, as determined by DamID-seq (Vazquez-Marin et al., 2019), and DEGs between WT and *yap1*$^{-/-}$ (P-value = 0.0002439) or WT and *yap1*$^{-/-}$;*yap1b*$^{-/-}$ (P-value = 8.99×10^{-7}) embryos. $N^{embryos} = 3$, the statistical significance of the differences between control and Yap1/Yap1b targeted regions was calculated applying a two-proportion Z-test. **(B)** Overview of Yap1 and Yap1b DamID-seq tracks (Vazquez-Marin et al., 2019), as well as RNA-seq profiling of WT and *yap* single and double mutants for *marcksl1b*.

Importantly, we could confirm within them relevant regulators of the cytoskeleton, such as *marcksl1b*; structural ECM encoding genes, such as *lamc1*; well-known Yap targets such as *ccn1/cyr61*; and Yap regulators such as *lats2* and *src* among the targeted genes (Fig 14B, S4 and Supplementary dataset 2).

In order to explore if the inhibition of the direct target *marcksl1b* results in gastrulation defects similar to those observed in *yap* mutants, we took advantage of the CRISPR/Cas13d tool. This approach allows the specific and efficient targeting of mRNAs in different species, including medaka (Kushawah et al., 2020). Knockdown of *marcksl1b* using Cas13d together with specific gRNAs resulted in an efficient depletion of its mRNA in 26% of the injected embryos (Fig S5A-B). These *marcksl1b* depleted embryos displayed a mild phenotype, including delayed development and epiboly (Fig S5C). However, unlike *yap* double mutants, the A-P axis was correctly formed in all of them (Fig 7C, S5C). This experiment strengthens the idea that yap mutants' phenotype is the result of a failure in the activation of a broad gene program rather than a single downstream effector. This complex program entails not only cytoskeleton remodelers but also ECM, and cell adhesion components.

Yap is active in migratory cells converging to the midline

Cell migration depends on actin polymerization at the leading edge to drive protrusions that adhere to the substrate through FAs (Shellard & Mayor, 2020). Our observation that Yap activates the transcriptional programs controlling cytoskeleton and FA components suggests that its activity may be required in migratory cells. To confirm this point, we checked the spatiotemporal dynamics of Yap activation by following both the transcriptional activity of a Tead sensor, and the expression of *marcksl1b,* a *bona fide* Yap target identified in our DamID-seq and RNA-seq analyses (Vázquez-Marín et al., 2019). Tead co-activators interact with Yap proteins acting as main mediators of their transcriptional response (Stein et al., 2015; Vázquez-Marín et al., 2019; Zanconato et al., 2015; Zhao et al., 2008). To monitor Yap activation, we generated a new medaka transgenic line in which the Tead-responsive *4xGTIIC* enhancer, previously tested in zebrafish, was coupled to GFP (*4xGTIIC::GFP*) (Mahoney et al., 2005; Miesfeld et al., 2015). To validate this transgenic line, we first checked that the GFP signal was undetectable in yap mutants (Fig S6A). Then, by injecting *yap1* mRNA fused to the mCherry reporter gene (*yap1::mCherry*), we confirmed that the cells with higher levels of nuclear Yap::mCherry are displaying higher intensity for the Tead reporter signal (Fig S6B).

These results corroborate that the *4xGTIIC::GFP* transgenic line responds specifically to Yap signaling. Using this tool, we could then follow *in vivo* the dynamics of Yap activation during gastrulation by live confocal imaging (Movie S3). Interestingly, we observed that Yap is active in cells migrating towards the midline, rather than in the midline itself, where cell density is higher (Movie S3 and Fig 15A). To validate these observations, we also examined the expression pattern of *marcksl1b* by *in situ* hybridization. Marcksl1b is a protein involved in cell motility, as it regulates actin cytoskeleton dynamics as well as filopodium and lamellipodium formation (El Amri et al., 2018). Matching our observations with the Tead reporter line, we saw that in gastrulating embryos, *marcksl1b* is expressed mainly in lateral cells (Fig 15B). As expected, we could confirm that *marcksl1b* expression is largely decreased in *yap1* mutant embryos (Fig S6C).

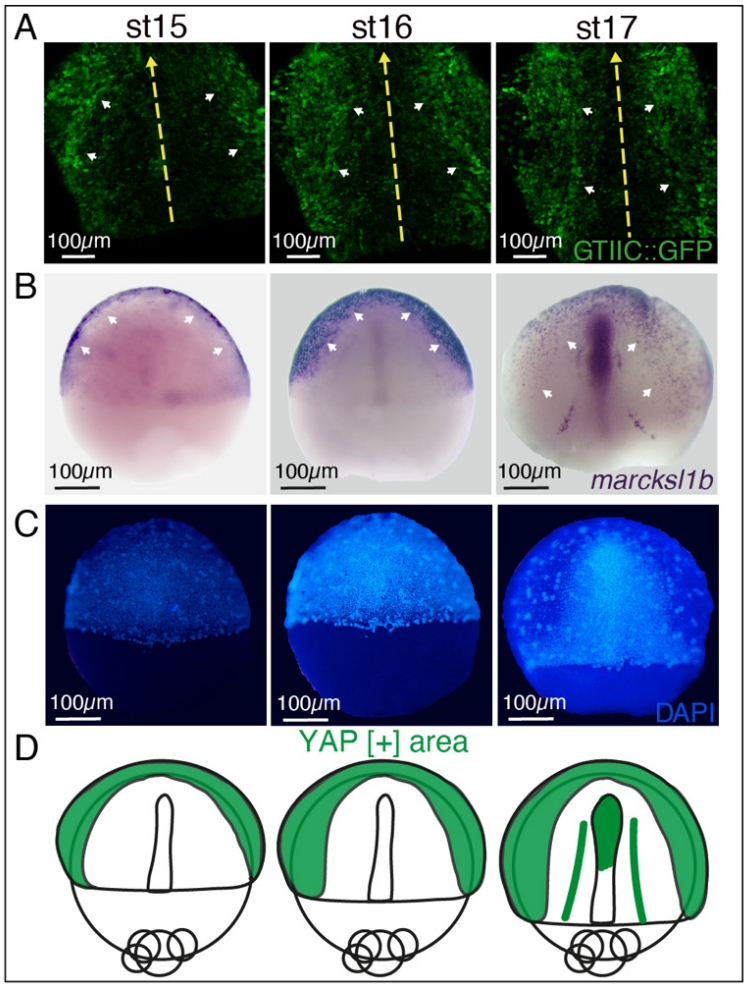

Figure 15. Yap activation in migratory precursors. (A) Still images from the confocal time-lapse analysis (movie S3) of transgenic embryos for the Tead/Yap sensor *GTIIC::GFP* at stages 15, 16 and 17. White arrowheads point to the GFP-positive cells. Yellow arrows indicate A-P axis **(B)** ISH analysis of the expression of *marcksl1b* in WT embryos at 15, 16 and 17. White arrowheads point to the cells expressing *marcksl1b*. **(C)** DAPI staining of the embryos in B. **(D)** Schematic representation of the expression of *marcksl1b* (Yap activation area) in green. Scale bars are 100 µm (A-C).

These results indicate that during gastrulation, Yap is specifically active in cells that are moving towards the midline, while inactive in the more compact cells forming the embryo axis (Fig 15C, D). Thus, we concluded that the migration defects observed specifically in dorsally-convergent yap mutant cells are consistent with the absence of Yap activation in these migratory cells.

Yap activity is inhibited by cell density

In agreement with our previous findings (Vázquez-Marín et al., 2019), we confirmed that *yap1* is ubiquitously expressed at early gastrula (stage 15), and that as gastrulation progresses its expression is enriched at the condensed axis (Fig 16).

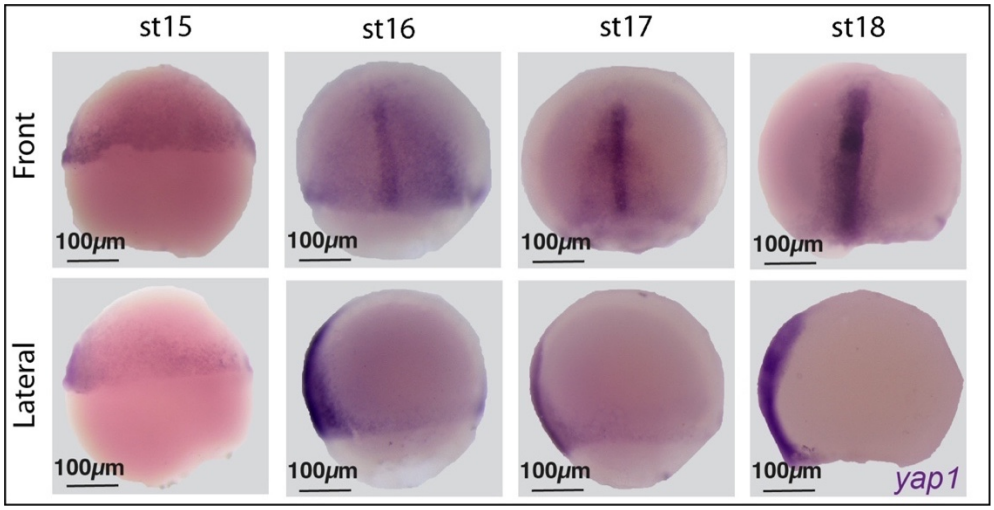

Figure 16. *yap1* expression pattern. Whole mount *ISH* showing *yap1* expression at stages 15, 16, 17 and 18 in medaka embryos. Front and lateral images are shown. Scale bars 100 µm.

This discrepancy between *yap* expression and Yap activation indicates that Yap signaling inhibition depends on post-transcriptional regulation. It has been described that Yap activity can be directly inhibited by cell density (Varelas et al., 2010; Zhao et al., 2007). To assess whether an anti-correlation between Yap activation and cell compaction was also significant in the gastrulation context, we examined density maps in relation to *marcksl1b* expression. We chose a region where active Yap became inactive, based on the *marcksl1b* expression pattern, and plot the centroids' position of the nuclei within this area (Fig 17 A-B). We could determine that the distance between neighbors is significantly higher (lower cell density) in Yap-active areas than in Yap-inactive areas (Fig 17C), suggesting that cell density may act as a modulator of Yap activity also during gastrulation.

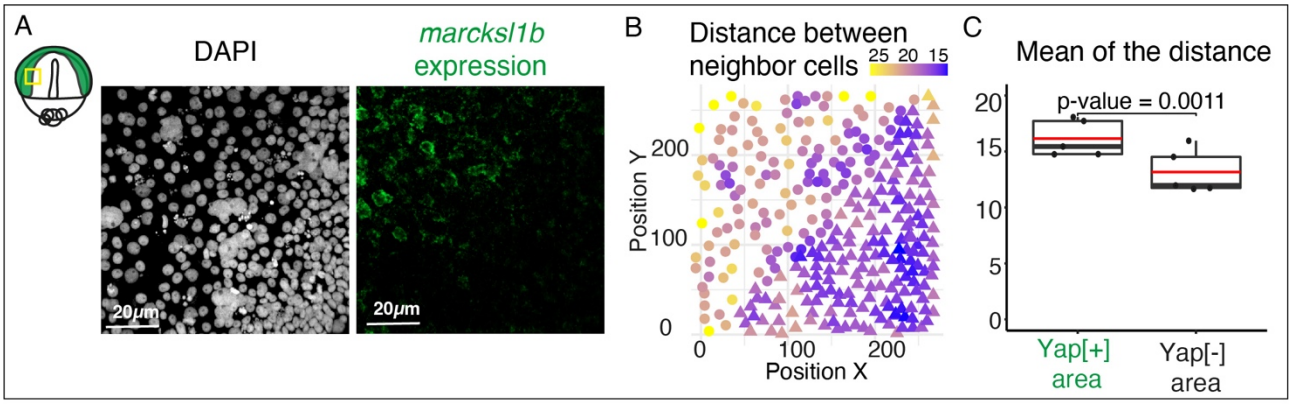

Figure 17. Anti-correlation between Yap activation and cell compaction. (A-B) Confocal image of *marcksl1b* fluorescent ISH stained with DAPI at the Yap activation margin in stage 16 embryos (A) and its corresponding cell density analysis (B). The position of the region considered in (A) is indicated with a yellow rectangle in the schematic stage 16 embryo, in which Yap activation is indicated in green. The XY position of the nuclei's centroids were represented. Circle: nuclei localized in a *marcksl1b* positive area; Triangle nuclei localized in a *marcksl1b* negative area. The color gradient refers to the mean of the distance between a cell and its five closest nuclei (B). **(C)** Quantification of the mean distance between nuclei in the *marcksl1b*-positive area (Yap active) and in the *marcksl1b*-negative area (Yap inactive). P-value = 0.0011. Boxes represent quartiles; whiskers indicate maximum minimum values; points indicate independent embryos ($N^{embryos} \geq 4$). Two-sided Student's t-tests were performed to evaluate statistical significances. Scales bars are 20 µm.

To further explore this hypothesis, we developed a method to increase cell density by extracting yolk material from 50% Epiboly WT embryos using microcapillaries (Fig 18A). This approach resulted in an average reduction of 40% of the embryo perimeter that was accompanied by a significant increase of the inner-mass cell density (~30 cells more per 100 µm^2) (Fig 18B-E). Dorsal migratory cells of yolk-reduced embryos display rounder shapes and reduced protrusions when compared to control embryo cells (Fig 18D). Interestingly, this increase in cell density and cell shape changes observed in the yolk-reduced embryos, correlated with a decrease in Yap activity, evidenced by a lower *marcksl1b* expression and Yap/Tead sensor activation (Fig 18C, F-G).

Altogether, these findings suggest that cell density acts as a negative regulator of Yap activity in midline regions of gastrulating embryos.

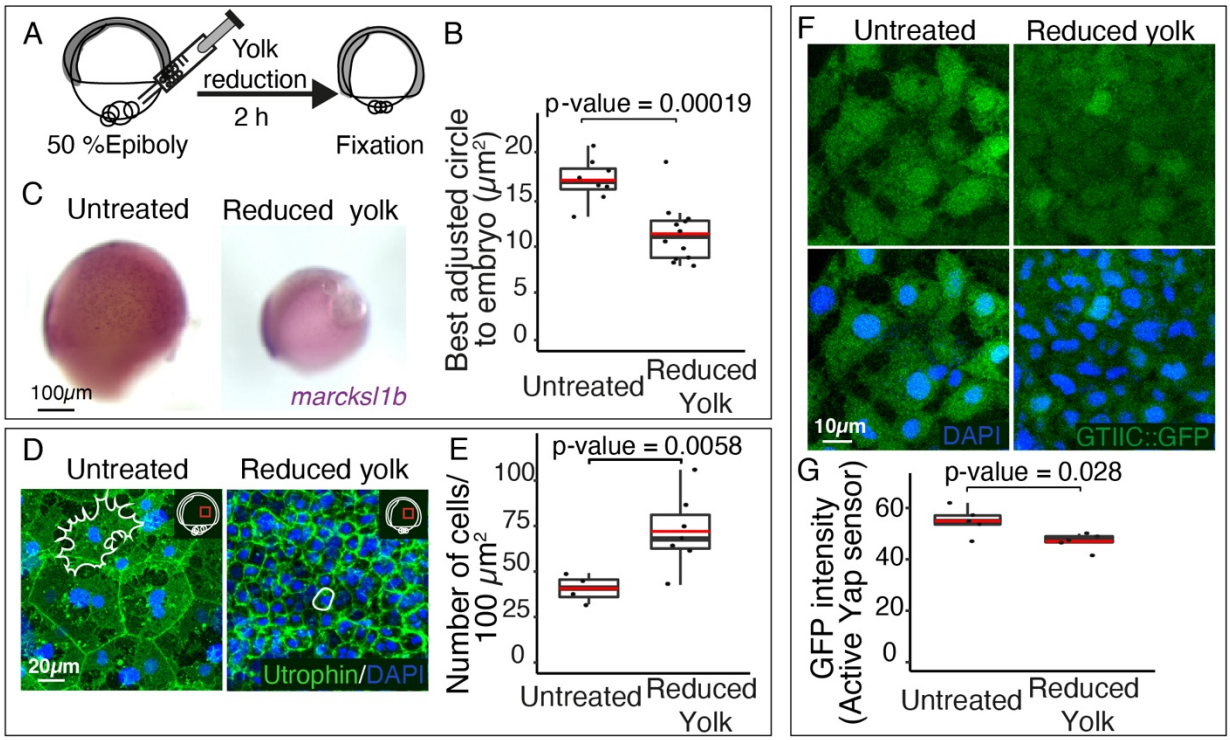

Figure 18. Yap activation is inhibited by cell density. (A) Schematic representation of the yolk removal protocol. **(B)** Quantification of embryo size, as determined by the area of the best adjusted circle to control and yolk reduced embryos. P-value: 0.00019. **(C)** ISH analysis of the expression of *marcksl1b* in control and reduced yolk embryos. **(D)** Confocal microscopy images of dorsally converging cells from control and yolk reduced embryos injected with *Utrophin::GFP* and stained with DAPI. A schematic representation of the embryo indicating the area of interest (red rectangle) is shown in the bottom left side of the image. Cell shapes are represented with white lines. **(E)** Quantification of cell density in control and yolk reduced embryos. P-value: 0.0058. **(F)** Confocal microscopy images of dorsally converging cells stained with DAPI from control and reduced yolk transgenic embryos for the Tead/Yap sensor *GTIIC::GFP*. **(G)** Quantification of GFP signal intensity in control and reduced yolk transgenic embryos for the Tead/Yap sensor *GTIIC::GFP*. P-value: 0.028. Boxes represent quartiles; whiskers indicate maximum minimum values; points indicate independent embryos ($N^{embryos} \geq 4$). Two-sided Student's t-tests were performed to evaluate statistical significances. Scales bars are 100 µm (C), 20 µm (D), and 10 µm (F).

Yap promotes cortical actin recruitment and focal adhesions assembly in migratory cells

We showed that Yap proteins are active in dorsally converging cells, in which they modulate the expression of cytoskeletal and ECM-adhesion components. To investigate the recruitment of these components to the cell cortex in convergent cells, embryos were injected at the one-cell stage with *Utrophin:GFP* mRNA, to label filamentous actin, and *Pax::mKate* mRNA, to reveal FAs assembly. Then, the distribution of these tracers was examined using high-resolution microscopy in WT and *yap* double mutants, focusing our attention on dorsal migratory cells of the inner mass (Fig 19), in which Yap is active (Fig 15). These inner mass cells display a monolayer distribution, positioned between the large polygonal cells of the enveloping layer (EVL) and the yolk syncytial layer (YSL). WT inner mass cells presented strong accumulation of filamentous actin (Fig 19A) and showed the spreading shape typical of migratory cells, with extended plasma membrane and protruding filopodia and lamellipodia. On the contrary, *yap* mutant cells accumulated less cortical actin, displaying a rounded shape with less noticeable protrusions (Fig 19A, C-E). We also observed that WT inner mass cells display FA stripes and foci, which are very reduced in *yap* double mutant cells (Fig 19A). This result suggests that Yap is essential for FA maturation, as these structures enlarge as they mature (Pasapera et al., 2010). By looking at the XZ projections of *Paxillin:mKate* in WT cells, we observed that FA clusters tend to accumulate at the surface contacting the YSL (Fig 19A'), thus suggesting that inner mass cells are migrating preferentially over the yolk surface. *Yap* mutant cells clearly lack these polarized adhesion clusters, which are significantly shorter (Fig 19A', Fig S7A).

To get further insight into the cells' morphology, we performed a similar experiment but now injecting *Utrophin:GFP* together with *Lyn-tdTomato (LynTm)* mRNA, to visualize the plasma membrane. These results confirmed the cortical accumulation of filamentous actin in WT cells, which presented multiple filopodia and membrane ruffles (Fig 19B-E). In contrast, *yap* mutant cells displayed a rounded morphology with lower number of filopodia (Fig 19B-E). By examining XZ projections of the nuclei, we observed that WT nuclei tend to appear less spherical than *yap* mutant cells (Fig 19B').

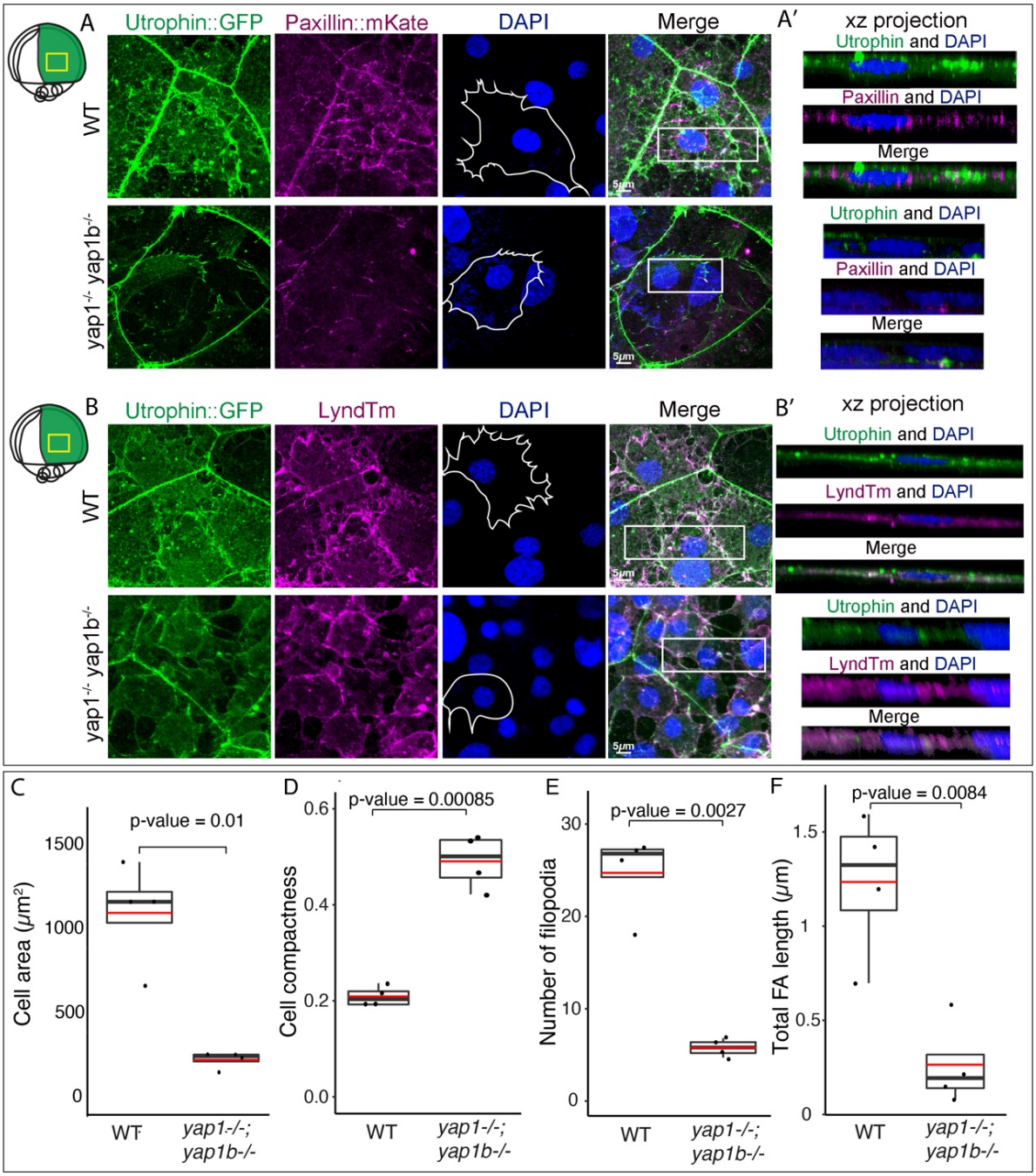

Figure 19. Defective recruitment of cortical actin and focal adhesions in *yap* mutants. (A, B) Confocal microscopy images of dorsally converging cells from WT and *yap1*$^{-/-}$*;yap1b*$^{-/-}$ embryos injected with *Utrophin::GFP*, *Paxillin::mKate* (A), *LyndTm* (B) and stained with DAPI. XZ projections from the sections indicated with white rectangles are shown (A', B'). Schematic representation of the embryo indicating the area of interest with a yellow rectangle is shown in the upper left side of the panel. Cell shapes are represented with white lines in the images corresponding to DAPI. **(C)** Quantification of average cell area in WT and *yap1-/-;yap1b-/-* embryos. P-value: 0.01. **(D)** Quantification of average cell compactness, as determined by the ratio between the cell area and the area of the circle having the same perimeter, in WT and *yap1-/-;yap1b-/-* embryos. P-value: 0.00085. **(E)** Quantification of the average number of filopodia in WT and *yap1-/-;yap1b-/-* embryos. P-value: 0.0027. **(F)** Quantification of the total focal adhesion length, as determined by the sum of all focal adhesions length within a 18225 μm^2 region of lateral converging cells, in WT and *yap1-/-;yap1b-/-* embryos. P-value: 0.0084. Boxes represent quartiles; whiskers indicate maximum minimum values; points indicate independent embryos ($N^{embryos}$ = 4). Two-sided Student's t-tests were performed to evaluate statistical significance. Scale bars = 5 μm

Since mechanical coupling to the ECM and nuclear deformation are required for Yap nuclear shuttling (Elosegui-Artola et al., 2016, 2017), we decided to explore this observation further. To this end, we performed a 3D nuclei reconstruction and measure two main morphological parameters of WT and *yap* mutant cells, flatness and sphericity (Fig 20, S7, Movie S4). We found that *yap* mutant nuclei display a lower flatness index and are significantly more spherical than those of WT cells (Fig 20B-C, S7B-C).

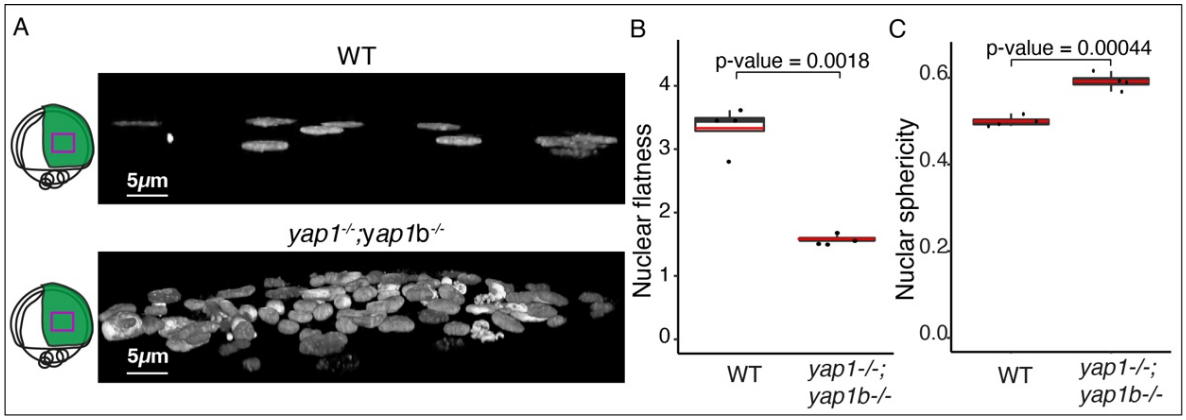

Figure 20. Nuclear morphology in mutant cells. (A) 3D nuclei reconstruction of DAPI stained nuclei (lateral) in stage 16 WT and *yap1-/-;yap1b-/-* embryos (see movie S4). **(B)** Quantification of average nuclei flatness, which refers to the ratio between the second and the third axis of an ellipsoid, in WT and *yap1*$^{-/-}$*;yap1b*$^{-/-}$ embryos. P-value: 0.0018. **(C)** Quantification of nuclei sphericity, which measures the degree to which a nucleus approaches the shape of a sphere, in WT and *yap1*$^{-/-}$*;yap1b*$^{-/-}$ embryos. P-value: 0.00044. See Figure S7 for a detailed plot. Boxes represent quartiles; whiskers indicate maximum minimum values; points indicate independent embryos ($N^{embryos}$ = 4). Two-sided Student's t-tests were performed to evaluate statistical significance. Scale bars = 5 µm.

From these measurements, we hypothesized that the noticeable reduction of cortical filamentous actin and FAs observed in *yap* mutant cells may lead to a decrease in intracellular tension, which is reflected in a more relaxed and rounded nuclei and cell morphology.

To examine if these morphological defects depend on cell-ECM adhesion we tested if the overexpression of *paxillin*, a central mechano-responsive FA component (Hytönen & Wehrle-Haller, 2016; Pasapera et al., 2010), was sufficient to alleviate *yap* mutants cellular phenotype. Injection of high levels of *paxillin::mKate* mRNA at one-cell stage in double mutant embryos partially rescued the defects at a cellular level; including spread cell morphology, cell compactness, filopodia number (Fig 21A-D) and nuclear morphology (Fig 22E-G).

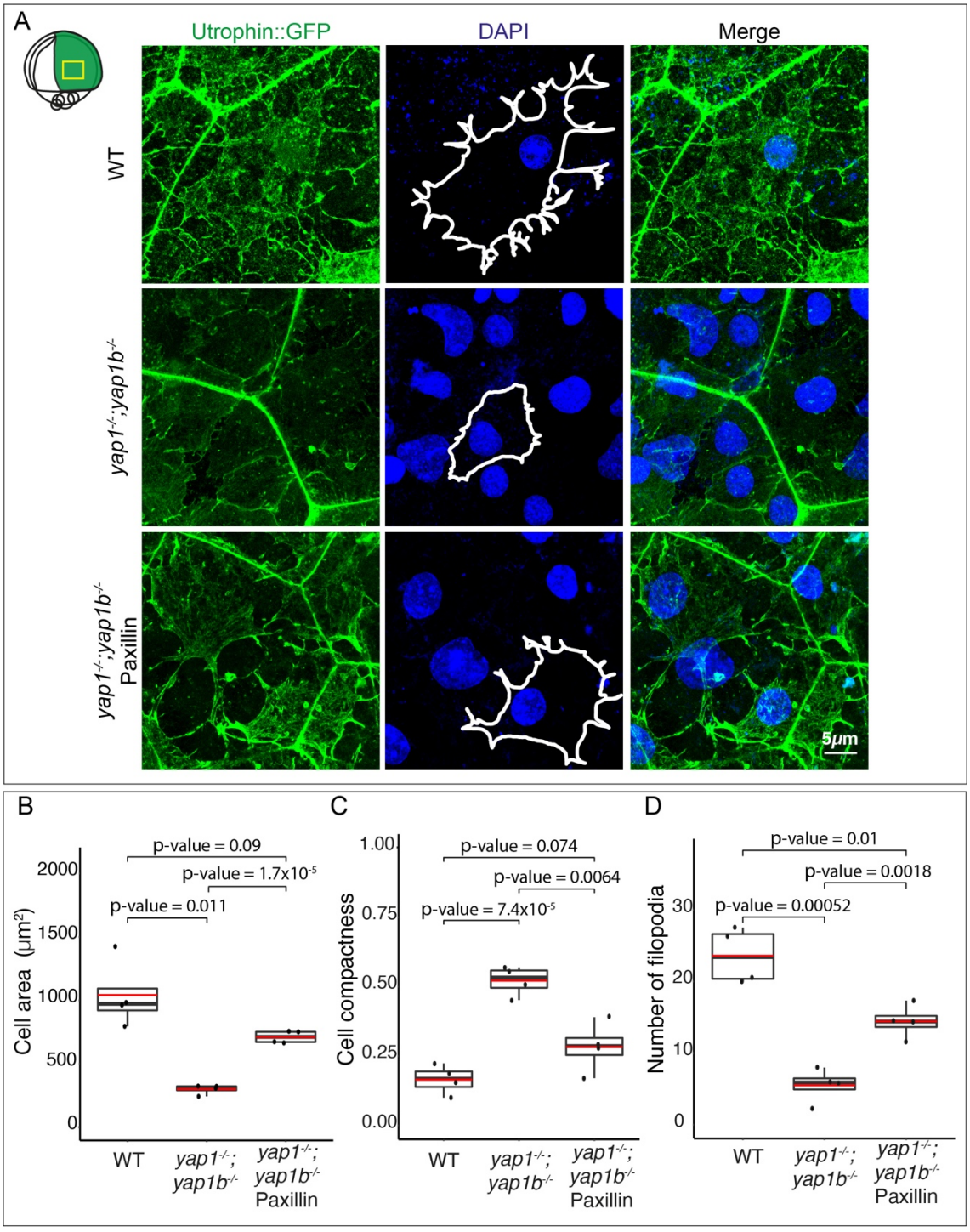

Figure 21. Paxillin overexpression rescues cell morphology in *yap* double mutant embryos. (A) Confocal microscopy images of dorsally converging cells from WT, *yap1-/-;yap1b-/-* and Paxillin-rescued *yap1-/-;yap1b-/-* embryos injected with *Utrophin::GFP* and stained with DAPI. Schematic representation of the embryo indicating the area of interest with a yellow rectangle is shown in the upper left side. Cell shapes are represented with white lines in the images corresponding to DAPI. **(B)** Quantification of average cell area in WT, as well as in *yap1-/-;yap1b-/-* and Paxillin-rescued *yap1-/-;yap1b-/-* embryos. **(C)** Quantification of average cell compactness in WT, *yap1-/-;yap1b-/-* and Paxillin-rescued *yap1-/-;yap1b-/-* embryos. **(D)** Quantification of the average number of filopodia in WT, *yap1-/-;yap1b-/-* and Paxillin-rescued *yap1-/-;yap1b-/-* embryos. Boxes represent quartiles; whiskers indicate maximum minimum values; points indicate independent embryos ($N^{embryos}$ = 4). P-values are indicated in the figure. Two-sided Student's t-tests were performed to evaluate statistical significance. Scale bars = 5 µm.

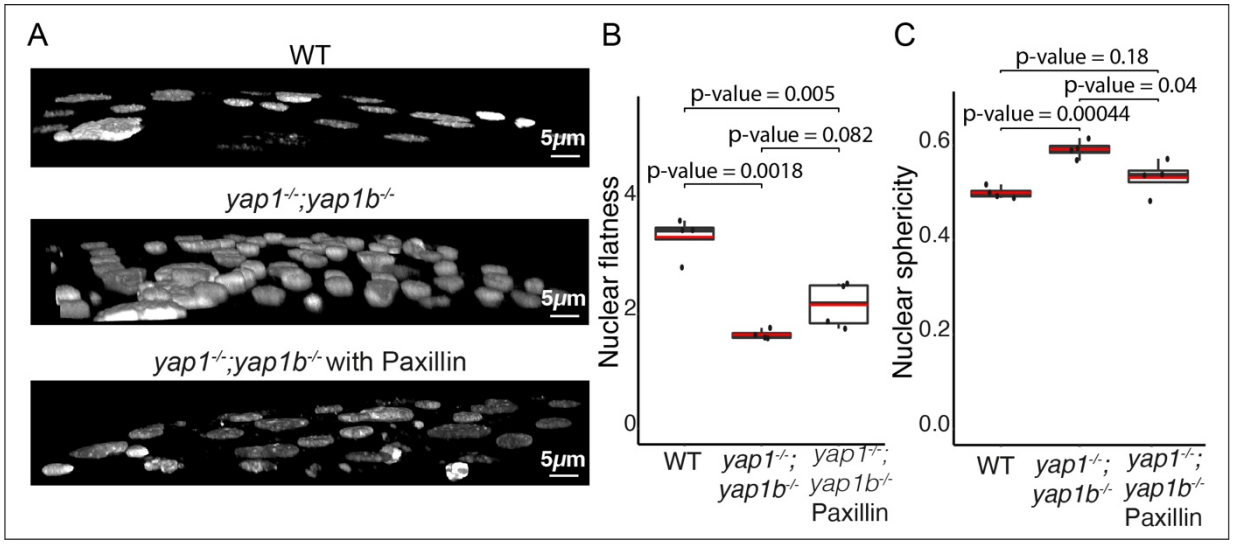

Figure 22. Paxillin overexpression rescues nuclear morphology in *yap* mutant embryos. (A) 3D reconstruction of DAPI stained nuclei (lateral) in stage 16 WT, *yap1*-/-;*yap1b*-/- and Paxillin-rescued *yap1*-/-;*yap1b*-/- embryos. **(B)** Quantification of average nuclei flatness, which refers to the ratio between the second and the third axis of an ellipsoid, in WT, *yap1*-/-;*yap1b*-/- and Paxillin-rescued *yap1*-/-;*yap1b*-/- embryos. **(C)** Quantification of average nuclei sphericity, which measures the degree to which a nucleus approaches the shape of a sphere, in WT, *yap1*-/-;*yap1b*-/- and Paxillin-rescued *yap1*-/-;*yap1b*-/- embryos. Boxes represent quartiles; whiskers indicate maximum minimum values; points indicate independent embryos ($N^{embryos} = 4$). P-values are indicated in the figure. Two-sided Student's t-tests were performed to evaluate statistical significance. Scale bars = 5 µm.

These observations further suggest the reduction of intracellular tension in our mutants is, at least in part, FA-dependent, which is in agreement with previous observations indicating reduced tissue tension in medaka mutant embryos for *yap1*, as well as in *yap/taz* knockdown embryos in zebrafish (S. Porazinski et al., 2015).

All these data suggest that Yap activity is promoting the formation and maturation of FAs and the polymerization of cortical actin in migratory cells. Thus, in the absence of Yap activity, cells would be unable to establish mature FAs and actin bundles, which are essential to respond to ECM cues.

Yap senses and activates intracellular tension within a positive feedback loop

Our results indicated that Yap activity regulates FAs and actomyosin cytoskeleton, which allows coupling intracellular tension to the ECM. In turn, Yap transcriptional regulators have been characterized as mechanosensors/mechanotransducers (Aragona et al., 2013; Dupont et al., 2011). Therefore, we wondered if Yap transcriptional response depends on mechanical strains, thus closing a mechano-regulatory feedback loop in gastrulating precursors. Integrins transmit information on the rigidity of the ECM through the Rho/Rock pathway, which modifies the F-actin cytoskeleton and mechanically activates Yap/Taz (Elosegui-Artola et al., 2016; Sero & Bakal, 2017; Totaro et al., 2018). When this pathway is inhibited, there is a reduction of stress fiber formation and FA maturation, which translates into reduced intracellular tension (Nardone et al., 2017; S. Piccolo et al., 2014). To test whether a mechanical feedback loop is operating in migrating cells, we applied the pharmacological inhibitor Rockout to interfere with the Rho/Rock pathway. Gastrulating embryos were treated with Rockout for a short developmental window (2h), after which cellular and nuclear morphologies, as well as Yap activation, were examined (Fig 23, 24, and S7). Rockout-treated embryos exhibited a similar phenotype to *yap* mutants, with lack of axis condensation and delayed epiboly when compared to a wild type embryo at an equivalent 17 stage (Fig 25A). To investigate the morphology of the cells, we injected *Utrophin:GFP* together with *Lyn-tdTomato (LynTm)* mRNA at the one-cell stage in control (DMSO) or Rockout treated embryos. In control embryos, we confirmed that, whereas compact cells at the midline display round shapes and spherical nuclei, lateral converging cells have a spread morphology with more filopodial protrusions and flattened nuclei (Fig 23, 24 and S7D, E). In contrast, cell and nuclei morphologies were significantly rounder for lateral cells in Rockout treated embryos, as determined by their area, compactness, nuclei flatness and sphericity indexes, as well as a reduced number of filopodia; all suggesting a reduced intracellular tension (Fig 23, 24, S7D, E; Movie S5).

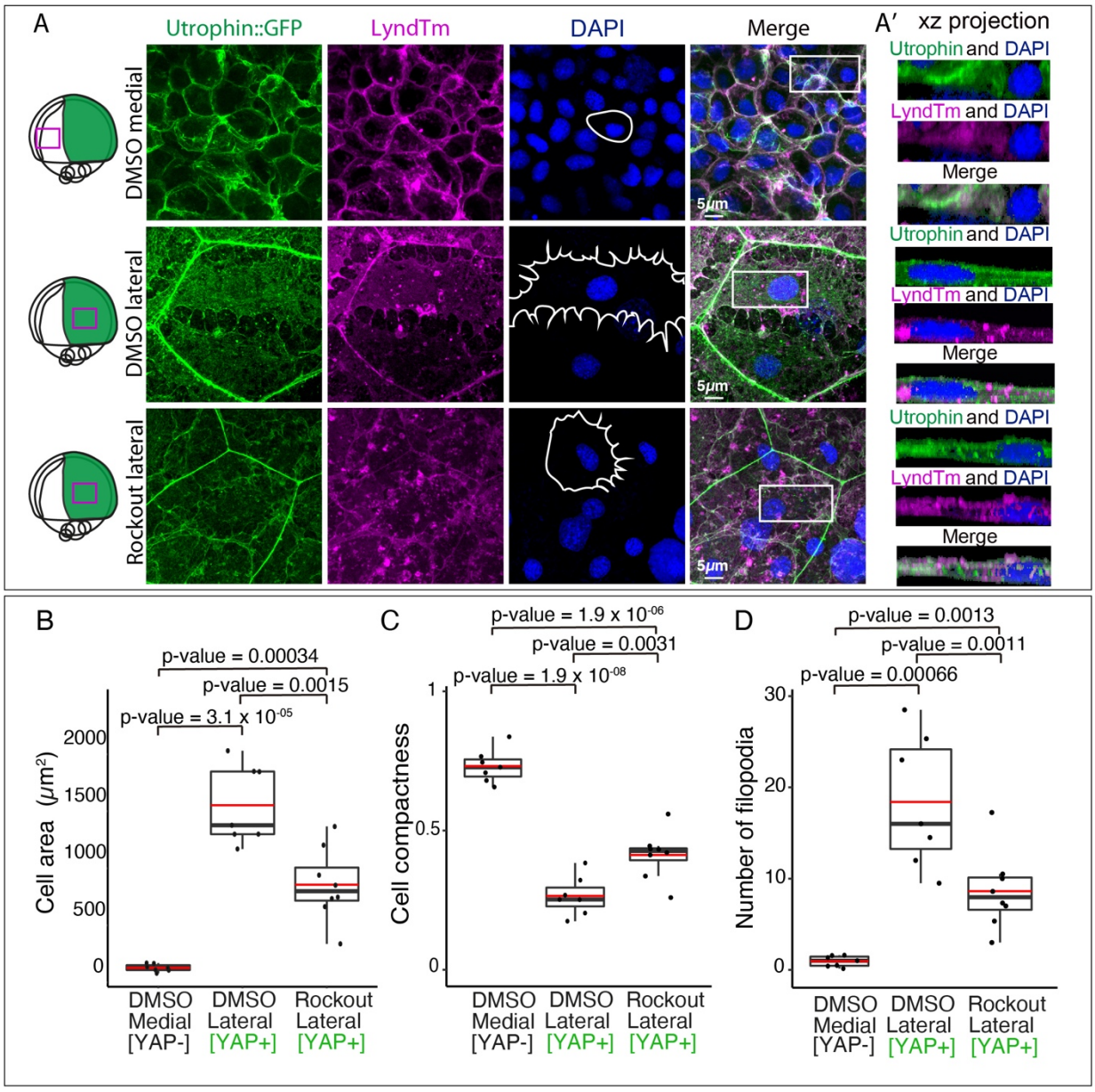

Figure 23. Cell morphology depends on Yap activity. (A) Confocal microscopy images of medial and lateral (DMSO) and lateral (Rockout-treated) converging cells from embryos injected with *Utrophin::GFP*, and *LyndTm* (B) and stained with DAPI. XZ projections from the sections indicated with white rectangles are shown (A'). Schematic representation of the embryo indicating the area of interest with a magenta rectangle is shown in the left side of the panel. Cell shapes are represented with white lines in the images corresponding to DAPI. **(B)** Quantification of average cell area in DMSO and Rockout treated embryos. **(C)** Quantification of average cell compactness in DMSO and Rockout treated embryos. **(D)** Quantification of the average number of filopodia in DMSO and Rockout treated embryos. Boxes represent quartiles; whiskers indicate maximum minimum values; points indicate independent embryos ($N^{embryos} \geq 7$). P-values are indicated in the figure. Two-sided Student's t-tests were performed to evaluate statistical significance. Scale bars = 5 µm.

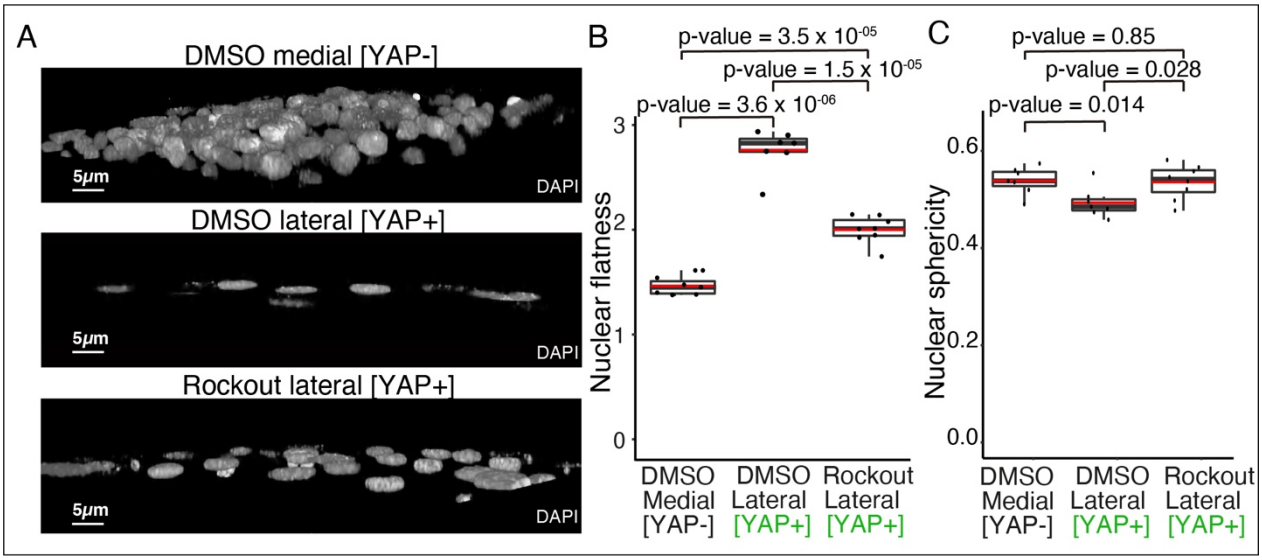

Figure 24. Cell and nuclear morphology depend on Yap activity. (A) 3D reconstruction of DAPI stained nuclei in stage 16 DMSO and Rockout treated embryos. **(B)** Quantification of average nuclei flatness, which refers to the ratio between the second and the third axis of an ellipsoid, in DMSO and Rockout treated embryos. See Figure S7D for a detailed plot. **(C)** Quantification of average nuclei sphericity, which measures the degree to which a nucleus approaches the shape of a sphere, in DMSO and Rockout treated embryos. See Figure S7E for a detailed plot. Boxes represent quartiles; whiskers indicate maximum minimum values; points indicate independent embryos ($N^{embryos} \geq 7$). P-values are indicated in the figure. Two-sided Student's t-tests were performed to evaluate statistical significance. Scale bars = 5 µm.

To determine if Rock inhibition impinges on Yap transcriptional activity, we followed *marcksl1b* expression, a potential direct target of Yap according to our data (Figs 14, 15), as well as the activation of the Tead/Yap sensor.

Quantitative imaging analysis revealed a significant reduction in *marcksl1b* expression and Tead/Yap activity in Rockout-treated embryos when compared to WT, thus indicating a diminished transcriptional activation by Yap (Fig 25BD, S8). Next, to further confirm the connection between tension and Yap activity in gastrulating cells, we applied alternative pharmacological treatments such as Blebblistatin, a selective Myosin II inhibitor (Kovács et al., 2004), and Dasatinib, a kinase inhibitor active against Src family kinases that interferes with both FAs dynamics and the Src/Yap signaling axis (Elbediwy et al., 2016; Logue et al., 2018). Similar to Rockout-, Blebblistatin- and Dasatinib-treated embryos, mimicked *yap* mutants' phenotype and displayed a marked reduction in *marcksl1b* expression and Tead/Yap activity (Fig 25A-D, S8).

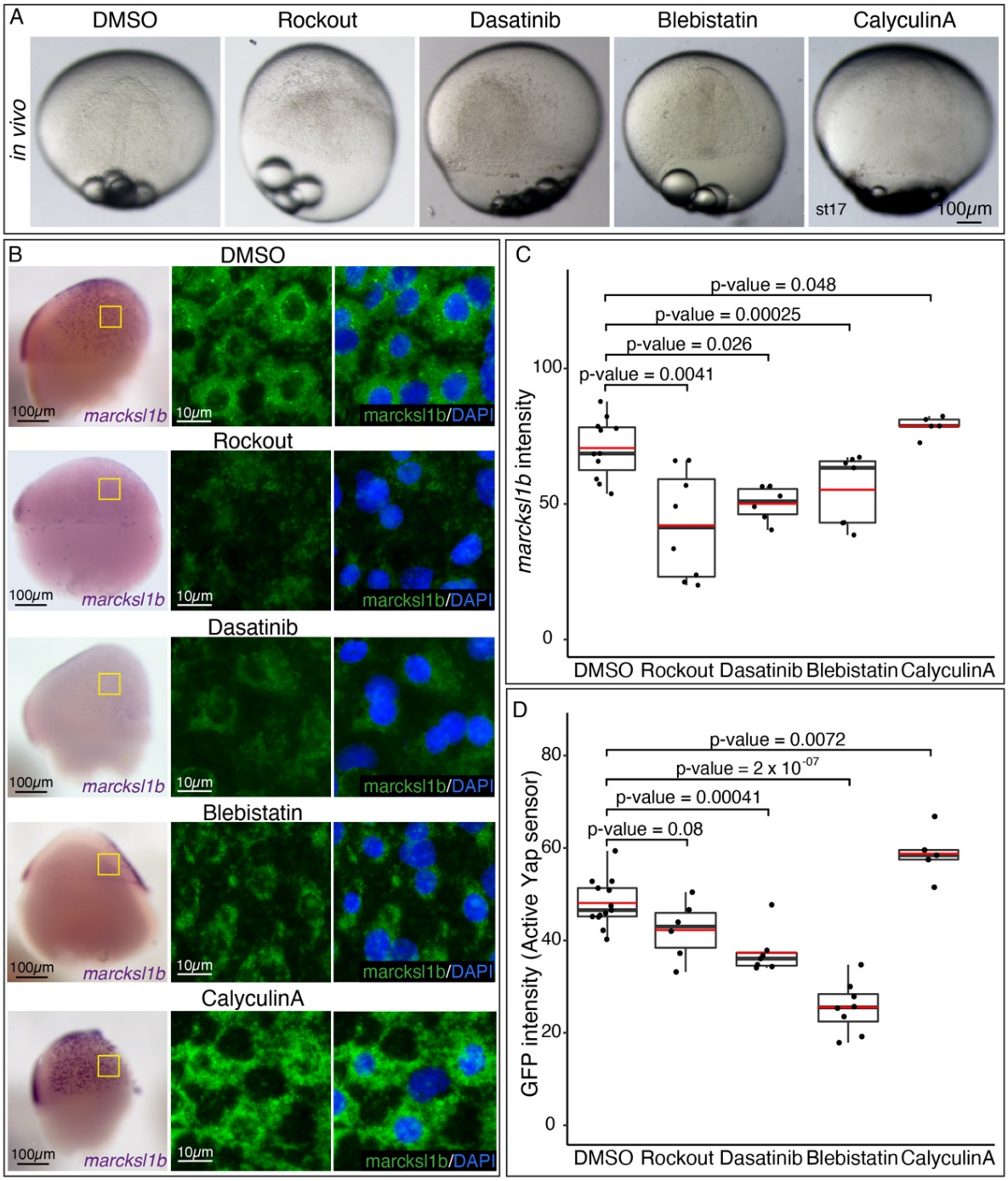

Figure 25. Gastrulation phenotype and Yap activity under intracellular tension alterations. (A) Brightfield images of stage 17 WT embryos treated with DMSO, Rockout, Dasatinib, Blebistatin or CalyculinA during 4 h. Frontal stereo microscope images of embryos are shown. **(B)** ISH analysis distribution of *marcksl1b* in WT embryos treated with DMSO, Rockout, Dasatinib, Blebistatin or CalyculinA for 2 h. Lateral stereo microscope images of stage 16 embryos are shown (first row). Confocal microscopy images of *marcksl1b* fluorescent ISH stained with DAPI (second and third rows) from the areas indicated with yellow rectangles are shown. **(C)** Quantification of *marcksl1b* fluorescent ISH signal in DMSO, Rockout, Dasatinib, Blebistatin or CalyculinA treated embryos. P-values are indicated in the figure. **(D)** Quantification of GFP signal intensity in DMSO, Rockout, Dasatinib, Blebistatin or CalyculinA-treated transgenic embryos for the Tead/Yap sensor *GTIIC::GFP*. See confocal images in Figure S8 P-values are indicated in the figure. Boxes represent quartiles; whiskers indicate maximum minimum values; points indicate independent embryos ($N^{embryos} \geq 5$). Two-sided Student's t-tests were performed to evaluate statistical significance. Scale bars are 100 µm (A-B) and 10 µm (B).

Finally, to close the loop, we investigated if an increase in the intracellular tension will as well translate in an increment of Yap nuclearization and activation of its transcriptional program. We followed two different approaches; first, a pharmacological activation of Myosin II using CalyculinA (Somlyo & Somlyo, 2000), and second, a direct mechanical stimulation of the embryos by using a customized mechanical tester (Fig S9) (Univert; CellScale) for simultaneous uniaxial compression of gastrulating embryos. CalyculinA treatment resulted indeed in a Yap over-activation in gastrulating embryos, as indicated by an enhanced *marcksl1b* expression and Tead reporter activity (Fig 25A-D, S6). Interestingly, the mechanical compression of the embryos for a short time window (20% axial deformation for 20 minutes) also produced a similar increase in *marcksl1b* expression (Fig 26A, B) following direct image quantification. In addition to *marcksl1b*, we also assessed the expression of other Yap bona-fide targets, such as *lamc1*, *ctgfa* and *lats2* by quantitative PCR (qPCR). This analysis showed a significant increment of the expression of the Yap targets *marcksl1b*, *lamc1* and *ctgfa* after embryo compression (Fig 26C).

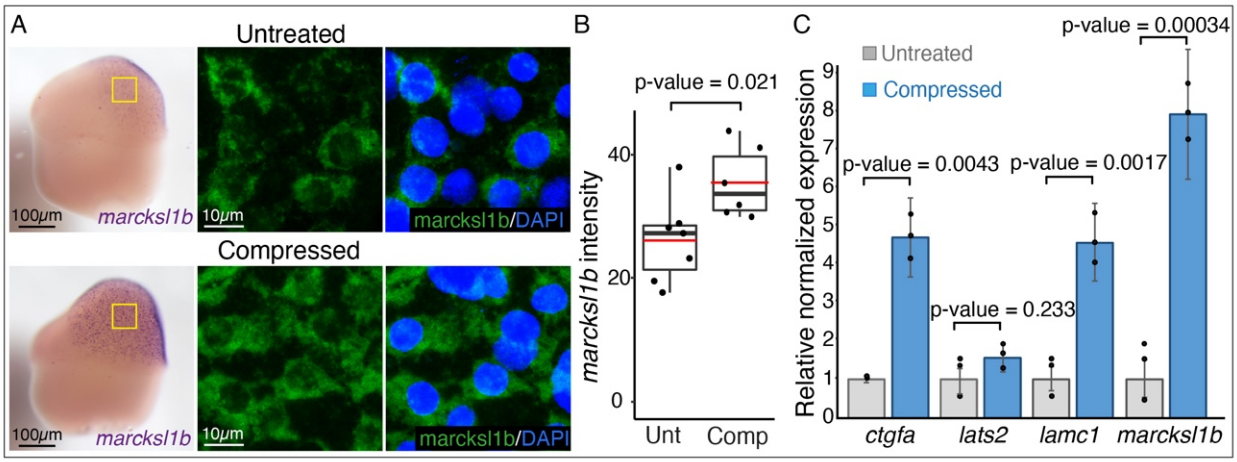

Figure 26. Yap activity under mechanical stimulation. (A) ISH analysis distribution of *marcksl1b* in control (untreated) and compressed WT embryos during 20 min. Lateral binocular images are shown. Confocal microscopy images of *marcksl1b* fluorescent ISH stained with DAPI from the sections indicated with yellow rectangles are shown. **(B)** Quantification of *marcksl1b* fluorescent ISH signal intensity in control and compressed embryos. P-value = 0.021. Boxes represent quartiles; whiskers indicate maximum minimum values; points indicate independent embryos ($N^{embryos} \geq 6$). **(C)** mRNA levels of *ctgfa*, *lats2*, *lamc1* and *marcksl1b* in control and compressed embryos as quantified by RT-qPCR. P-values are indicated in the figure. Data are represented as mean ± SD; points indicate technical replicates ($N^{embryos} = 20$). Two-sided Student's t-tests were performed to evaluate statistical significance. Scale bars are 100 μm and 10 μm (A).

Finally, we checked the effect of mechanical compression in embryos after pharmacological inhibition by Rockout treatment. We saw that, in Rock inhibited embryos, the impact of the mechanical perturbation on the Yap-dependent transcriptional activation is largely reduced (Fig 27A-C). This observation is in agreement with our previous findings (Fig 25), indicating that Yap ability to mechanotransduce relies on the generation of intracellular tension.

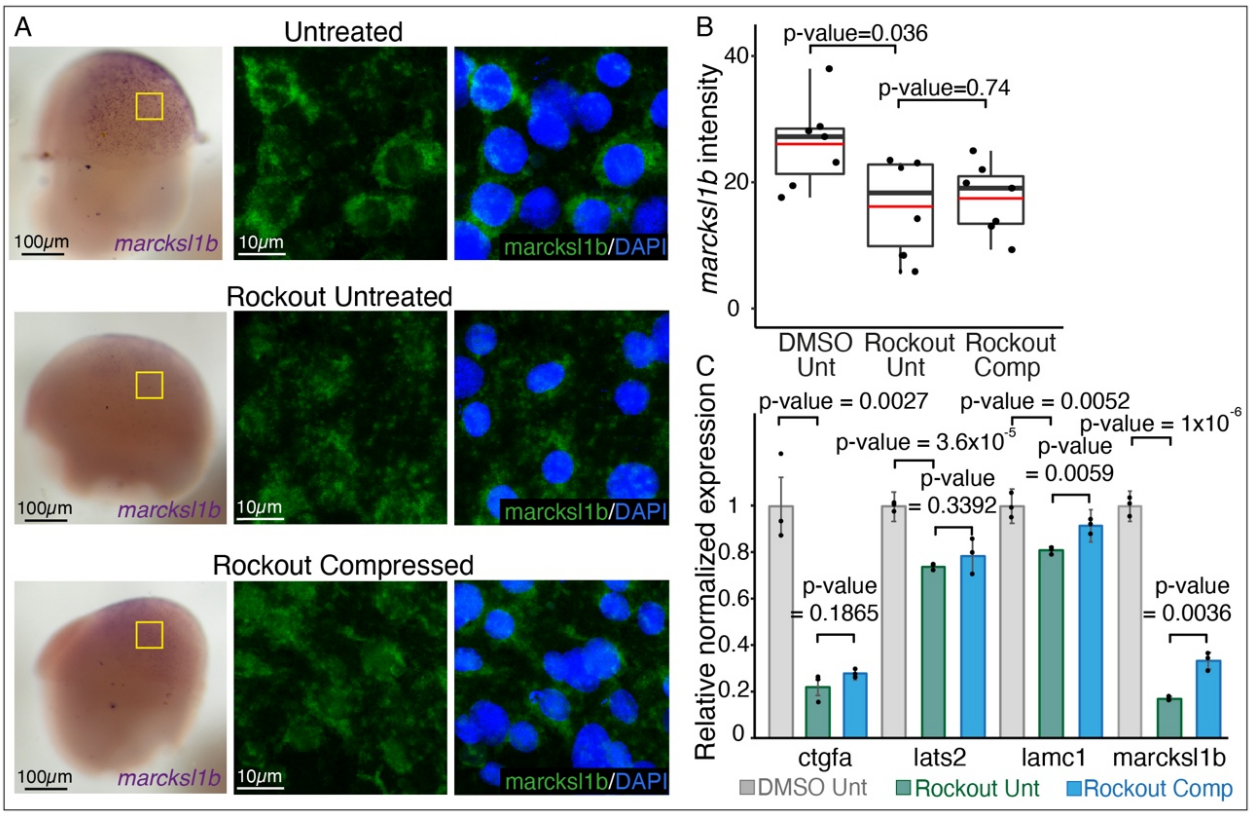

Figure 27. Rho/ROCK-dependent response of Yap activity to compression. **(A)** ISH analysis distribution of *marcksl1b* in DMSO untreated (not compressed), Rockout untreated and Rockout compressed WT embryos during 20 min. Lateral stereo microscope images are shown. Confocal microscopy images of *marcksl1b* fluorescent ISH stained with DAPI from the sections indicated with yellow rectangles are shown. **(B)** Quantification of *marcksl1b* fluorescent ISH signal intensity in DMSO untreated, Rockout untreated and Rockout compressed embryos. P-values are indicated in the figure. Boxes represent quartiles; whiskers indicate maximum minimum values; points indicate independent embryos ($N^{embryos} \geq 6$). **(C)** mRNA levels of *ctgfa*, *lats2*, *lamc1* and *marcksl1b* in DMSO untreated, Rockout untreated and Rockout compressed embryos as quantified by RT-qPCR. P-values are indicated in the figure. Data are represented as mean ± SD; points indicate technical replicates ($N^{embryos} = 20$). Two-sided Student's t-tests were performed to evaluate statistical significance. Scale bars are 100 µm and 10 µm (A).

Taken together, our data demonstrate the existence of a mechano-regulatory loop between intracellular tension and Yap activation, which is essential to maintain directed cell migration during gastrulation.

Discussion

The sophisticated and diverse body architecture found in animals is acquired during embryonic development through a step wise process in which gastrulation plays a fundamental role. Gastrulation involves complex morphogenetic movements that will transform a homogenous mass of cells into a more complex 3D structure, in which the axes and the germ layers are established. Understanding which mechanisms drive, coordinate and regulate these complex rearrangements of cells is crucial not only to understand how tissues and organs are formed but also to investigate how tumor progression can be controlled, as there are striking parallelisms between the mechanisms that govern gastrulation movements and those that regulate oncogenic growth and metastasis (Leptin, 1999; Solnica-Krezel & Sepich, 2012; Zhao et al., 2010). Recently, mechanical cues have been proven to have a crucial function in modulating morphogenetic processes, however little is known about how gastrulating cells interpret them. Yap proteins are well-known transcriptional co-activators that mediate the response of cells to mechanical signals (Aragona et al., 2013; S. Piccolo et al., 2014), however, its role in gastrulation remains elusive . Here we show that the double knockout of *yap1* and its paralog *yap1b* in medaka results in an axis assembly failure, due to a defective migration of dorsally converging cells. Accordingly, we uncover the role of Yap as a transcriptional hub that activates the expression of genes mostly involved in cell-ECM adhesion, cytoskeleton organization and cell migration. Finally, our results indicate that Yap coordinates a mechano-regulatory loop to sustain intracellular tension and maintain the directed cell migration for embryo axis development.

Yap is required for a proper posterior axis assembly

YAP proteins are involved in a broad range of processes, such as the control of cell fate, proliferation, apoptosis and movement, and thus, have a key role in development, tissue remodeling, and tumor progression (Varelas, 2014; Zanconato et al., 2016). However, we show that during gastrulation, YAP paralogs play mainly a role in controlling morphogenetic movements. We observed that *yap* double mutants fail to assemble their posterior axis, and that these defects were not due to variations in cell death or proliferation, as none of these parameters were significantly altered when compared to

WT embryos. Previous findings indicate that these *yap* mutants display increased cell death and lower rates of cell proliferation, however, these observations were done at later stages of development, once the gastrulation was ended (S. Porazinski et al., 2015; Vázquez-Marín et al., 2019).

Moreover, our RNA-seq and ISH data also indicate that, in general terms, defects of germ layers specification (i.e. endoderm, mesoderm and neuroectoderm) are not behind *yap* double mutants' phenotype. The exception to this is the specification of the non-neural/epidermal lineage. We showed that key non-neural specifiers, such as *dlx3b*, *gata2a* and *tp63* appear downregulated in double mutant embryos. This finding is in agreement with recent reports indicating a crucial role for Yap/Tead in the determination of the non-neural/epidermal lineage (F. M. Piccolo et al., 2022). However, it is very unlikely that epidermal lineage misspecification is behind the strong axial defects observed in *yap* double mutants, as the mutation of key non-neural/epidermal specifiers, such as *tp63* do not result in gastrulation defects in teleosts (Santos-Pereira et al., 2019). In addition, our data is in consonance with previous studies in mice, in which *Yap* mutants (with functional *Taz*) display shortened and highly disorganized body axis, but normal cell specification, as determined by histological and ISH data (Morin-Kensicki et al., 2006). However, we cannot discard the requirement of YAP in fate specification during whole embryonic development. In mammals, YAP overexpression leads to a defective specification of extraembryonic tissues, and in 2D human gastruloids, YAP is required for the ectoderm determination (Giraldez et al., 2021; S. Piccolo et al., 2014).

Yap directs the migration of dorsally converging cells towards the midline

Identifying the underlying cues of cell migration is key, both to understand self-organization principles behind tissue assembly and homeostasis, as well as to identify molecular targets to fight malignant metastasis. Directed cell migration is one of the main mechanisms behind gastrulation movements. The weight of this mechanism

during the different gastrulation stages varies among species, as egg geometry, developmental speed or the environment are key determinants shaping embryonic development. It has been shown that in teleost and chicken, directed cell migration towards the midline mediates the convergence movements (Pézeron et al., 2008; Sepich et al., 2005; Solnica-Krezel, 2005). Here, we uncover the role of Yap as a transcriptional hub that coordinates the genetic program required for directed cell migration during gastrulation.

We found that Yap is active just in lateral cells that are far from the midline and need to undergo long displacement. In fact, Yap function promotes these cells to move long distances, and hold the persistence and velocity required to reach the midline. When Yap is absent, lateral cells move slower and are unable to maintain their directionality resulting in shorter displacements and thus in a reduced accumulation of cells at the midline. This migratory behavior of dorsally converging cells is also essential during zebrafish body axis assembly (Zeng et al., 2007). In this case, authors indicate that fast and persistent migration of cardiac precursors (i.e. a population of lateral mesodermal cells) required the signaling via the GPCR Agtrl1b/Apnrb and its ligands Apelin and Toddler, the latter of which act only inducing cell motility without providing directionality. Similar to our results, wider and shorter body axes were observed upon the disruption of the convergence movements (F. Lin et al., 2005; Williams & Solnica-Krezel, 2020; Zeng et al., 2007).

Once dorsally converging cells approach the midline region, they display a decrease in Yap activity. In consonance with this, in the A-P axis, the migratory parameters of *yap* mutant cells were not significantly altered when compared to WT, with the exception of a slightly reduced displacement, which might be the consequence of the shorter *yap* mutant axis. Therefore, we can hypothesize that cells in midline regions would perform the convergence and extension movements in a Yap-independent manner, being Wnt/planar cell polarity (PCP)-dependent mediolateral intercalation the most likely responsible mechanism (Heisenberg et al., 2000; Jessen et al., 2002; Wallingford et al., 2000).

Yap programs primarily regulate cytoskeleton organization and cell adhesions components

In order for a cell to migrate directionally it needs to polymerize actin at the leading edge, forming protrusions that adhere to the substrate by focal adhesions. Bundles of actomyosin filaments bind focal adhesions and generate forces that mature the adhesion, and these forces are transferred onto the substrate in the form of traction. The forces of actin polymerization together with myosin contractility drive the cell movement forward (SenGupta et al., 2021; Shellard & Mayor, 2020). Our findings suggest that these principles underlying adherent cell migration were controlled by Yap function.

Yap-activated cells display a spreading shape, with numerous protrusions, mature FAs and flattened nuclei. In contrast, *yap* mutant cells in equivalent regions do not have this migratory state, presenting less accumulation of filamentous actin, reduced FAs, and lower intracellular tension, based on their rounder shape and more spherical nuclei. Moreover, our rescue experiments with *paxillin::mkate* suggest that the intracellular tension of dorsally converging cells is, at least in part, FA-dependent. Paxillin is a central scaffolding protein of FAs, which promote the recruitment of structural and signaling molecules involved in cell movement and migration (López-Colomé et al., 2017; Pasapera et al., 2010). Interestingly, its overexpression in *yap* double mutants was sufficient to partially rescue mutants' defects, such as spread cell morphology, cell compactness, filopodia number and nuclear morphology. This link between FA and F-actin accumulation has been extensively reported in the literature (Bachir et al., 2017; Hynes & Destree, 1978; Martino et al., 2018; Schwarz & Gardel, 2012). Therefore, we propose a central role for YAP in promoting cell migration, by controlling cytoskeleton tension and FA maturation. This is in agreement with previous *in vitro* studies of endothelial cells that mediate vasculogenesis and angiogenesis, in which YAP is identified as an essential regulator of directed cell migration, modulating cytoskeleton and FAs remodeling (Mason et al., 2019; Sakabe et al., 2017). However, opposite to our observations, Mason and collaborators indicate that YAP absence leads to a motility

arrest because of excessive cytoskeleton tension and over-maturation of FAs. In contrast, our data are consistent with reports that implicate YAP in a feed-forward promotion of cytoskeleton tension and FA reinforcement (Aragona et al., 2013; C. Lin et al., 2017; Nardone et al., 2017). While YAP proteins might have a context and cell type-dependent function, it is clear that YAP proteins mediate cell migration and modulate cell mechanics, maintaining the cytoskeleton responsive to mechanical cues.

In addition, our bulk RNA-seq results confirm the tight relationship between Yap activation and an increase in the expression of genes mostly involved in cell-ECM adhesion, cytoskeleton organization and cell migration. Furthermore, a significant proportion of these identified genes are putative direct targets of Yap1/Yap1b, according to our previous DamID-seq datasets (Vázquez-Marín et al., 2019). This suggests a straightforward regulatory role in cell adhesion and cell migration during gastrulation. A similar transcriptional program, coupling intrinsic cell tension with adhesion to the ECM, has also been reported in migratory endothelial and breast cancer cells (Mason et al., 2019; Nardone et al., 2017). In agreement with our transcriptome data, part of the gene set identified as downregulated in *yap1*/*yap1b* medaka mutants was also found as differentially expressed in *yap1*/*wwtr1* zebrafish mutants (Kimelman et al., 2017) (e.g. *amotl2b*, *cyr61*, *cdc42ep*, *sorbs3*, *ctgfa*, *col1a1b* and *pcdh7*). In this study, the authors analyzed the role of *yap1* and its paralog *wwtr1* (a.k.a. *taz*) in zebrafish embryo development. They reported that double mutant embryos show a defect in the elongation of the posterior part of the embryo, by regulating the deposition of Fibronectin (a main ECM component) in the presumptive epidermis. The main difference with our results is that the phenotype observed in zebrafish was first evident at 15-16 somite stage, much after gastrulation was completed, and did not interfere with the assembly of the primary embryo axis. A logical explanation is that Yap signaling cooperates with other mechanisms to direct cell migration, and thus it is possible that its early role has remained elusive due to compensatory mechanisms. Additionally, it is important to take into account that the spatial configuration of the gastrulating cells varies among species. Due to the much larger size of the yolk, dorsally converging cells in medaka embryos form a flattened monolayer, and they have to travel longer distances to arrive at the midline compared to their equivalent in zebrafish. Therefore,

it is likely that the particular geometry of the medaka gastrula has facilitated uncovering the role of Yap proteins in directed cell migration during gastrulation.

Finally, the Knockdown of *marcksl1b*, a direct downstream of Yap involved in actin cytoskeleton dynamics, corroborates the crucial role of cytoskeleton remodeling during convergence movements. *marckl1b* depleted embryos presented a delay in development and epiboly, however, the A-P axis was formed in all of them. This less severe phenotype compared to those of *yap* double mutant embryos confirm that Yap activates a broad gene program, involving many other cytoskeleton remodelers, as well as a battery of cell-ECM adhesion components.

Yap activity is inhibited by the high cell density at the midline

Classically, YAP proteins have been mainly identified as downstream effectors of the Hippo pathway, a kinase cascade that ends up phosphorylating and inhibiting YAP/TAZ. However, recent studies question whether, and to what extent, YAP activation pattern observed in diverse contexts is determined by the Hippo signaling. In fact, the Hippo pathway is a crucial regulator of YAP activity, but undeniably not the only one. Mechanical signals, provided by cellular shape and the structural properties of the environment, are also a central pillar for YAP function. However, the mechanism behind this biomechanical regulation remains unknown. As YAP proteins play a central role in morphogenesis and cancer malignancy, it is essential to better understand the inputs that regulate YAP mechanical activation (S. Piccolo et al., 2014; S. Porazinski et al., 2015; Varelas, 2014; Zanconato et al., 2016).

Since we observed a significant correlation between Yap activity silencing and increased cell density closer to the embryo midline, we propose that the shape changes imposed by the spatial restrictions in more crowded areas (e.g. cells become rounded, reducing their ECM contact surface and protrusions) might mediate Yap inhibition as previously demonstrated (Aragona et al., 2013; Zhao et al., 2007). Aragona et al. reported that the main determinant for Yap/Taz inhibition is actually to accommodate to a smaller cell

size. Small cells attach to a smaller ECM substrate area, displaying "decreased integrin-mediated focal adhesions, reduced actin stress fibers, and blunted cell contractility" (Aragona et al., 2013). Thus, culturing cells in soft substrates, placing them in suspension, or disrupting the F-actin cytoskeleton are all scenarios that result in Yap/Taz signaling inhibition (Aragona et al., 2013; Grannas et al., 2015; Wada et al., 2011; Yu et al., 2012). In the opposite cell configuration (i.e., spreading cells), mechanical cues have been shown to be essential for Yap/Taz nuclear localization and activity (Dupont et al., 2011; Wada et al., 2011). The work of Elosegui-Artola et al. illustrates how cytoskeletal and cell shape changes affect Yap activation. They describe how cell flattening triggers nuclear pores relaxation, allowing transcription factors, such as Yap, to enter the nucleus upon cell deformation (Elosegui-Artola et al., 2016).

To confirm whether cell density is a key regulator of Yap activity in the context of gastrulation, we highly reduced embryos' size by extracting yolk material, resulting in a significant increase in the inner cell mass density. This made dorsally converging cells acquire rounder shapes that were accompanied by a decrease in Yap activity when compared to equivalent regions in control embryos. Therefore, our data indicate that high cell density is a crucial factor that inhibits Yap activity in the midline region, where cells move in a Yap-independent manner. The inactivation of YAP by cell density has also been shown to play a crucial role in other biological contexts. YAP proteins underlie the contact inhibition of proliferation, a classic paradigm of epithelial biology in which cultured cells stop dividing when they became confluent. The loss of this cell density control has been shown to be a hallmark of most cancer. Interestingly, these studies point out again the geometrical information as the principal controller of YAP activity, being the Hippo pathway dispensable for this process (S. Piccolo et al., 2014; Zhao et al., 2007).

Yap senses and maintains tension in a mechano-regulatory loop

The way that forces are generated, sensed, and transmitted within tissues is increasingly being understood as a continuous interplay between the cells and their environment.

This results in regulatory feedback loops in which cells perceive mechanical cues and respond in turn modifying their own mechanical properties (Hannezo & Heisenberg, 2019; Petridou et al., 2017). In the case of Yap, the general agreement is that the cytoskeletal organization reflects the mechanical state of the tissue and serves as a universal Yap regulator; while Yap will transform these inputs into transcriptional changes inducing cytoskeletal and cell adhesions rearrangements (Totaro et al., 2018).

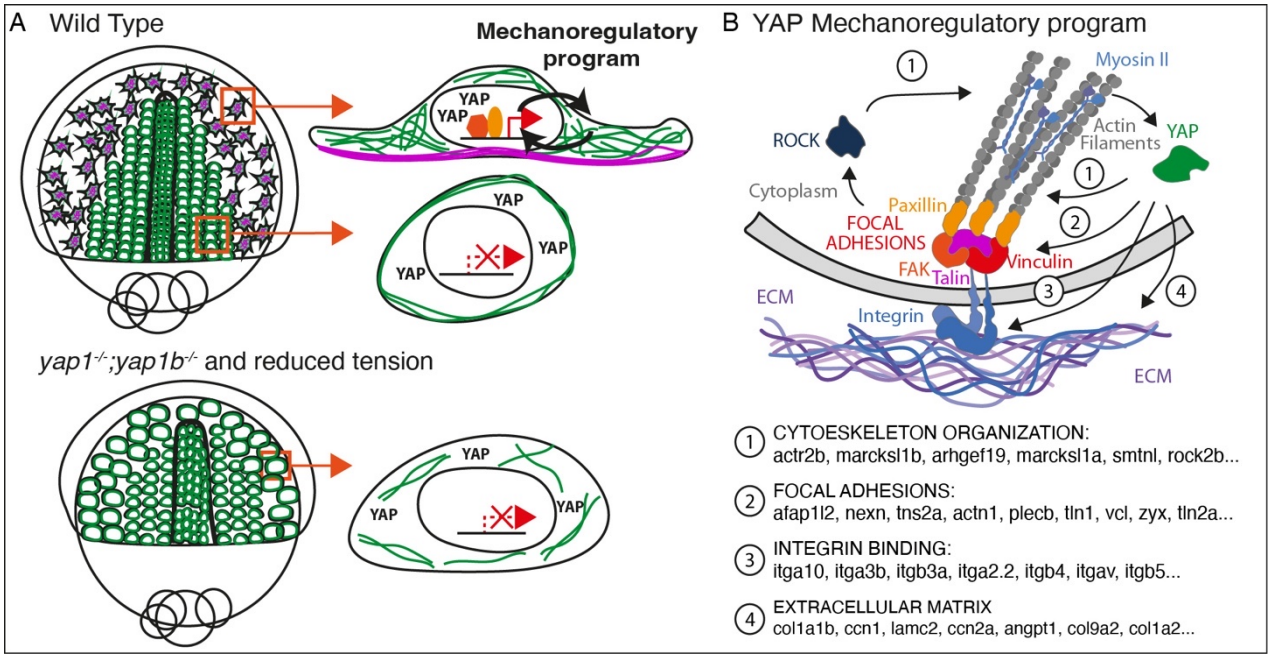

Figure 28. Yap senses intracellular tension within a mechano-regulatory feedback loop. (A) Summarizing scheme representing the differences between medial and lateral migrating cells converging to the midline in WT, *yap1-/-;yap1b-/-* and reduced tension embryos. **(B)** Main components of the Yap-dependent transcriptional program encode for proteins that are involved in the link between the ECM and the actin cytoskeleton.

Here, our results suggest that, in the context of gastrulation, Yap plays a pivotal role in the establishment of a mechano-regulatory feedback loop (Fig 28). We show that physical and pharmacological alterations of the intracellular tension impact Yap activity. High mechanical inputs, such as mechanical compression or activation of Myosin II, activate Yap. Then, nuclear Yap triggers a genetic program that will contribute to sustain tension levels by maintaining the spreading shape of converging cells. Consistently, Inhibition of intracellular tension leads to the inactivation of Yap, which results in cells acquiring rounder shapes and spherical nuclei. Interestingly, the compression-induced activation of Yap was largely reduced in Rock inhibited embryos. These results were in

agreement with our previous findings, which indicate that the generation of intracellular tension is required for the ability of Yap to mechanotransduce. In other words, if mechanical information cannot be transmitted upon Rock inhibition, exogenous tension won't be able to activate Yap. In line with this, we also propose that in our model cell density induces intracellular tension changes, by the remodeling of cytoskeleton and FAs, that cause the inhibition of Yap activity, thus determining the region controlled by Yap. Yap-dependent feedback mechanisms have been described in diverse cellular contexts, ranging from cardiomyocyte regeneration (Morikawa et al., 2015), breast cancer cells (Chang et al., 2015), mesenchymal stem cell cultures (Nardone et al., 2017) and endothelial cells migration (Mason et al., 2019). What our results and all these examples have in common is that mechanically activated Yap/Taz promotes F-actin remodeling, FA assembly, and integrin and ECM components expression; all essential elements mediating ECM-cell communication (Totaro et al., 2018).

Concluding remarks/ Conclusiones

1. *yap* mutant embryos present gastrulation defects. Notably, *yap* double mutants have a more severe phenotype displaying a failure in the axis assembly. Therefore, Yap activity is essential for medaka gastrulation and axis formation.

2. Cell death and proliferation rates were not significantly altered in *yap* double mutant embryos when compared to WT, indicating that variations in these parameters are not behind the gastrulation defects.

3. The general specification of the germ layers does not depend on Yap function.

4. Yap proteins activate the expression of genes mainly involved in cell-ECM adhesion, Hippo signaling, and actin cytoskeleton regulation/organization.

5. Yap is specifically active in dorsally migrating precursors.

6. Yap function promotes dorsally converging cells to move long distances, and hold the persistence and velocity required to reach the midline.

7. Cells in the midline region move in a Yap-independent manner.

8. Spatial restrictions upon an increase in cell density lead to Yap inhibition.

9. In the absence of Yap function, dorsally converging cells show reduced focal adhesions and cortical actin recruitment, and fail to acquire the characteristic spread and flattened morphology of WT migratory cells.

10. Yap activation depends on the intracellular tension, being activated upon mechanical compression of the embryos and the increase of myosin contractility, and silenced upon inhibition of the actin cytoskeleton polymerization, myosin II or the focal adhesions-dependent signaling. This suggests the existence of a Yap-dependent mechano-regulatory loop that sustains intracellular tension.

1. Los embriones mutantes *yap* presentan defectos de gastrulación. Siendo los mutantes dobles de *yap* los más afectados, mostrando un fallo en el ensamblaje del eje.

2. Las tasas de proliferación y de muerte celular no variaron significativamente en los embriones dobles mutantes *yap* en comparación con WT, lo que indica que los cambios en estos parámetros no están detrás de los defectos de gastrulación.

3. La especificación general de las capas germinales no depende de la función Yap.

4. Las proteínas Yap activan la expresión de genes implicados principalmente en la adhesión célula-matriz extracelular, señalización Hippo y regulación/organización del citoesqueleto de actina.

5. Yap está específicamente activo en precursores que migran dorsalmente.

6. La función Yap promueve que las células que convergen dorsalmente migren largas distancias y mantengan la persistencia y la velocidad necesarias para alcanzar la línea media.

7. Las células en la línea media se mueven de manera independiente a Yap.

8. Las restricciones espaciales debido a un aumento en la densidad celular causan la inhibición de Yap.

9. En ausencia de la función Yap, las células que convergen dorsalmente muestran una reducción en las adherencias focales, en el reclutamiento de actina cortical, y el área celular.

10. La activación del Yap depende de la tensión intracelular, siendo activada por la compresión mecánica de los embriones y la contración de la miosina II, y silenciada por la inhibición de la polimerización del citoesqueleto de actina, la miosina II o la señalización dependiente de adherencias focales. Esto sugiere la existencia de un ciclo mecano-regulador dependiente de Yap que sostiene la tensión intracelular.

Supplementary Data

A

```
run("Options...", "iterations=1 count=1 black do=Nothing");
run("Convert to Mask");
run("Skeletonize");
run("Analyze Skeleton (2D/3D)", "prune=[shortest branch]");
```

B

```
////////////////////////////////////////////////////////////////////////
//////////////////////
/* Author: Ale Campoy
 * Date: 25.09.2022
 * User: Ana Sousa
 * Description: Medida de morfologia
 * Input: imagenes en PDF.
////////////////////////////////////////////////////////////////////////
//////////////////////

run("Close All");
run("Clear Results");
counts = roiManager("count");
if(counts !=0) {roiManager("delete");}
// set configuration
run("Options...", "iterations=1 count=1 black");
setBackgroundColor(0, 0, 0);
run("Set Measurements...", "area centroid center perimeter fit shape
feret's area_fraction stack redirect=None decimal=2");

// añadir aqui la ruta del archivo
path = File.openDialog("Selecciona un archivo pdf");
run("PDF ...", "choose=["+path+"] scale=300 page=0");
setOption("BlackBackground", true);
run("Convert to Mask");
run("Fill Holes");
original = getImageID();
rename("original");

run("Analyze Particles...", "display add");
 /*
  *  Medidas importantes para ver lo "compacto" -abrupto- de la celula
  *  Perimetro & Area -> para calcular el compactness definido como: the
ratio of the area of the shape to the area of a circle (the most compact
shape) having the same perimeter
  *  Circularity -> 4π*area/perimeter^2
  *  Solidity -> area/convex area
  */

run("Select None");
roiManager("Show None");

// loop para cada celula
n_celulas = roiManager("count");
for (i = 0; i < n_celulas; i++) {
 selectImage(original);
 roiManager("Select", i);
 run("Duplicate...", "title=roi_"+i);
 run("Clear Outside");
 roi = getImageID();
 /*
  *  En la siguiente linea "radius" indica  el tamaño del erode, lo que
define el tamaño de los 'filopodios' que van a borrarse de la imagen.
  *  Para tener una referencia del tamaño real, calcular el area de una
circunferencia de ese area (y pasarlo a unidades de la imagen).
  *  Un elemento de la imagen se contabilizará como filopodio si esa
esfera no entra
 */
 run("Morphological Filters", "operation=Opening element=Disk
radius=25");
```

```
 morph = getImageID();
 imageCalculator("Difference create", "roi_"+i,"roi_"+i+"-Opening");
 selectImage(roi);
 close();
 selectImage(morph);
 close();
}

// medida de los filopodios de cada celula
for (i = 0; i < n_celulas; i++) {
 counts2 = roiManager("count");
 if(counts2 !=0) {roiManager("delete");}
 selectWindow("Result of roi_"+i);
 /* Size filtra particulas pequeñas para que no cuenten como filopodio -
en pixel- */
 run("Analyze Particles...", "size=40-Infinity add");
 close();
 n_filo = roiManager("count");
 setResult("N_Filopodios", i, n_filo);
}

// pintado de los filopodios
selectImage(original);
run("Morphological Filters", "operation=Opening element=Disk radius=25");
run("Merge Channels...", "c2=original-Opening c1=original ignore");
```

C

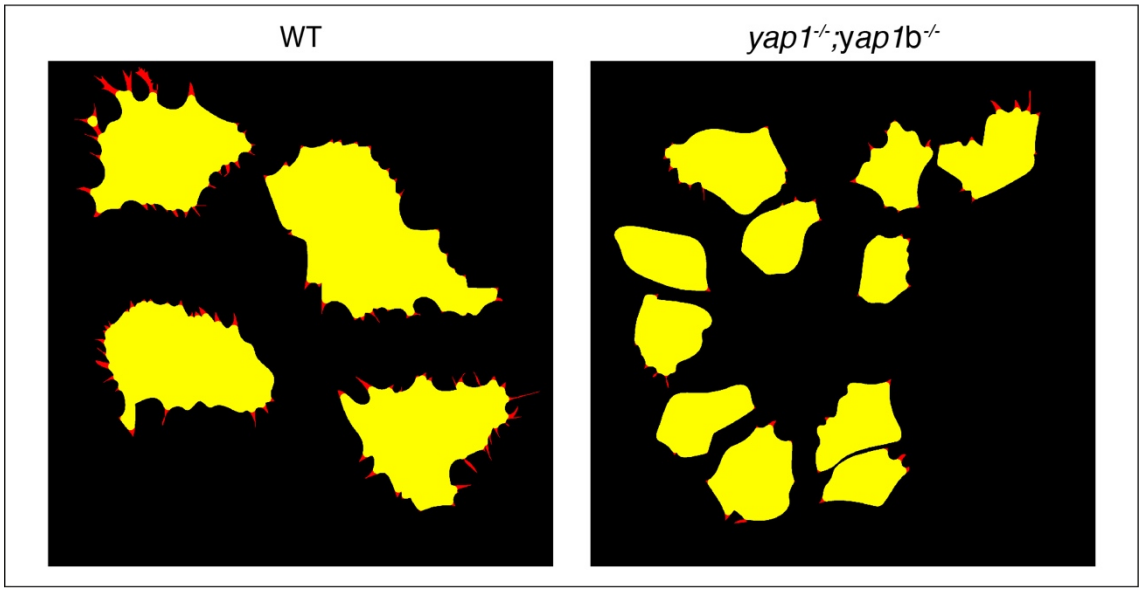

Supplementary Figure 1. Focal adhesions and cell morphology quantifications. (A) Analysis performed in ImageJ to the paxillin::mKate manually segmented signal to obtain FA lengths. Script done by Alejandro Campoy. **(B)** Analysis performed in ImageJ to the LynTdTomato and/or utrophin::GFP manually segmented signal to measure cell morphology parameters. Script done by Alejandro Campoy. **(C)** Example of cell morphology analysis of WT and *yap1*$^{-/-}$*;yap1b*$^{-/-}$ cells. The cell area when applying an opening morphology filter is indicated in yellow. In red are the elements considered filopodia.

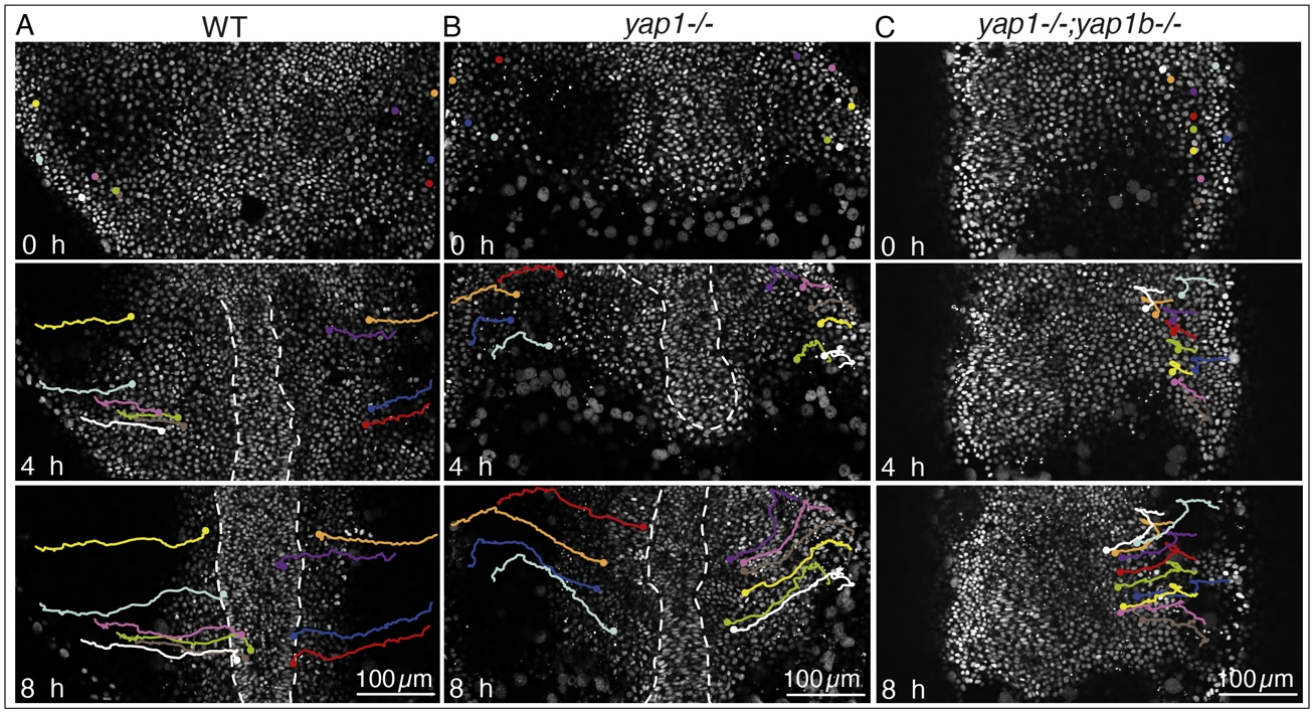

Supplementary Figure 2. Analysis of cell migration during gastrulation. (A-C) Manual tracking of representative cells of gastrulating WT (A), *yap1*$^{-/-}$ mutant (B) and *yap1*$^{-/-}$*;yap1b*$^{-/-}$ mutant embryos (C) injected with *Histone2B*::GFP for nuclei visualization. Still images from movie S2 at 0h, 4h and 8h are shown. Each cell trajectory is represented with a color line. When present, the midline is represented with white, dashed lines. Scale bars are 100 µm(A-C).

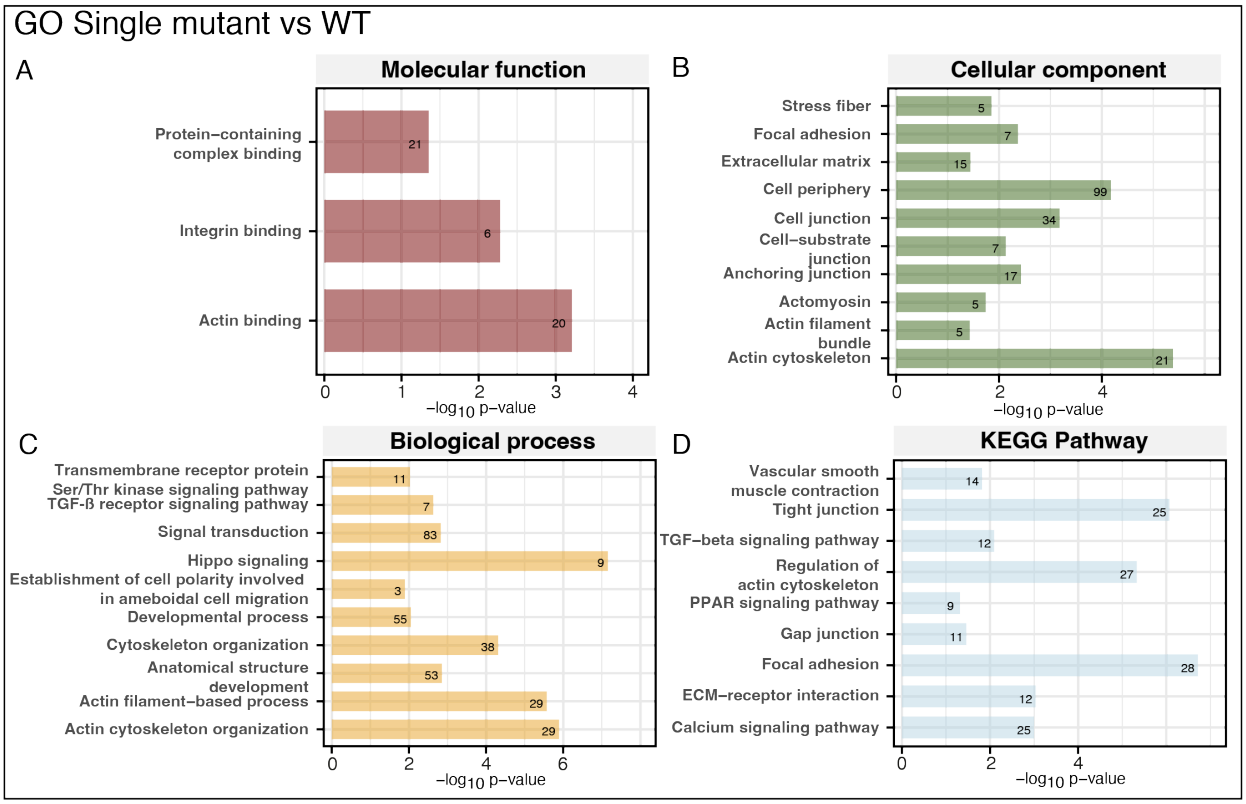

Supplementary Figure 3. Characterization of yap single mutant transcriptional programs. (A-D) Gene Ontology (GO) enrichment of the DEGs in yap1-/- embryos compared with WT, classified in molecular function (A), cellular component (B), biological processes (C) and KEGG Pathway (D).

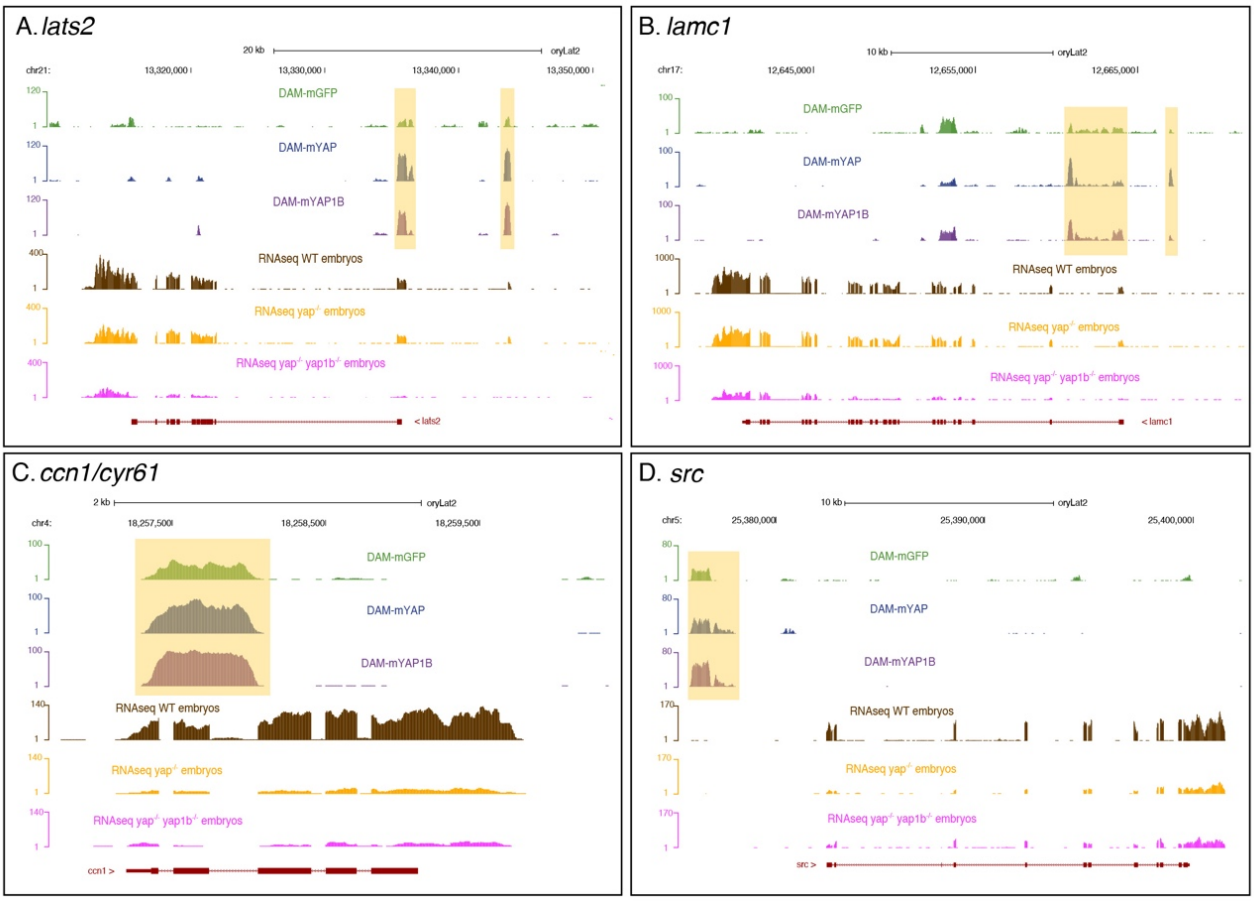

Supplementary Figure 4. Binding of Yap1/Yap1b to the chromatin is associated to significant DEGs. Overview of Yap1 and Yap1b DamID-seq tracks (Vazquez-Marin et al., 2019), as well as RNA-seq profiling of WT and *yap* single and double mutants for four representative loci: *lats2* (A), *lamc1* (B), ccn2/cyr61 (C) and src (D). Specific binding of Yap1 and Yap1b to the genome is highlighted in yellow.

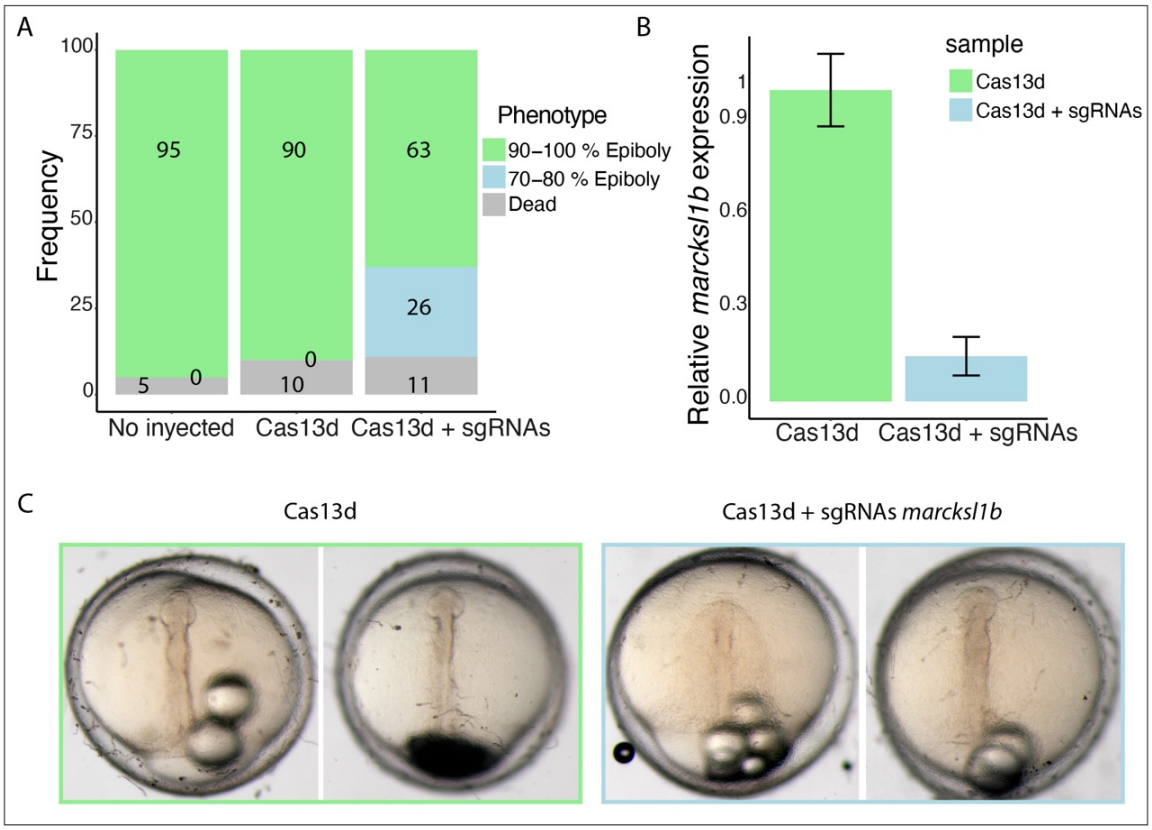

Supplementary Figure 5. Phenotype of *marcksl1b* depleted embryos. (A) Stacked barplots showing percentage of epiboly in embryos no injected, injected with Cas13d protein alone, or together with *marcksl1b* gRNAs. ($N^{embryos} \geq 30$). **(B)** RT-qPCR analysis of mRNA levels of *marcksl1b* in embryos injected only with Cas13d protein and in affected embryos injected with Cas13d and *marcksl1b* gRNAs. Data are represented as mean ± SD; ($N^{embryos} \geq 8$). The housekeeping gene *ef1a* mRNA was used as normalization control. **(C)** Brightfield images of stage 18 embryos injected only with Cas13d protein and affected embryos injected with Cas13d and *marcksl1b* gRNAs. Frontal stereo microscope images of embryos are shown.

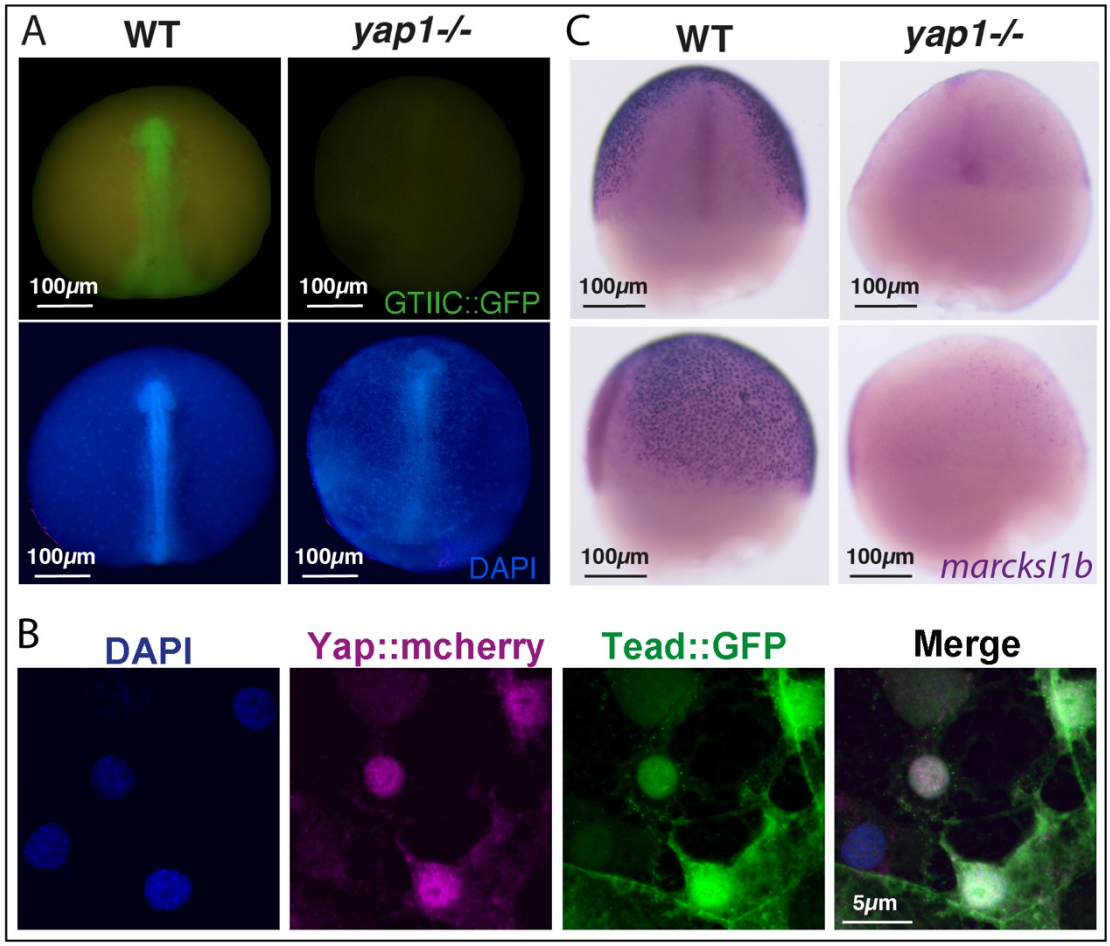

Supplementary Figure 6. Yap activity dynamics during gastrulation. (A) Activity of the Tead/Yap sensor (*GTIIC::GFP)* in WT and *yap1*$^{-/-}$ transgenic embryos shown under the fluorescent stereo microscope at stage 18. DAPI staining of these embryos is also shown. **(B)** DAPI counterstained confocal images of dorsally converging cells from *GTIIC::GFP* transgenic embryos injected with *yap1*::mCherry. Blue channel: DAPI; Magenta channel: *yap1*::mCherry signal; Green channel: GFP signal. **(C)** ISH analysis of the expression of *marcksl1b* in WT and *yap1*$^{-/-}$ embryos at stage 16. Front and lateral images are shown. Scale bars 100 µm (A, C) and 5 µm (B).

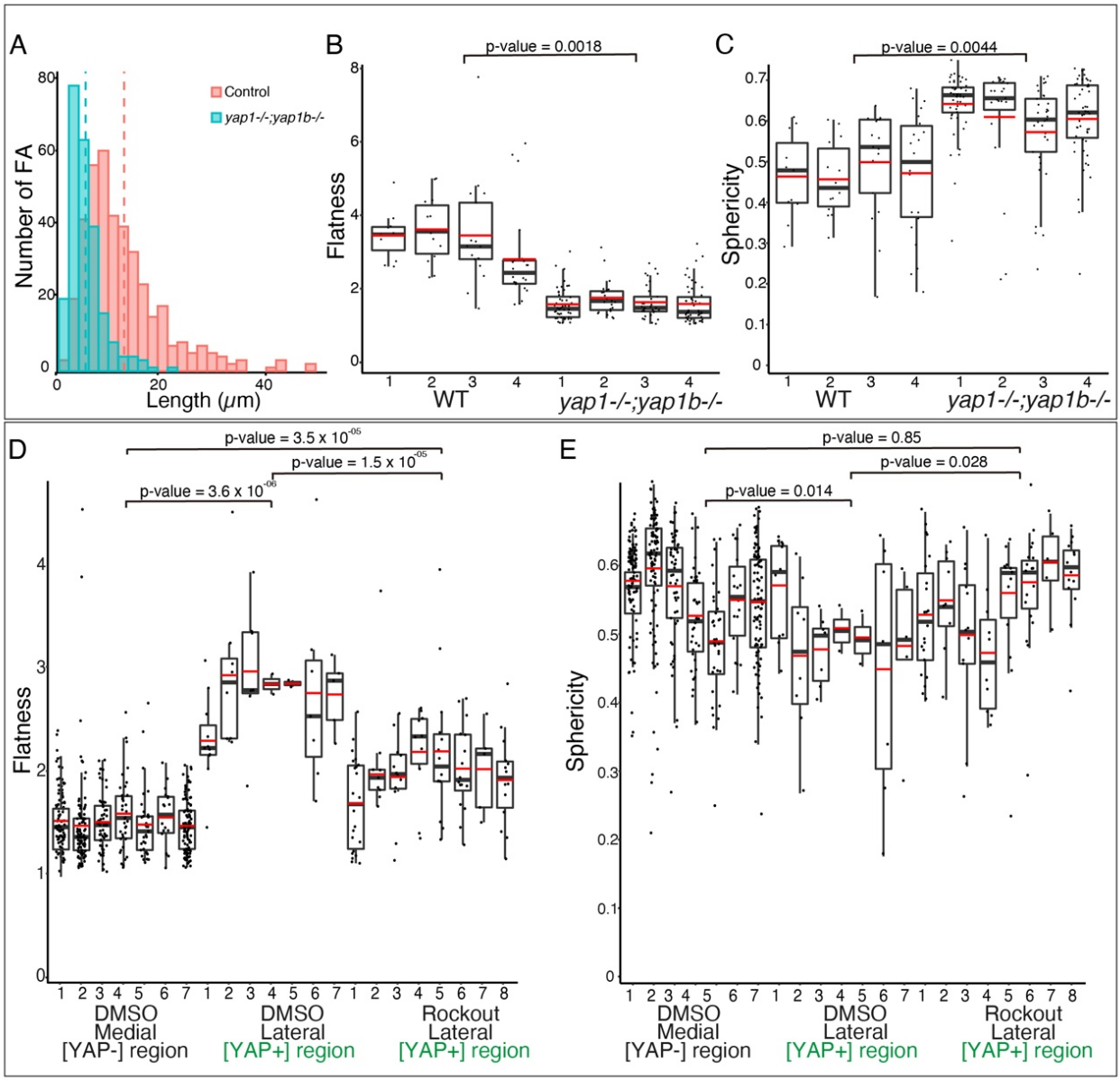

Supplementary Figure 7. Nuclear morphology in mutant and Rockout treated cells. (A) Distribution of focal adhesions according to their length in WT and *yap1-/-;yap1b-/-* embryos. Red line: mean of focal adhesions length in WT embryos. Blue line: mean of focal adhesions length in *yap1-/-;yap1b-/-* embryos. **(B-C)** Quantification of nuclei flatness (B), average values are shown in figure R15, and sphericity (C) for individual stage 16 WT and *yap1-/-;yap1b-/-* embryos. **(D-E)** Quantification of nuclei flatness (D), average values are shown in figure R17, and sphericity (G) for individual stage 16 embryos treated with DMSO (lateral and medial) or Rockout (lateral). P-value are indicated in the figure. Boxes represent quartiles; whiskers indicate maximum minimum values; points indicate cells ($N^{embryos} \geq 4$). Two-sided Student's t-tests were performed to evaluate statistical significance.

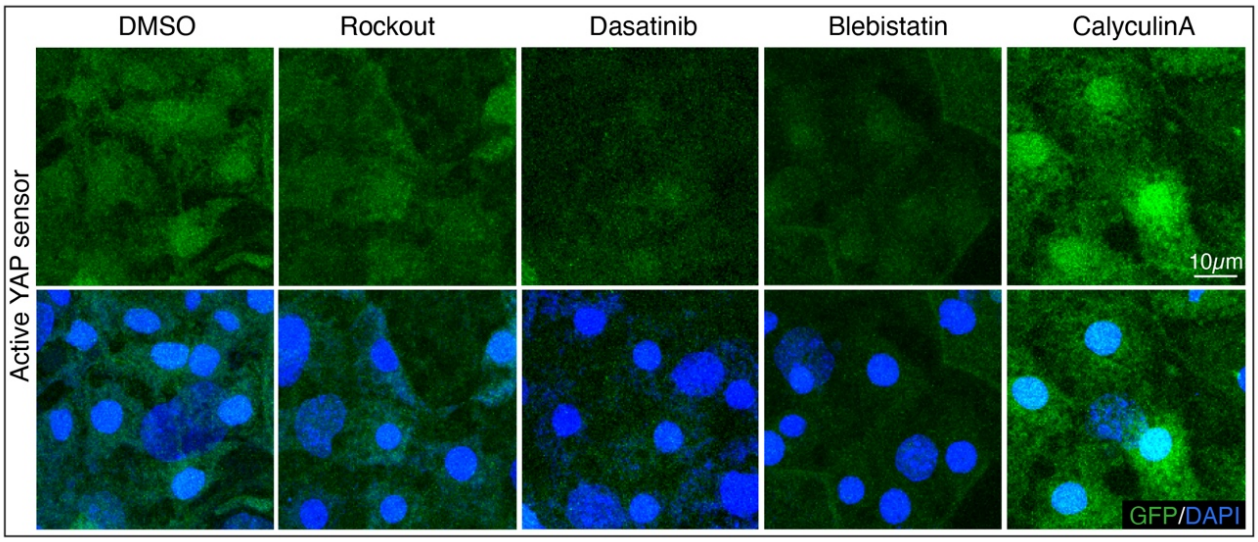

Supplementary Figure 8. Yap activity under intracellular tension alterations. Confocal microscopy images of dorsally converging cells stained with DAPI from stage 16 transgenic embryos for the Tead/Yap sensor *GTIIC::GFP* treated with DMSO, Rockout, Dasatinib, Blebistatin or CalyculinA for 2 h. Scale bars are 10 µm.

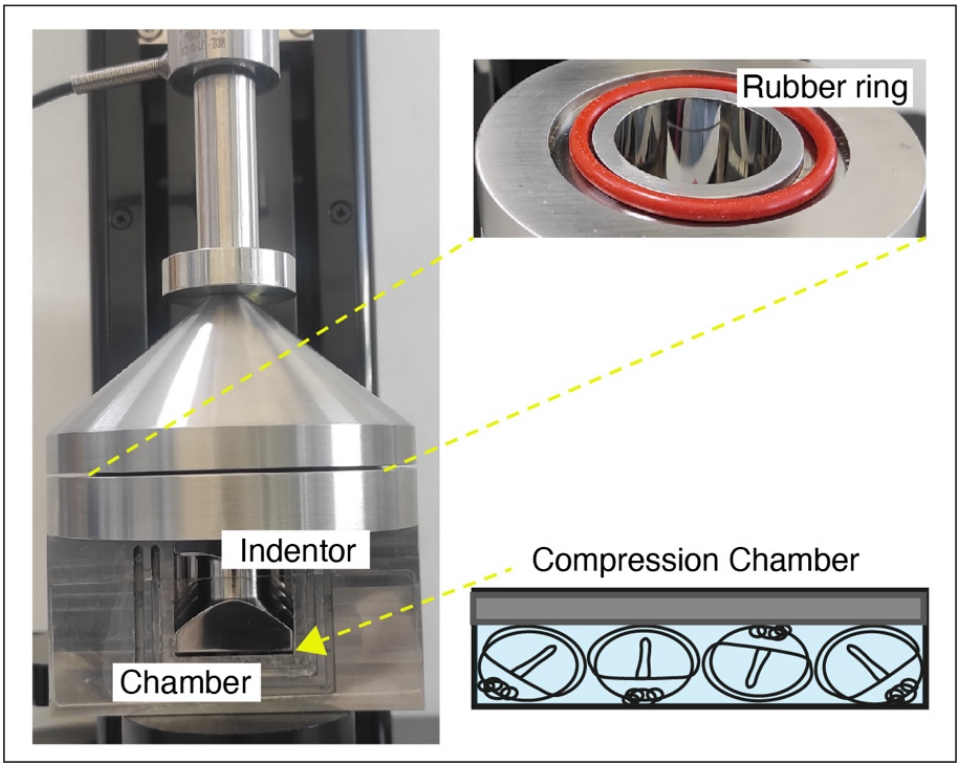

Supplementary Figure 9. Motorized mechanical tester (Univert). Motorized mechanical tester (Univert), equipped with a customized chamber for embryo compression.

Gene name	Primers (5'-3')
no-tail (ntl)	AGAGTTAACCAACGAGATGATCG
	CAACCTCCAAGTTGGGAGTATC
goosecoid (gsc)	GTTCAGCATCGACAGCATCTTG
	TTTTCCTCCCTCAAATGGACCTT
sox3	TGATGGAAACCGAGATCAAGACC
	GAGGACATCATAGGGTACTGCAG
yap1	ACTCCAGATGACTTCCTCAACAG
	AGCCTTGAAGACACAGACACAAT
***marcksl1b* (probe)**	ATGGGATCCCAGTCATCCAAGGG
	ACTCCACCCTGCTTCACCTCATGG
Universal primer (Cas13d)	TAATACGACTCACTATAGGTACCCCTACCAACTGGTCGGGGTTTGAAAC
***marcksl1b* (gRNAs Cas13d)**	GTGCTGCCGCCGCTGCCCCCTCCGTTTCAAACCCCGACCAGTT
	GGCGGTGGGACGGTCAGCGTGCGGTTTCAAACCCCGACCAGTT
***ef1a* (qPCR)**	AAACCCAGAAACACCGAAACAT
	CCTCCGCACTTGTAGATCAG
***ctgfa* (qPCR)**	GCCGACAGGAGATCCACTTG
	CCTGCAGCCGCGTATGAGTA
***cyr61* (qPCR)**	GAGCTCTCCCTGCCCAATTT
	CTGTATGCAGGCAGGGTCTT
***lats2* (qPCR)**	AACGAGCAACTTTTTCCCGC
	CATCTGCGCCATGTGTGATG
***lmc1* (qPCR)**	GAGCGCAGAGTGTTACTTCG
	GAGGAGACAGAGAGCCGATG
***marcksl1b* (qPCR)**	AAGACCAACGGACAGGAGAAC
	CTTCGGGTTTGGTGGCTTCC

Supplementary Table 1: List of primers used.

Gene ID	Gene name	log2FoldChange	GeneOntology
ENSORLG00000027007	mfap4	-1,99	Extracellular Matrix
ENSORLG00000011273	col1a1b	-1,87	Extracellular Matrix
ENSORLG00000010226	angpt1	-1,85	Extracellular Matrix
ENSORLG00000010756	ccn1	-1,62	Integrin Binding, Extracellular Matrix
ENSORLG00000008004	actr2b	-1,62	Cytoskeleton Organization
ENSORLG00000018064	ccn2a	-1,59	Integrin Binding, Extracellular Matrix
ENSORLG00000014159	marcksl1b	-1,53	Cytoskeleton Organization
ENSORLG00000003389	itgb3a	-1,35	Integrin Binding, Focal Adhesion
ENSORLG00000008993	ptk2bb	-1,23	Focal Adhesion
ENSORLG00000024658	arhgef19	-1,14	Cytoskeleton Organization
ENSORLG00000020765	itgb4	-1,12	Integrin Binding, Focal Adhesion
ENSORLG00000004319	col1a2	-1,04	Extracellular Matrix
ENSORLG00000009834	fermt1	-1,01	Integrin Binding, Focal Adhesion
ENSORLG00000013126	unknown	-1,01	Cytoskeleton Organization
ENSORLG00000016273	amotl2b	-0,96	Hippo Signalling, Cytoskeleton Organization
ENSORLG00000024032	marcksl1a	-0,95	Cytoskeleton Organization
ENSORLG00000009847	smtnl	-0,94	Cytoskeleton Organization
ENSORLG00000002553	tead4	-0,93	Hippo Signalling
ENSORLG00000009876	muc17	-0,92	Extracellular Matrix
ENSORLG00000004966	ADAMTS5	-0,85	Extracellular Matrix
ENSORLG00000007439	tead1b	-0,84	Hippo Signalling
ENSORLG00000029189	tuba1l2	-0,84	Cytoskeleton Organization
ENSORLG00000002708	yap1	-0,83	Hippo Signalling
ENSORLG00000016655	lima1a	-0,82	Cytoskeleton Organization
ENSORLG00000014658	col5a2a	-0,82	Extracellular Matrix
ENSORLG00000012987	tubb5	-0,81	Cytoskeleton Organization
ENSORLG00000015488	bmper	-0,80	Extracellular Matrix
ENSORLG00000002046	coro1a	-0,79	Cytoskeleton Organization
ENSORLG00000001953	NCKAP5	-0,78	Cytoskeleton Organization
ENSORLG00000001946	unknown	-0,78	Extracellular Matrix
ENSORLG00000019677	lama5	-0,77	Integrin Binding, Extracellular Matrix
ENSORLG00000000178	adamtsl5	-0,77	Extracellular Matrix
ENSORLG00000015895	sptb	-0,75	Cytoskeleton Organization
ENSORLG00000000761	vwa1	-0,73	Extracellular Matrix
ENSORLG00000012731	rock2b	-0,72	Cytoskeleton Organization
ENSORLG00000024836	map1ab	-0,72	Cytoskeleton Organization
ENSORLG00000005263	svild	-0,69	Cytoskeleton Organization
ENSORLG00000017032	tpm4a	-0,69	Cytoskeleton Organization
ENSORLG00000005664	col11a1a	-0,68	Extracellular Matrix
ENSORLG00000018013	ccn6	-0,64	Integrin Binding, Extracellular Matrix
ENSORLG00000000815	evpla	-0,64	Cytoskeleton Organization
ENSORLG00000015065	evplb	-0,64	Cytoskeleton Organization
ENSORLG00000003176	coro6	-0,63	Cytoskeleton Organization
ENSORLG00000009740	myo1cb	-0,63	Cytoskeleton Organization
ENSORLG00000026496	synpo	-0,63	Cytoskeleton Organization
ENSORLG00000012150	MYO1D	-0,62	Cytoskeleton Organization
ENSORLG00000015457	amotl2a	-0,62	Hippo Signalling, Cytoskeleton Organization
ENSORLG00000018617	fgl1	-0,61	Extracellular Matrix
ENSORLG00000005573	yap1b	-0,61	Hippo Signalling
ENSORLG00000029757	wtip	-0,60	Hippo Signalling, Cytoskeleton Organization
ENSORLG00000025663	paplna	-0,59	Extracellular Matrix
ENSORLG00000004990	adamts1	-0,56	Extracellular Matrix
ENSORLG00000019746	cav1	-0,54	Focal Adhesion
ENSORLG00000023311	plecb	-0,53	Focal Adhesion, Citoskeleton Organization
ENSORLG00000018677	pard6a	-0,53	Cytoskeleton Organization
ENSORLG00000008336	PKP1	-0,53	Cytoskeleton Organization
ENSORLG00000007419	lamc1	-0,52	Extracellular Matrix
ENSORLG00000014111	pdlim1	-0,52	Cytoskeleton Organization
ENSORLG00000019702	pacsin3	-0,51	Cytoskeleton Organization
ENSORLG00000001861	pard6b	-0,50	Cytoskeleton Organization

Supplementary Table 2: List of significant DEGs between WT and yap1-/-;yap1b-/- stage 16 embryos (FC ≤ -0.5) linked to most significant GO terms identified in the comparative RNA-seq analysis.

Supplementary Movie 1: Tridimensional (3D) reconstruction of DAPI (blue) and Phalloidin (green) immunostained posterior axis in WT, *yap1*$^{-/-}$, and *yap1*$^{-/-}$*;yap1b*$^{-/-}$ embryos.

Supplementary Movie 2: WT, *yap1*$^{-/-}$, and *yap1*$^{-/-}$*;yap1b*$^{-/-}$ embryos injected with *histone2b*::GFP for nuclei visualization were imaged in 4-min intervals over 8 hours. Manual cell tracking trajectories are represented with color lines.

Supplementary Movie 3: Time-lapse confocal imaging of WT *GTIIC::GFP* transgenic embryos.

Supplementary Movie 4: Tridimensional (3D) reconstruction of DAPI stained nuclei in stage 16 WT and *yap1*$^{-/-}$*;yap1b*$^{-/-}$ embryos.

Supplementary Movie S5: Tridimensional (3D) reconstruction of DAPI stained nuclei (stage 16) at medial and lateral regions of a DMSO treated embryo, as well as at lateral region of Rockout treated embryo.

References

Abercrombie, M. (1997). The crawling movement of metazoan cells. *Proceedings of the Royal Society of London. Series B. Biological Sciences*, *207*(1167), 129–147. https://doi.org/10.1098/rspb.1980.0017

Alberts, B., Johnson, A., Lewis, J., Raff, M., Roberts, K., & Walter, P. (2002). The Extracellular Matrix of Animals. *Molecular Biology of the Cell. 4th Edition*. https://www.ncbi.nlm.nih.gov/books/NBK26810/

Almuedo-Castillo, M., Bläßle, A., Mörsdorf, D., Marcon, L., Soh, G. H., Rogers, K. W., Schier, A. F., & Müller, P. (2018). Scale-invariant patterning by size-dependent inhibition of Nodal signalling. *Nature Cell Biology*, *20*(9), Article 9. https://doi.org/10.1038/s41556-018-0155-7

Angulo-Urarte, A., van der Wal, T., & Huveneers, S. (2020). Cell-cell junctions as sensors and transducers of mechanical forces. *Biochimica Et Biophysica Acta. Biomembranes*, *1862*(9), 183316. https://doi.org/10.1016/j.bbamem.2020.183316

Aragona, M., Panciera, T., Manfrin, A., Giulitti, S., Michielin, F., Elvassore, N., Dupont, S., & Piccolo, S. (2013). A Mechanical Checkpoint Controls Multicellular Growth through YAP/TAZ Regulation by Actin-Processing Factors. *Cell*, *154*(5), 1047–1059. https://doi.org/10.1016/j.cell.2013.07.042

Bachir, A. I., Horwitz, A. R., Nelson, W. J., & Bianchini, J. M. (2017). Actin-Based Adhesion Modules Mediate Cell Interactions with the Extracellular Matrix and Neighboring Cells. *Cold Spring Harbor Perspectives in Biology*, *9*(7), a023234. https://doi.org/10.1101/cshperspect.a023234

Balda, M. S., & Matter, K. (2000). The tight junction protein ZO-1 and an interacting transcription factor regulate ErbB-2 expression. *The EMBO Journal*, *19*(9), 2024–2033. https://doi.org/10.1093/emboj/19.9.2024

Balemans, W., & Van Hul, W. (2002). Extracellular regulation of BMP signaling in vertebrates: A cocktail of modulators. *Developmental Biology*, *250*(2), 231–250.

Blum, M., Gaunt, S. J., Cho, K. W., Steinbeisser, H., Blumberg, B., Bittner, D., & De Robertis, E. M. (1992). Gastrulation in the mouse: The role of the homeobox gene goosecoid. *Cell*, *69*(7), 1097–1106. https://doi.org/10.1016/0092-8674(92)90632-m

Bolger, A. M., Lohse, M., & Usadel, B. (2014). Trimmomatic: A flexible trimmer for Illumina sequence data. *Bioinformatics*, *30*(15), 2114–2120. https://doi.org/10.1093/bioinformatics/btu170

Calvo, F., Ege, N., Grande-Garcia, A., Hooper, S., Jenkins, R. P., Chaudhry, S. I., Harrington, K., Williamson, P., Moeendarbary, E., Charras, G., & Sahai, E. (2013). Mechanotransduction and YAP-dependent matrix remodelling is required for the generation and maintenance of cancer-associated fibroblasts. *Nature Cell Biology*, *15*(6), Article 6. https://doi.org/10.1038/ncb2756

Camargo, F. D., Gokhale, S., Johnnidis, J. B., Fu, D., Bell, G. W., Jaenisch, R., & Brummelkamp, T. R. (2007). YAP1 increases organ size and expands undifferentiated progenitor cells. *Current Biology: CB*, *17*(23), 2054–2060. https://doi.org/10.1016/j.cub.2007.10.039

Chan, S. S.-K., & Kyba, M. (2013). What is a Master Regulator? *Journal of Stem Cell Research & Therapy*, *3*, 114. https://doi.org/10.4172/2157-7633.1000e114

Chang, C., Goel, H. L., Gao, H., Pursell, B., Shultz, L. D., Greiner, D. L., Ingerpuu, S., Patarroyo, M., Cao, S., Lim, E., Mao, J., McKee, K. K., Yurchenco, P. D., & Mercurio, A. M. (2015). A laminin 511 matrix is regulated by TAZ and functions as the ligand for the α6Bβ1 integrin to sustain breast cancer stem cells. *Genes & Development*, *29*(1), 1–6. https://doi.org/10.1101/gad.253682.114

Chea, H. K., Wright, C. V., & Swalla, B. J. (2005). Nodal signaling and the evolution of deuterostome gastrulation. *Developmental Dynamics*, *234*(2), 269–278. https://doi.org/10.1002/dvdy.20549

Choi, H.-J., Gross, J. C., Pokutta, S., & Weis, W. I. (2009). Interactions of Plakoglobin and β-Catenin with Desmosomal Cadherins. *Journal of Biological Chemistry*, *284*(46), 31776–31788. https://doi.org/10.1074/jbc.M109.047928

Collinet, C., & Lecuit, T. (2021). Programmed and self-organized flow of information during morphogenesis. *Nature Reviews Molecular Cell Biology*, *22*(4), Article 4. https://doi.org/10.1038/s41580-020-00318-6

Coutelis, J.-B., González-Morales, N., Géminard, C., & Noselli, S. (2014). Diversity and convergence in the mechanisms establishing L/R asymmetry in metazoa. *EMBO Reports*, *15*(9), 926–937. https://doi.org/10.15252/embr.201438972

Dasbiswas, K., Hannezo, E., & Gov, N. S. (2018). Theory of Epithelial Cell Shape Transitions Induced by Mechanoactive Chemical Gradients. *Biophysical Journal*, *114*(4), 968–977. https://doi.org/10.1016/j.bpj.2017.12.022

De Robertis, & M, E. (2006). Spemann's organizer and self-regulation in amphibian embryos. *Nature Reviews Molecular Cell Biology*, *7*(4), Article 4. https://doi.org/10.1038/nrm1855

Dicko, M., Saramito, P., Blanchard, G. B., Lye, C. M., Sanson, B., & Étienne, J. (2017). Geometry can provide long-range mechanical guidance for embryogenesis. *PLOS Computational Biology*, *13*(3), e1005443. https://doi.org/10.1371/journal.pcbi.1005443

Dong, J., Feldmann, G., Huang, J., Wu, S., Zhang, N., Comerford, S. A., Gayyed, M. F., Anders, R. A., Maitra, A., & Pan, D. (2007). Elucidation of a universal size-control mechanism in Drosophila and mammals. *Cell*, *130*(6), 1120–1133. https://doi.org/10.1016/j.cell.2007.07.019

Duchemin, A.-L., Vignes, H., & Vermot, J. (2019). Mechanically activated piezo channels modulate outflow tract valve development through the Yap1 and Klf2-Notch signaling axis. *ELife*, *8*, e44706. https://doi.org/10.7554/eLife.44706

Dupont, S., Morsut, L., Aragona, M., Enzo, E., Giulitti, S., Cordenonsi, M., Zanconato, F., Le Digabel, J., Forcato, M., Bicciato, S., Elvassore, N., & Piccolo, S. (2011). Role of YAP/TAZ in mechanotransduction. *Nature*, *474*(7350), Article 7350. https://doi.org/10.1038/nature10137

Durdu, S., Iskar, M., Revenu, C., Schieber, N., Kunze, A., Bork, P., Schwab, Y., & Gilmour, D. (2014). Luminal signalling links cell communication to tissue architecture during organogenesis. *Nature*, *515*(7525), Article 7525. https://doi.org/10.1038/nature13852

Dzamba, B. J., & DeSimone, D. W. (2018). Chapter Seven—Extracellular Matrix (ECM) and the Sculpting of Embryonic Tissues. In E. S. Litscher & P. M. Wassarman (Eds.), *Current Topics in Developmental Biology* (Vol. 130, pp. 245–274). Academic Press. https://doi.org/10.1016/bs.ctdb.2018.03.006

El Amri, M., Fitzgerald, U., & Schlosser, G. (2018). MARCKS and MARCKS-like proteins in development and regeneration. *Journal of Biomedical Science*, *25*(1), 43. https://doi.org/10.1186/s12929-018-0445-1

Elbediwy, A., Vincent-Mistiaen, Z. I., Spencer-Dene, B., Stone, R. K., Boeing, S., Wculek, S. K., Cordero, J., Tan, E. H., Ridgway, R., Brunton, V. G., Sahai, E., Gerhardt, H., Behrens, A., Malanchi, I., Sansom, O. J., & Thompson, B. J. (2016). Integrin signalling regulates YAP

and TAZ to control skin homeostasis. *Development (Cambridge, England)*, *143*(10), 1674–1687. https://doi.org/10.1242/dev.133728

Elosegui-Artola, A., Andreu, I., Beedle, A. E. M., Lezamiz, A., Uroz, M., Kosmalska, A. J., Oria, R., Kechagia, J. Z., Rico-Lastres, P., Le Roux, A.-L., Shanahan, C. M., Trepat, X., Navajas, D., Garcia-Manyes, S., & Roca-Cusachs, P. (2017). Force Triggers YAP Nuclear Entry by Regulating Transport across Nuclear Pores. *Cell*, *171*(6), 1397-1410.e14. https://doi.org/10.1016/j.cell.2017.10.008

Elosegui-Artola, A., Oria, R., Chen, Y., Kosmalska, A., Pérez-González, C., Castro, N., Zhu, C., Trepat, X., & Roca-Cusachs, P. (2016). Mechanical regulation of a molecular clutch defines force transmission and transduction in response to matrix rigidity. *Nature Cell Biology*, *18*(5), Article 5. https://doi.org/10.1038/ncb3336

Farge, E. (2011). Chapter eight—Mechanotransduction in Development. In M. Labouesse (Ed.), *Current Topics in Developmental Biology* (Vol. 95, pp. 243–265). Academic Press. https://doi.org/10.1016/B978-0-12-385065-2.00008-6

Fink, R. D., & McClay, D. R. (1985). Three cell recognition changes accompany the ingression of sea urchin primary mesenchyme cells. *Developmental Biology*, *107*(1), 66–74. https://doi.org/10.1016/0012-1606(85)90376-8

Fletcher, D. A., & Mullins, R. D. (2010). Cell mechanics and the cytoskeleton. *Nature*, *463*(7280), Article 7280. https://doi.org/10.1038/nature08908

Forlani, S., Lawson, K. A., & Deschamps, J. (2003). Acquisition of Hox codes during gastrulation and axial elongation in the mouse embryo. *Development (Cambridge, England)*, *130*(16), 3807–3819. https://doi.org/10.1242/dev.00573

Friedl, P., & Gilmour, D. (2009). Collective cell migration in morphogenesis, regeneration and cancer. *Nature Reviews Molecular Cell Biology*, *10*(7), Article 7. https://doi.org/10.1038/nrm2720

Galli, G. G., Carrara, M., Yuan, W.-C., Valdes-Quezada, C., Gurung, B., Pepe-Mooney, B., Zhang, T., Geeven, G., Gray, N. S., de Laat, W., Calogero, R. A., & Camargo, F. D. (2015). YAP Drives Growth by Controlling Transcriptional Pause Release from Dynamic Enhancers. *Molecular Cell*, *60*(2), 328–337. https://doi.org/10.1016/j.molcel.2015.09.001

Gehring, W. J., & Ikeo, K. (1999). Pax 6: Mastering eye morphogenesis and eye evolution. *Trends in Genetics*, *15*(9), 371–377. https://doi.org/10.1016/S0168-9525(99)01776-X

Gilmour, D., Rembold, M., & Leptin, M. (2017). From morphogen to morphogenesis and back. *Nature*, *541*(7637), Article 7637. https://doi.org/10.1038/nature21348

Giraldez, S., Stronati, E., Huang, L., Hsu, H.-T., Abraham, E., Jones, K. A., & Estaras, C. (2021). *YAP1 Regulates the Self-organized Fate Patterning of hESCs-Derived Gastruloids* (p. 2021.03.12.434631). bioRxiv. https://doi.org/10.1101/2021.03.12.434631

Gong, Y., Mo, C., & Fraser, S. E. (2004). Planar cell polarity signalling controls cell division orientation during zebrafish gastrulation. *Nature*, *430*(7000), Article 7000. https://doi.org/10.1038/nature02796

Gottardi, C. J., Arpin, M., Fanning, A. S., & Louvard, D. (1996). The Junction-Associated Protein, Zonula Occludens-1, Localizes to the Nucleus before the Maturation and during the Remodeling of Cell-Cell Contacts. *Proceedings of the National Academy of Sciences of the United States of America*, *93*(20), 10779–10784.

Grannas, K., Arngården, L., Lönn, P., Mazurkiewicz, M., Blokzijl, A., Zieba, A., & Söderberg, O. (2015). Crosstalk between Hippo and TGFβ: Subcellular Localization of YAP/TAZ/Smad Complexes. *Journal of Molecular Biology*, *427*(21), 3407–3415. https://doi.org/10.1016/j.jmb.2015.04.015

Gray, R. S., Roszko, I., & Solnica-Krezel, L. (2011). Planar Cell Polarity: Coordinating Morphogenetic Cell Behaviors with Embryonic Polarity. *Developmental Cell*, *21*(1), 120–133. https://doi.org/10.1016/j.devcel.2011.06.011

Gumbiner, B. M. (1995). Signal transduction of beta-catenin. *Current Opinion in Cell Biology*, *7*(5), 634–640. https://doi.org/10.1016/0955-0674(95)80104-9

Halder, G., Callaerts, P., & Gehring, W. J. (1995). Induction of ectopic eyes by targeted expression of the eyeless gene in Drosophila. *Science (New York, N.Y.)*, *267*(5205), 1788–1792. https://doi.org/10.1126/science.7892602

Hannezo, E., & Heisenberg, C.-P. (2019). Mechanochemical Feedback Loops in Development and Disease. *Cell*, *178*(1), 12–25. https://doi.org/10.1016/j.cell.2019.05.052

Heisenberg, C.-P., & Bellaïche, Y. (2013). Forces in Tissue Morphogenesis and Patterning. *Cell*, *153*(5), 948–962. https://doi.org/10.1016/j.cell.2013.05.008

Heisenberg, C.-P., Tada, M., Rauch, G.-J., Saúde, L., Concha, M. L., Geisler, R., Stemple, D. L., Smith, J. C., & Wilson, S. W. (2000). Silberblick/Wnt11 mediates convergent extension movements during zebrafish gastrulation. *Nature*, *405*(6782), Article 6782. https://doi.org/10.1038/35011068

Hirose, Y., Varga, Z. M., Kondoh, H., & Furutani-Seiki, M. (2004). Single cell lineage and regionalization of cell populations during Medaka neurulation. *Development*, *131*(11), 2553–2563. https://doi.org/10.1242/dev.01140

Hong, S., Troyanovsky, R. B., & Troyanovsky, S. M. (2013). Binding to F-actin guides cadherin cluster assembly, stability, and movement. *Journal of Cell Biology*, *201*(1), 131–143. https://doi.org/10.1083/jcb.201211054

Huang, J., Wu, S., Barrera, J., Matthews, K., & Pan, D. (2005). The Hippo signaling pathway coordinately regulates cell proliferation and apoptosis by inactivating Yorkie, the Drosophila Homolog of YAP. *Cell*, *122*(3), 421–434. https://doi.org/10.1016/j.cell.2005.06.007

Hubaud, A., & Pourquié, O. (2014). Signalling dynamics in vertebrate segmentation. *Nature Reviews Molecular Cell Biology*, *15*(11), Article 11. https://doi.org/10.1038/nrm3891

Huttenlocher, A., & Horwitz, A. R. (2011). Integrins in Cell Migration. *Cold Spring Harbor Perspectives in Biology*, *3*(9), a005074. https://doi.org/10.1101/cshperspect.a005074

Hynes, R. O., & Destree, A. T. (1978). 10 nm filaments in normal and transformed cells. *Cell*, *13*(1), 151–163. https://doi.org/10.1016/0092-8674(78)90146-0

Hytönen, V. P., & Wehrle-Haller, B. (2016). Mechanosensing in cell–matrix adhesions – Converting tension into chemical signals. *Experimental Cell Research*, *343*(1), 35–41. https://doi.org/10.1016/j.yexcr.2015.10.027

Jessen, J. R., Topczewski, J., Bingham, S., Sepich, D. S., Marlow, F., Chandrasekhar, A., & Solnica-Krezel, L. (2002). Zebrafish trilobite identifies new roles for Strabismus in gastrulation and neuronal movements. *Nature Cell Biology*, *4*(8), 610–615. https://doi.org/10.1038/ncb828

Kang, Y., & Massagué, J. (2004). Epithelial-Mesenchymal Transitions: Twist in Development and Metastasis. *Cell*, *118*(3), 277–279. https://doi.org/10.1016/j.cell.2004.07.011

Karaman, R., & Halder, G. (2018). Cell Junctions in Hippo Signaling. *Cold Spring Harbor Perspectives in Biology*, *10*(5), a028753. https://doi.org/10.1101/cshperspect.a028753

Keller, R. (2005). Cell migration during gastrulation. *Current Opinion in Cell Biology*, *17*(5), 533–541. https://doi.org/10.1016/j.ceb.2005.08.006

Keller, R. E. (1981). An experimental analysis of the role of bottle cells and the deep marginal zone in gastrulation of Xenopus laevis. *The Journal of Experimental Zoology*, *216*(1), 81–101. https://doi.org/10.1002/jez.1402160109

Khatau, S. B., Hale, C. M., Stewart-Hutchinson, P. J., Patel, M. S., Stewart, C. L., Searson, P. C., Hodzic, D., & Wirtz, D. (2009). A perinuclear actin cap regulates nuclear shape. *Proceedings of the National Academy of Sciences of the United States of America*, *106*(45), 19017–19022. https://doi.org/10.1073/pnas.0908686106

Kim, D., Paggi, J. M., Park, C., Bennett, C., & Salzberg, S. L. (2019). Graph-based genome alignment and genotyping with HISAT2 and HISAT-genotype. *Nature Biotechnology*, *37*(8), Article 8. https://doi.org/10.1038/s41587-019-0201-4

Kim, N.-G., & Gumbiner, B. M. (2015). Adhesion to fibronectin regulates Hippo signaling via the FAK-Src-PI3K pathway. *Journal of Cell Biology*, *210*(3), 503–515. Scopus. https://doi.org/10.1083/jcb.201501025

Kim, N.-G., Koh, E., Chen, X., & Gumbiner, B. M. (2011). E-cadherin mediates contact inhibition of proliferation through Hippo signaling-pathway components. *Proceedings of the National Academy of Sciences*, *108*(29), 11930–11935. https://doi.org/10.1073/pnas.1103345108

Kimelman, D., Smith, N. L., Lai, J. K. H., & Stainier, D. Y. (2017). Regulation of posterior body and epidermal morphogenesis in zebrafish by localized Yap1 and Wwtr1. *ELife*, *6*, e31065. https://doi.org/10.7554/eLife.31065

Kindberg, A., Hu, J. K., & Bush, J. O. (2020). Forced to communicate: Integration of mechanical and biochemical signaling in morphogenesis. *Current Opinion in Cell Biology*, *66*, 59–68. https://doi.org/10.1016/j.ceb.2020.05.004

Ko, C. S., & Martin, A. C. (2020). Chapter Five—The cellular and molecular mechanisms that establish the mechanics of Drosophila gastrulation. In L. Solnica-Krezel (Ed.), *Current Topics in Developmental Biology* (Vol. 136, pp. 141–165). Academic Press. https://doi.org/10.1016/bs.ctdb.2019.08.003

Kopylova, E., Noé, L., & Touzet, H. (2012). SortMeRNA: Fast and accurate filtering of ribosomal RNAs in metatranscriptomic data. *Bioinformatics (Oxford, England)*, *28*(24), 3211–3217. https://doi.org/10.1093/bioinformatics/bts611

Kovács, M., Tóth, J., Hetényi, C., Málnási-Csizmadia, A., & Sellers, J. R. (2004). Mechanism of blebbistatin inhibition of myosin II. *The Journal of Biological Chemistry*, *279*(34), 35557–35563. https://doi.org/10.1074/jbc.M405319200

Kucukural, A., Yukselen, O., Ozata, D. M., Moore, M. J., & Garber, M. (2019). DEBrowser: Interactive differential expression analysis and visualization tool for count data. *BMC Genomics*, *20*(1), 6. https://doi.org/10.1186/s12864-018-5362-x

Kushawah, G., Hernandez-Huertas, L., Abugattas-Nuñez Del Prado, J., Martinez-Morales, J. R., DeVore, M. L., Hassan, H., Moreno-Sanchez, I., Tomas-Gallardo, L., Diaz-Moscoso, A., Monges, D. E., Guelfo, J. R., Theune, W. C., Brannan, E. O., Wang, W., Corbin, T. J., Moran, A. M., Sánchez Alvarado, A., Málaga-Trillo, E., Takacs, C. M., … Moreno-Mateos, M. A. (2020). CRISPR-Cas13d Induces Efficient mRNA Knockdown in Animal Embryos. *Developmental Cell*, *54*(6), 805-817.e7. https://doi.org/10.1016/j.devcel.2020.07.013

Leptin, M. (1999). Gastrulation in Drosophila: The logic and the cellular mechanisms. *The EMBO Journal*, *18*(12), 3187–3192. https://doi.org/10.1093/emboj/18.12.3187

Leptin, M. (2005). Gastrulation Movements: The Logic and the Nuts and Bolts. *Developmental Cell*, *8*(3), 305–320. https://doi.org/10.1016/j.devcel.2005.02.007

Lewis, J. M., Baskaran, R., Taagepera, S., Schwartz, M. A., & Wang, J. Y. J. (1996). Integrin Regulation of c-Abl Tyrosine Kinase Activity and Cytoplasmic-Nuclear Transport. *Proceedings of the National Academy of Sciences of the United States of America*, *93*(26), 15174–15179.

Lin, C., Yao, E., Zhang, K., Jiang, X., Croll, S., Thompson-Peer, K., & Chuang, P.-T. (2017). YAP is essential for mechanical force production and epithelial cell proliferation during lung branching morphogenesis. *ELife*, *6*, e21130. https://doi.org/10.7554/eLife.21130

Lin, F., Chen, S., Sepich, D. S., Panizzi, J. R., Clendenon, S. G., Marrs, J. A., Hamm, H. E., & Solnica-Krezel, L. (2009). Gα12/13 regulate epiboly by inhibiting E-cadherin activity and modulating the actin cytoskeleton. *Journal of Cell Biology*, *184*(6), 909–921. https://doi.org/10.1083/jcb.200805148

Lin, F., Sepich, D. S., Chen, S., Topczewski, J., Yin, C., Solnica-Krezel, L., & Hamm, H. (2005). Essential roles of Gα12/13 signaling in distinct cell behaviors driving zebrafish convergence and extension gastrulation movements. *Journal of Cell Biology*, *169*(5), 777–787. https://doi.org/10.1083/jcb.200501104

Logue, J. S., Cartagena-Rivera, A. X., & Chadwick, R. S. (2018). C-Src activity is differentially required by cancer cell motility modes. *Oncogene*, *37*(16), Article 16. https://doi.org/10.1038/s41388-017-0071-5

López-Colomé, A. M., Lee-Rivera, I., Benavides-Hidalgo, R., & López, E. (2017). Paxillin: A crossroad in pathological cell migration. *Journal of Hematology & Oncology*, *10*(1), 50. https://doi.org/10.1186/s13045-017-0418-y

Mahoney, W. M., Hong, J.-H., Yaffe, M. B., & Farrance, I. K. G. (2005). The transcriptional co-activator TAZ interacts differentially with transcriptional enhancer factor-1 (TEF-1) family members. *The Biochemical Journal*, *388*(Pt 1), 217–225. https://doi.org/10.1042/BJ20041434

Marsal, M., Hernández-Vega, A., & Martin-Blanco, E. (2017). Contractility, differential tension and membrane removal lead zebrafish epiboly biomechanics. *Cell Cycle*, *16*(14), 1328–1335. https://doi.org/10.1080/15384101.2017.1327489

Martin, A. C., & Goldstein, B. (2014). Apical constriction: Themes and variations on a cellular mechanism driving morphogenesis. *Development*, *141*(10), 1987–1998. https://doi.org/10.1242/dev.102228

Martin, B. L., & Kimelman, D. (2010). Brachyury establishes the embryonic mesodermal progenitor niche. *Genes & Development*, *24*(24), 2778–2783. https://doi.org/10.1101/gad.1962910

Martinez-Morales, J. R., Rembold, M., Greger, K., Simpson, J. C., Brown, K. E., Quiring, R., Pepperkok, R., Martin-Bermudo, M. D., Himmelbauer, H., & Wittbrodt, J. (2009). Ojoplano-mediated basal constriction is essential for optic cup morphogenesis. *Development*, *136*(13), 2165–2175. https://doi.org/10.1242/dev.033563

Martino, F., Perestrelo, A. R., Vinarský, V., Pagliari, S., & Forte, G. (2018). Cellular Mechanotransduction: From Tension to Function. *Frontiers in Physiology*, *9*. https://www.frontiersin.org/articles/10.3389/fphys.2018.00824

Mason, D. E., Collins, J. M., Dawahare, J. H., Nguyen, T. D., Lin, Y., Voytik-Harbin, S. L., Zorlutuna, P., Yoder, M. C., & Boerckel, J. D. (2019). YAP and TAZ limit cytoskeletal and focal adhesion maturation to enable persistent cell motility. *Journal of Cell Biology*, *218*(4), 1369–1389. https://doi.org/10.1083/jcb.201806065

Mayer, M., Depken, M., Bois, J. S., Jülicher, F., & Grill, S. W. (2010). Anisotropies in cortical tension reveal the physical basis of polarizing cortical flows. *Nature*, *467*(7315), Article 7315. https://doi.org/10.1038/nature09376

Méjat, A., & Misteli, T. (2010). LINC complexes in health and disease. *Nucleus*, *1*(1), 40–52. https://doi.org/10.4161/nucl.1.1.10530

Miesfeld, J. B., Gestri, G., Clark, B. S., Flinn, M. A., Poole, R. J., Bader, J. R., Besharse, J. C., Wilson, S. W., & Link, B. A. (2015). Yap and Taz regulate retinal pigment epithelial cell fate. *Development (Cambridge, England)*, *142*(17), 3021–3032. https://doi.org/10.1242/dev.119008

Mongera, A., Rowghanian, P., Gustafson, H. J., Shelton, E., Kealhofer, D. A., Carn, E. K., Serwane, F., Lucio, A. A., Giammona, J., & Campàs, O. (2018). A fluid-to-solid jamming transition underlies vertebrate body axis elongation. *Nature*, *561*(7723), Article 7723. https://doi.org/10.1038/s41586-018-0479-2

Morgan, T. H. (1895). Half-embryos and whole-embryos from one of the first two blastomeres of the frog's egg. *Anat. Anz.*, *10*, 623–628.

Morikawa, Y., Zhang, M., Heallen, T., Leach, J., Tao, G., Xiao, Y., Bai, Y., Li, W., Willerson, J. T., & Martin, J. F. (2015). Actin cytoskeletal remodeling with protrusion formation is essential for heart regeneration in Hippo-deficient mice. *Science Signaling*, *8*(375), ra41–ra41. https://doi.org/10.1126/scisignal.2005781

Morin-Kensicki, E. M., Boone, B. N., Howell, M., Stonebraker, J. R., Teed, J., Alb, J. G., Magnuson, T. R., O'Neal, W., & Milgram, S. L. (2006). Defects in Yolk Sac Vasculogenesis, Chorioallantoic Fusion, and Embryonic Axis Elongation in Mice with Targeted Disruption of Yap65. *Molecular and Cellular Biology*, *26*(1), 77–87. https://doi.org/10.1128/MCB.26.1.77-87.2006

Nardone, G., Oliver-De La Cruz, J., Vrbsky, J., Martini, C., Pribyl, J., Skládal, P., Pešl, M., Caluori, G., Pagliari, S., Martino, F., Maceckova, Z., Hajduch, M., Sanz-Garcia, A., Pugno, N. M., Stokin, G. B., & Forte, G. (2017). YAP regulates cell mechanics by controlling focal adhesion assembly. *Nature Communications*, *8*(1), Article 1. https://doi.org/10.1038/ncomms15321

Nelson, C. M., Jean, R. P., Tan, J. L., Liu, W. F., Sniadecki, N. J., Spector, A. A., & Chen, C. S. (2005). Emergent patterns of growth controlled by multicellular form and mechanics. *Proceedings of the National Academy of Sciences*, *102*(33), 11594–11599. https://doi.org/10.1073/pnas.0502575102

Nelson, W. J. (2009). Remodeling epithelial cell organization: Transitions between front-rear and apical-basal polarity. *Cold Spring Harbor Perspectives in Biology*, *1*(1), a000513. https://doi.org/10.1101/cshperspect.a000513

Neto-Silva, R. M., de Beco, S., & Johnston, L. A. (2010). Evidence for a Growth-Stabilizing Regulatory Feedback Mechanism between Myc and Yorkie, the Drosophila Homolog of Yap. *Developmental Cell*, *19*(4), 507–520. https://doi.org/10.1016/j.devcel.2010.09.009

Nicolás-Pérez, M., Kuchling, F., Letelier, J., Polvillo, R., Wittbrodt, J., & Martínez-Morales, J. R. (2016). Analysis of cellular behavior and cytoskeletal dynamics reveal a constriction mechanism driving optic cup morphogenesis. *ELife*, *5*, e15797. https://doi.org/10.7554/eLife.15797

Oliver-De La Cruz, J., Nardone, G., Vrbsky, J., Pompeiano, A., Perestrelo, A. R., Capradossi, F., Melajová, K., Filipensky, P., & Forte, G. (2019). Substrate mechanics controls adipogenesis through YAP phosphorylation by dictating cell spreading. *Biomaterials*, *205*, 64–80. https://doi.org/10.1016/j.biomaterials.2019.03.009

Orsulic, S., & Peifer, M. (1996). An in vivo structure-function study of armadillo, the beta-catenin homologue, reveals both separate and overlapping regions of the protein required for cell adhesion and for wingless signaling. *The Journal of Cell Biology*, *134*(5), 1283–1300. https://doi.org/10.1083/jcb.134.5.1283

Pasapera, A. M., Schneider, I. C., Rericha, E., Schlaepfer, D. D., & Waterman, C. M. (2010). Myosin II activity regulates vinculin recruitment to focal adhesions through FAK-mediated paxillin phosphorylation. *Journal of Cell Biology*, *188*(6), 877–890. https://doi.org/10.1083/jcb.200906012

Pathak, M. M., Nourse, J. L., Tran, T., Hwe, J., Arulmoli, J., Le, D. T. T., Bernardis, E., Flanagan, L. A., & Tombola, F. (2014). Stretch-activated ion channel Piezo1 directs lineage choice in human neural stem cells. *Proceedings of the National Academy of Sciences*, *111*(45), 16148–16153. https://doi.org/10.1073/pnas.1409802111

Petridou, N. I., Spiró, Z., & Heisenberg, C.-P. (2017). Multiscale force sensing in development. *Nature Cell Biology*, *19*(6), 581–588. https://doi.org/10.1038/ncb3524

Pézeron, G., Mourrain, P., Courty, S., Ghislain, J., Becker, T. S., Rosa, F. M., & David, N. B. (2008). Live Analysis of Endodermal Layer Formation Identifies Random Walk as a Novel Gastrulation Movement. *Current Biology*, *18*(4), 276–281. https://doi.org/10.1016/j.cub.2008.01.028

Piccolo, F. M., Kastan, N. R., Haremaki, T., Tian, Q., Laundos, T. L., De Santis, R., Beaudoin, A. J., Carroll, T. S., Luo, J.-D., Gnedeva, K., Etoc, F., Hudspeth, A., & Brivanlou, A. H. (2022).

Role of YAP in early ectodermal specification and a Huntington's Disease model of human neurulation. *ELife*, *11*, e73075. https://doi.org/10.7554/eLife.73075

Piccolo, S., Dupont, S., & Cordenonsi, M. (2014). The Biology of YAP/TAZ: Hippo Signaling and Beyond. *Physiological Reviews*, *94*(4), 1287–1312. https://doi.org/10.1152/physrev.00005.2014

Pinheiro, D., & Heisenberg, C.-P. (2020). Chapter Twelve - Zebrafish gastrulation: Putting fate in motion. In L. Solnica-Krezel (Ed.), *Current Topics in Developmental Biology* (Vol. 136, pp. 343–375). Academic Press. https://doi.org/10.1016/bs.ctdb.2019.10.009

Plattner, R., Kadlec, L., DeMali, K. A., Kazlauskas, A., & Pendergast, A. M. (1999). C-Abl is activated by growth factors and Src family kinases and has a role in the cellular response to PDGF. *Genes & Development*, *13*(18), 2400–2411.

Porazinski, S. R., Wang, H., & Furutani-Seiki, M. (2010). Dechorionation of medaka embryos and cell transplantation for the generation of chimeras. *Journal of Visualized Experiments: JoVE*, *46*, 2055. https://doi.org/10.3791/2055

Porazinski, S., Wang, H., Asaoka, Y., Behrndt, M., Miyamoto, T., Morita, H., Hata, S., Sasaki, T., Krens, S. F. G., Osada, Y., Asaka, S., Momoi, A., Linton, S., Miesfeld, J. B., Link, B. A., Senga, T., Shimizu, N., Nagase, H., Matsuura, S., … Furutani-Seiki, M. (2015). YAP is essential for tissue tension to ensure vertebrate 3D body shape. *Nature*, *521*(7551), 217–221. https://doi.org/10.1038/nature14215

Pradel, J., & White, R. A. (2002). From selectors to realizators. *International Journal of Developmental Biology*, *42*(3), Article 3. https://doi.org/10.1387/ijdb.9654026

Raudvere, U., Kolberg, L., Kuzmin, I., Arak, T., Adler, P., Peterson, H., & Vilo, J. (2019). g:Profiler: A web server for functional enrichment analysis and conversions of gene lists (2019 update). *Nucleic Acids Research*, *47*(W1), W191–W198. https://doi.org/10.1093/nar/gkz369

Rivera-Pérez, J. A., Mallo, M., Gendron-Maguire, M., Gridley, T., & Behringer, R. R. (1995). Goosecoid is not an essential component of the mouse gastrula organizer but is required for craniofacial and rib development. *Development (Cambridge, England)*, *121*(9), 3005–3012. https://doi.org/10.1242/dev.121.9.3005

Rogers, K. W., & Schier, A. F. (2011). Morphogen gradients: From generation to interpretation. *Annual Review of Cell and Developmental Biology*, *27*, 377–407. https://doi.org/10.1146/annurev-cellbio-092910-154148

Ross, J. J., Shimmi, O., Vilmos, P., Petryk, A., Kim, H., Gaudenz, K., Hermanson, S., Ekker, S. C., O'Connor, M. B., & Marsh, J. L. (2001). Twisted gastrulation is a conserved extracellular BMP antagonist. *Nature*, *410*(6827), Article 6827. https://doi.org/10.1038/35068578

Ruprecht, V., Wieser, S., Callan-Jones, A., Smutny, M., Morita, H., Sako, K., Barone, V., Ritsch-Marte, M., Sixt, M., Voituriez, R., & Heisenberg, C.-P. (2015). Cortical Contractility Triggers a Stochastic Switch to Fast Amoeboid Cell Motility. *Cell*, *160*(4), 673–685. https://doi.org/10.1016/j.cell.2015.01.008

Sagner, A., & Briscoe, J. (2017). Morphogen interpretation: Concentration, time, competence, and signaling dynamics. *WIREs Developmental Biology*, *6*(4), e271. https://doi.org/10.1002/wdev.271

Sakabe, M., Fan, J., Odaka, Y., Liu, N., Hassan, A., Duan, X., Stump, P., Byerly, L., Donaldson, M., Hao, J., Fruttiger, M., Lu, Q. R., Zheng, Y., Lang, R. A., & Xin, M. (2017). YAP/TAZ-CDC42 signaling regulates vascular tip cell migration. *Proceedings of the National Academy of Sciences*, *114*(41), 10918–10923. https://doi.org/10.1073/pnas.1704030114

Sanaki-Matsumiya, M., Matsuda, M., Gritti, N., Nakaki, F., Sharpe, J., Trivedi, V., & Ebisuya, M. (2022). Periodic formation of epithelial somites from human pluripotent stem cells. *Nature Communications*, *13*(1), Article 1. https://doi.org/10.1038/s41467-022-29967-1

Santos-Pereira, J. M., Gallardo-Fuentes, L., Neto, A., Acemel, R. D., & Tena, J. J. (2019). Pioneer and repressive functions of p63 during zebrafish embryonic ectoderm specification. *Nature Communications*, *10*(1), Article 1. https://doi.org/10.1038/s41467-019-11121-z

Sausedo, R. A., Smith, J. L., & Schoenwolf, G. C. (1997). Role of nonrandomly oriented cell division in shaping and bending of the neural plate. *The Journal of Comparative Neurology*, *381*(4), 473–488.

Schiller, H. B., & Fässler, R. (2013). Mechanosensitivity and compositional dynamics of cell–matrix adhesions. *EMBO Reports*, *14*(6), 509–519. https://doi.org/10.1038/embor.2013.49

Schindelin, J., Arganda-Carreras, I., Frise, E., Kaynig, V., Longair, M., Pietzsch, T., Preibisch, S., Rueden, C., Saalfeld, S., Schmid, B., Tinevez, J.-Y., White, D. J., Hartenstein, V., Eliceiri, K., Tomancak, P., & Cardona, A. (2012). Fiji—An Open Source platform for biological image analysis. *Nature Methods*, *9*(7), 10.1038/nmeth.2019. https://doi.org/10.1038/nmeth.2019

Schwarz, U. S., & Gardel, M. L. (2012). United we stand: Integrating the actin cytoskeleton and cell-matrix adhesions in cellular mechanotransduction. *Journal of Cell Science*, *125*(Pt 13), 3051–3060. https://doi.org/10.1242/jcs.093716

SenGupta, S., Parent, C. A., & Bear, J. E. (2021). The principles of directed cell migration. *Nature Reviews Molecular Cell Biology*, *22*(8), Article 8. https://doi.org/10.1038/s41580-021-00366-6

Sepich, D. S., Calmelet, C., Kiskowski, M., & Solnica-Krezel, L. (2005). Initiation of convergence and extension movements of lateral mesoderm during zebrafish gastrulation. *Developmental Dynamics*, *234*(2), 279–292. https://doi.org/10.1002/dvdy.20507

Sero, J. E., & Bakal, C. (2017). Multiparametric Analysis of Cell Shape Demonstrates that β-PIX Directly Couples YAP Activation to Extracellular Matrix Adhesion. *Cell Systems*, *4*(1), 84-96.e6. https://doi.org/10.1016/j.cels.2016.11.015

Sharpe, J. (2019). Wolpert's French Flag: What's the problem? *Development*, *146*(24), dev185967. https://doi.org/10.1242/dev.185967

Shellard, A., & Mayor, R. (2020). All Roads Lead to Directional Cell Migration. *Trends in Cell Biology*, *30*(11), 852–868. https://doi.org/10.1016/j.tcb.2020.08.002

Shyer, A. E., Huycke, T. R., Lee, C., Mahadevan, L., & Tabin, C. J. (2015). Bending Gradients: How the Intestinal Stem Cell Gets Its Home. *Cell*, *161*(3), 569–580. https://doi.org/10.1016/j.cell.2015.03.041

Sidhaye, J., & Norden, C. (2017). Concerted action of neuroepithelial basal shrinkage and active epithelial migration ensures efficient optic cup morphogenesis. *ELife*, *6*, e22689. https://doi.org/10.7554/eLife.22689

Slack, J. M. W. (2002). Conrad Hal Waddington: The last Renaissance biologist? *Nature Reviews Genetics*, *3*(11), Article 11. https://doi.org/10.1038/nrg933

Smith, J. C., Price, B. M., Green, J. B., Weigel, D., & Herrmann, B. G. (1991). Expression of a Xenopus homolog of Brachyury (T) is an immediate-early response to mesoderm induction. *Cell*, *67*(1), 79–87. https://doi.org/10.1016/0092-8674(91)90573-h

Solnica-Krezel, L. (2005). Conserved Patterns of Cell Movements during Vertebrate Gastrulation. *Current Biology*, *15*(6), R213–R228. https://doi.org/10.1016/j.cub.2005.03.016

Solnica-Krezel, L. (2020). Chapter Thirteen—Maternal contributions to gastrulation in zebrafish. In F. L. Marlow (Ed.), *Current Topics in Developmental Biology* (Vol. 140, pp. 391–427). Academic Press. https://doi.org/10.1016/bs.ctdb.2020.05.001

Solnica-Krezel, L., & Sepich, D. S. (2012). Gastrulation: Making and Shaping Germ Layers. *Annual Review of Cell and Developmental Biology*, *28*(1), 687–717. https://doi.org/10.1146/annurev-cellbio-092910-154043

Somlyo, A. P., & Somlyo, A. V. (2000). Signal transduction by G-proteins, Rho-kinase and protein phosphatase to smooth muscle and non-muscle myosin II. *The Journal of Physiology*, *522*(Pt 2), 177–185. https://doi.org/10.1111/j.1469-7793.2000.t01-2-00177.x

Spadaro, D., Le, S., Laroche, T., Mean, I., Jond, L., Yan, J., & Citi, S. (2017). Tension-Dependent Stretching Activates ZO-1 to Control the Junctional Localization of Its Interactors. *Current Biology: CB*, *27*(24), 3783-3795.e8. https://doi.org/10.1016/j.cub.2017.11.014

Standring, S. (2021). Chapter teen—Cell populations at gastrulation. In *Gray's Anatomy* (42nd ed.). Elsevier. https://www.clinicalkey.com/#!/content/book/3-s2.0-B9780702077050000100

Stein, C., Bardet, A. F., Roma, G., Bergling, S., Clay, I., Ruchti, A., Agarinis, C., Schmelzle, T., Bouwmeester, T., Schübeler, D., & Bauer, A. (2015). YAP1 Exerts Its Transcriptional Control via TEAD-Mediated Activation of Enhancers. *PLOS Genetics*, *11*(8), e1005465. https://doi.org/10.1371/journal.pgen.1005465

Stern, C. D. (2004). *Gastrulation: From Cells to Embryo*. CSHL Press.

Su, Y.-H., Chen, Y.-C., Ting, H.-C., Fan, T.-P., Lin, C.-Y., Wang, K.-T., & Yu, J.-K. (2019). BMP controls dorsoventral and neural patterning in indirect-developing hemichordates providing insight into a possible origin of chordates. *Proceedings of the National Academy of Sciences of the United States of America*, *116*(26), 12925–12932. https://doi.org/10.1073/pnas.1901919116

Tam, P. P. L., & Loebel, D. A. F. (2007). Gene function in mouse embryogenesis: Get set for gastrulation. *Nature Reviews Genetics*, *8*(5), Article 5. https://doi.org/10.1038/nrg2084

Technau, U. (2001). Brachyury, the blastopore and the evolution of the mesoderm. *BioEssays: News and Reviews in Molecular, Cellular and Developmental Biology*, *23*(9), 788–794. https://doi.org/10.1002/bies.1114

Thiery, J. P., Acloque, H., Huang, R. Y. J., & Nieto, M. A. (2009). Epithelial-Mesenchymal Transitions in Development and Disease. *Cell*, *139*(5), 871–890. https://doi.org/10.1016/j.cell.2009.11.007

Thisse, C., & Thisse, B. (2008). High-resolution in situ hybridization to whole-mount zebrafish embryos. *Nature Protocols*, *3*(1), Article 1. https://doi.org/10.1038/nprot.2007.514

Tinevez, J.-Y., Perry, N., Schindelin, J., Hoopes, G. M., Reynolds, G. D., Laplantine, E., Bednarek, S. Y., Shorte, S. L., & Eliceiri, K. W. (2017). TrackMate: An open and extensible platform for single-particle tracking. *Methods (San Diego, Calif.)*, *115*, 80–90. https://doi.org/10.1016/j.ymeth.2016.09.016

Totaro, A., Panciera, T., & Piccolo, S. (2018). YAP/TAZ upstream signals and downstream responses. *Nature Cell Biology*, *20*(8), 888–899. https://doi.org/10.1038/s41556-018-0142-z

Varelas, X. (2014). The Hippo pathway effectors TAZ and YAP in development, homeostasis and disease. *Development*, *141*(8), 1614–1626. https://doi.org/10.1242/dev.102376

Varelas, X., Samavarchi-Tehrani, P., Narimatsu, M., Weiss, A., Cockburn, K., Larsen, B. G., Rossant, J., & Wrana, J. L. (2010). The Crumbs complex couples cell density sensing to Hippo-dependent control of the TGF-β-SMAD pathway. *Developmental Cell*, *19*(6), 831–844. https://doi.org/10.1016/j.devcel.2010.11.012

Vázquez-Marín, J., Gutiérrez-Triana, J. A., Almuedo-Castillo, M., Buono, L., Gómez-Skarmeta, J. L., Mateo, J. L., Wittbrodt, J., & Martínez-Morales, J. R. (2019). Yap1b, a divergent Yap/Taz family member, cooperates with yap1 in survival and morphogenesis via common transcriptional targets. *Development*, *146*(13), dev173286. https://doi.org/10.1242/dev.173286

Wada, K.-I., Itoga, K., Okano, T., Yonemura, S., & Sasaki, H. (2011). Hippo pathway regulation by cell morphology and stress fibers. *Development (Cambridge, England)*, *138*(18), 3907–3914. https://doi.org/10.1242/dev.070987

Walck-Shannon, E., & Hardin, J. (2014). Cell intercalation from top to bottom. *Nature Reviews Molecular Cell Biology*, *15*(1), Article 1. https://doi.org/10.1038/nrm3723

Wallingford, J. B., Rowning, B. A., Vogeli, K. M., Rothbächer, U., Fraser, S. E., & Harland, R. M. (2000). Dishevelled controls cell polarity during Xenopus gastrulation. *Nature*, *405*(6782), 81–85. https://doi.org/10.1038/35011077

Warga, R. M., & Kimmel, C. B. (1990). Cell movements during epiboly and gastrulation in zebrafish. *Development (Cambridge, England)*, *108*(4), 569–580. https://doi.org/10.1242/dev.108.4.569

Wartlick, O., Mumcu, P., Kicheva, A., Bittig, T., Seum, C., Jülicher, F., & González-Gaitán, M. (2011). Dynamics of Dpp Signaling and Proliferation Control. *Science*, *331*(6021), 1154–1159. https://doi.org/10.1126/science.1200037

Weber, G. F., Bjerke, M. A., & DeSimone, D. W. (2012). A Mechanoresponsive Cadherin-Keratin Complex Directs Polarized Protrusive Behavior and Collective Cell Migration. *Developmental Cell*, *22*(1), 104–115. https://doi.org/10.1016/j.devcel.2011.10.013

Weintraub, H., Tapscott, S. J., Davis, R. L., Thayer, M. J., Adam, M. A., Lassar, A. B., & Miller, A. D. (1989). Activation of muscle-specific genes in pigment, nerve, fat, liver, and fibroblast cell lines by forced expression of MyoD. *Proceedings of the National Academy of Sciences of the United States of America*, *86*(14), 5434–5438. https://doi.org/10.1073/pnas.86.14.5434

Williams, M. L. K., & Solnica-Krezel, L. (2020). Chapter Thirteen—Cellular and molecular mechanisms of convergence and extension in zebrafish. In L. Solnica-Krezel (Ed.), *Current Topics in Developmental Biology* (Vol. 136, pp. 377–407). Academic Press. https://doi.org/10.1016/bs.ctdb.2019.08.001

Wolpert, L. (1969). Positional information and the spatial pattern of cellular differentiation. *Journal of Theoretical Biology*, *25*(1), 1–47. https://doi.org/10.1016/S0022-5193(69)80016-0

Wu, S.-Y., Ferkowicz, M., & McClay, D. R. (2007). Ingression of primary mesenchyme cells of the sea urchin embryo: A precisely timed epithelial mesenchymal transition. *Birth Defects Research Part C: Embryo Today: Reviews*, *81*(4), 241–252. https://doi.org/10.1002/bdrc.20113

Yang, Y., & Mlodzik, M. (2015). Wnt-Frizzled/Planar Cell Polarity Signaling: Cellular Orientation by Facing the Wind (Wnt). *Annual Review of Cell and Developmental Biology*, *31*, 623–646. https://doi.org/10.1146/annurev-cellbio-100814-125315

Yin, C., Ciruna, B., & Solnica-Krezel, L. (2009). Convergence and extension movements during vertebrate gastrulation. *Current Topics in Developmental Biology*, *89*, 163–192. https://doi.org/10.1016/S0070-2153(09)89007-8

Yosefzon, Y., Soteriou, D., Feldman, A., Kostic, L., Koren, E., Brown, S., Ankawa, R., Sedov, E., Glaser, F., & Fuchs, Y. (2018). Caspase-3 Regulates YAP-Dependent Cell Proliferation and Organ Size. *Molecular Cell*, *70*(4), 573-587.e4. https://doi.org/10.1016/j.molcel.2018.04.019

Yu, F.-X., Zhao, B., Panupinthu, N., Jewell, J. L., Lian, I., Wang, L. H., Zhao, J., Yuan, H., Tumaneng, K., Li, H., Fu, X.-D., Mills, G. B., & Guan, K.-L. (2012). Regulation of the Hippo-YAP pathway by G-protein-coupled receptor signaling. *Cell*, *150*(4), 780–791. https://doi.org/10.1016/j.cell.2012.06.037

Zanconato, F., Cordenonsi, M., & Piccolo, S. (2016). YAP/TAZ at the roots of cancer. *Cancer Cell*, *29*(6), 783–803. https://doi.org/10.1016/j.ccell.2016.05.005

Zanconato, F., Forcato, M., Battilana, G., Azzolin, L., Quaranta, E., Bodega, B., Rosato, A., Bicciato, S., Cordenonsi, M., & Piccolo, S. (2015). Genome-wide association between YAP/TAZ/TEAD and AP-1 at enhancers drives oncogenic growth. *Nature Cell Biology*, *17*(9), 1218–1227. https://doi.org/10.1038/ncb3216

Zeng, X.-X. I., Wilm, T. P., Sepich, D. S., & Solnica-Krezel, L. (2007). Apelin and its receptor control heart field formation during zebrafish gastrulation. *Developmental Cell*, *12*(3), 391–402. https://doi.org/10.1016/j.devcel.2007.01.011

Zhao, B., Li, L., Lei, Q., & Guan, K.-L. (2010). The Hippo–YAP pathway in organ size control and tumorigenesis: An updated version. *Genes & Development*, *24*(9), 862–874. https://doi.org/10.1101/gad.1909210

Zhao, B., Li, L., Lu, Q., Wang, L. H., Liu, C.-Y., Lei, Q., & Guan, K.-L. (2011). Angiomotin is a novel Hippo pathway component that inhibits YAP oncoprotein. *Genes & Development*, *25*(1), 51–63. https://doi.org/10.1101/gad.2000111

Zhao, B., Wei, X., Li, W., Udan, R. S., Yang, Q., Kim, J., Xie, J., Ikenoue, T., Yu, J., Li, L., Zheng, P., Ye, K., Chinnaiyan, A., Halder, G., Lai, Z.-C., & Guan, K.-L. (2007). Inactivation of YAP oncoprotein by the Hippo pathway is involved in cell contact inhibition and tissue growth control. *Genes & Development*, *21*(21), 2747–2761. https://doi.org/10.1101/gad.1602907

Zhao, B., Ye, X., Yu, J., Li, L., Li, W., Li, S., Yu, J., Lin, J. D., Wang, C.-Y., Chinnaiyan, A. M., Lai, Z.-C., & Guan, K.-L. (2008). TEAD mediates YAP-dependent gene induction and growth control. *Genes & Development*, *22*(14), 1962–1971. https://doi.org/10.1101/gad.1664408